Asteroseismology of β Cephei and Be type stars

by

Kym Jeanette Frances Goss

A thesis submitted to
The University of Birmingham
for the degree of
Doctor of Philosophy

School of Physics and Astronomy
The University of Birmingham
May 2012

Abstract

The thesis focuses on the asteroseismology of main sequence B-type stars, particularly β Cephei and Be stars. Photometric observations of these stars were analysed in order to detect stellar oscillations. The photometric data analysed in this thesis were collected using the Solar Mass Ejection Imager *(SMEI)*.

The analysis initially focussed on known β Cephei stars, to refine information on previously detected frequencies and detect further oscillations. A survey was then conducted using data from the *SMEI* instrument to search for further β Cephei stars. The results from this survey were analysed, and individual stars were examined in more detail which may possibly be β Cephei like.

Due to the long duration of light curves obtained with the *SMEI* instrument, stellar oscillations can be analysed for evidence of amplitude and phase change. This type of analysis was completed on two Be stars, Achernar and ζ Oph, and significant amplitude changes in the oscillations of both of these stars were detected. There is evidence that the amplitude variations may be linked with the outburst events that occur on Be stars, and therefore this analysis may be used to help solve the puzzle of the *Be phenomenon*.

For Mum, Dad and Jon

Without your love and support this would not have been possible

Acknowledgments

Many thanks go to my supervisors, Prof Yvonne Elsworth and Prof Bill Chaplin, for their much appreciated support, encouragement and advice during my PhD. Particular thanks go to Dr Ian Stevens, with whom I have worked with over the last 3 years, also Dr Christoffer Karoff and Dr Andrea Miglio for their collaborative work.

I would also like to thank the rest of the members in the HiROS research group for their help and support with my work and company and fun over the last 3 years: Neil Tarrant, Guy Davies, Elizabeth George, Anne-Marie Broomhall, Saskia Hekker, Graham Verner, Brek Miller, Steven Hale, Ian Barnes and Barry Jackson.

And last, but definitely not least, I would like to say a big thank you to my family. My parents have always been dedicated to my education and supportive with whatever decisions I have made. My fiancé, Jon, has kept me sane (with regards to work) and provided me with continuous encouragement. Their love and support throughout has made this possible.

The work presented in this thesis, unless stated otherwise, is the original work of the author, which has been prepared under the supervision of Prof Y. Elsworth and Prof W. Chaplin.

Particular credit should be made to the following people:

- Dr Steven Spreckley for his work in developing the *SMEI* pipeline.
- Dr Ian Stevens for his collaborative work on the analysis of the confirmed β Cephei stars.
- Dr Christoffer Karoff for providing the basics of a computer program to analyse photometric light curves for pulsations.
- Dr Andrea Miglio for his help in modelling the star HIP 30122.
- Dr Derek Buzasi for creating the time frequency analysis diagram on ζ Oph.
- Dr Petr Harmanec for providing spectroscopic data on ζ Oph.
- Dr Ian Howarth for analysing the spectroscopic data on ζ Oph.

Contents

List of Figures

List of Tables

Chapter 1

An Introduction to asteroseismology

> At first sight it would seem that the deep interior of the Sun and stars is less accessible to scientific investigations than any other region of the universe. Our telescopes may probe further and farther into the depths of space; but how can we ever obtain certain knowledge of that which is hidden behind substantial barriers? What appliance can pierce through the outer layers of a star and test the conditions within?
>
> *Arthur Eddington, 1926.*

In the *Internal constitution of stars* [Eddington, 1926] Eddington points out the difficulties in taking scientific measurements of the interior of our Sun and other stars. The observations that are obtained from a star are of radiation and only tell us information about the surface of the star, as the stellar interior is opaque to radiation.

Therefore a more indirect approach needs to be used to provide information about stellar interiors. What observations can be made of the Sun and other stars that would tell us more about their internal structure? This is where the field of asteroseismology comes into play.

Asteroseismology derives from the Greek, *aster* to mean star and *seismos* to mean

quake. It is the study of the internal structure of pulsating stars, by interpreting their oscillations.

Asteroseismology is one of the only ways of inferring information about the interior structure of stars. By analysing the oscillations in stars we are able to determine the density of the material the oscillations have travelled through. Another way of probing the conditions in the solar interior is to study solar neutrinos. Different nuclear reactions within the Sun produce neutrinos of different energies. However, for the present the study of solar neutrinos can only provide bulk information on the solar core.

The theory behind asteroseismology is something that has been used before to determine the internal structure of the Earth. Earthquakes that give waves that travel through the interior of the Earth have been used to infer information about the Earth's interior, allowing geophysicists to improve their understanding of the internal structure of the Earth. In the case of stars, analogous information can be used to test the input parameters of stellar models and hence supply observational evidence that these models are accurate or need to be corrected or improved. Not only would improvement of the stellar models increase the accuracy of the calculated global parameters but also allows scientists a deeper knowledge of these stars by using them as a laboratory to test physics e.g. physics of convection, opacities etc.

Asteroseismology can also be used in the study of extrasolar planets. Observed oscillations of the parent star can put constraints on the radius of the star. If a planet is detected using the transit method, this means that the radius of the planet can then be estimated very accurately and hence further information about the dynamics of the system can be calculated.

This thesis is focused on analysing photometric data on B-type stars which lie on the main sequence. These stars are much larger than our Sun with high effective temperatures and luminosities in comparison. The following sections of this chapter explain in more detail the different characteristics of B type stars and how they compare

with our Sun. This is also accompanied by an introduction to asteroseismology and any background information that is required for this thesis.

1.1 Oscillations

The study of oscillations can give us valuable information about the internal structure of stars. Let us consider, for example, sound waves travelling through a simple open ended resonance tube. The resonance frequencies that form in an open ended tube will depend on the length of the tube and also the speed of sound of the gas within the tube, which depends on the temperature and composition of the gas that the sound wave is travelling through. If you treat the resonance tube as a black box and are only able to observe the resonance frequencies, it is possible to infer characteristics of the size and composition of the gas in the tube. This theory can be extended to the study of stellar oscillations within stars.

There are two main types of oscillation that can occur within stars. These are called p- and g-mode oscillations and are described in more details below.

Pressure (p-mode) oscillations, also known as acoustic oscillations, are longitudinal standing waves of compression and decompression which propagate through the interior of the star. Like a basic resonance tube, in order for a standing wave to be set up the wave must be trapped between certain boundaries. In a star these boundaries are known as the upper and lower turning surfaces. The boundary for the upper turning surface is at the surface of the star where the acoustic cutoff frequency becomes very high and the waves are reflected back into the interior of the star. The isothermal acoustic cutoff frequency is defined as

$$\omega_a = \frac{c}{2H}, \tag{1.1}$$

where c is the adiabatic sound speed of the wave and H is the density scale height which is defined by

$$H = \frac{\Re T}{\mu g}, \tag{1.2}$$

with $\Re$, the gas constant, T the local temperature, μ the mean molecular mass and g the local gravitational force.

At the surface of the star there is a sharp decrease in density and temperature. When this happens H decreases and the ω_a becomes very high. At the stellar surface a wave travelling through the star with a wavelength λ will be considerably larger than H. For the wave to be a wave it must maintain the compression and rarefraction of the gas. However if $\lambda >> H$ then the wave smoothes out and no longer propagates and reflection back into the interior of the star occurs.

Whilst the wave travels into the stellar interior, the temperature of the gas that the wave travels through increases at greater depths. This in turn increases the speed at which the wave travels at and the wave is refracted. If the wave is launched at an angle that is not 90° to the surface, the direction of the wave bends away from the inward radial direction until the wave is refracted back towards the surface of the star. The depth at which the acoustic wave travels horizontally defines the lower turning surface. An example of the paths of propagation for acoustic waves are shown in Figure 1.1, where the dotted rings indicate the lower turning surfaces for the waves shown. A wave launched at 90° to the surface of the star (radially) will travel straight through the centre.

As shown by Figure 1.1 acoustic waves with small spatial scales (small separation between successive reflections) are shallow waves and are confined to layers close to the surface of the star. Those which have large spatial scales have much longer wavelengths and travel to greater depths. It is the waves with longer wavelengths that provide us with valuable information about the most central regions of the star where nuclear reactions take place.

Gravity (g-mode) oscillations, also known as buoyancy oscillations, are waves where gravity is the restoring force. Consider a small bubble of gas that has been

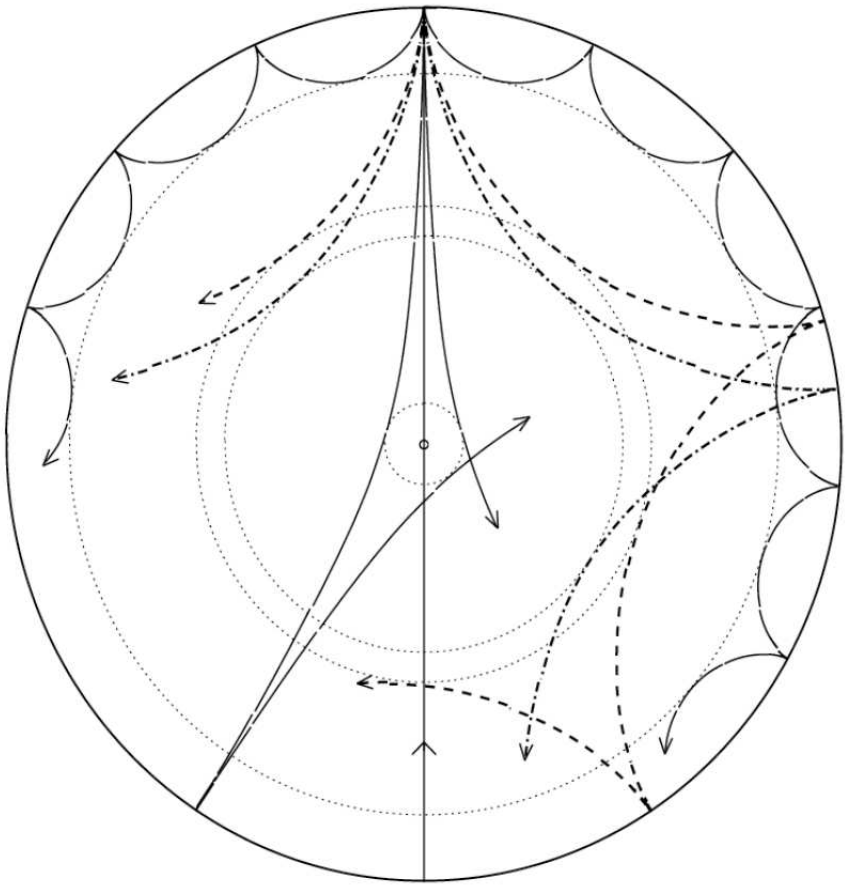

Figure 1.1: A diagram to show the paths of propagation for p-mode oscillations, penetrating to different depths within the stellar interior [Christensen-Dalsgaard, 2003].

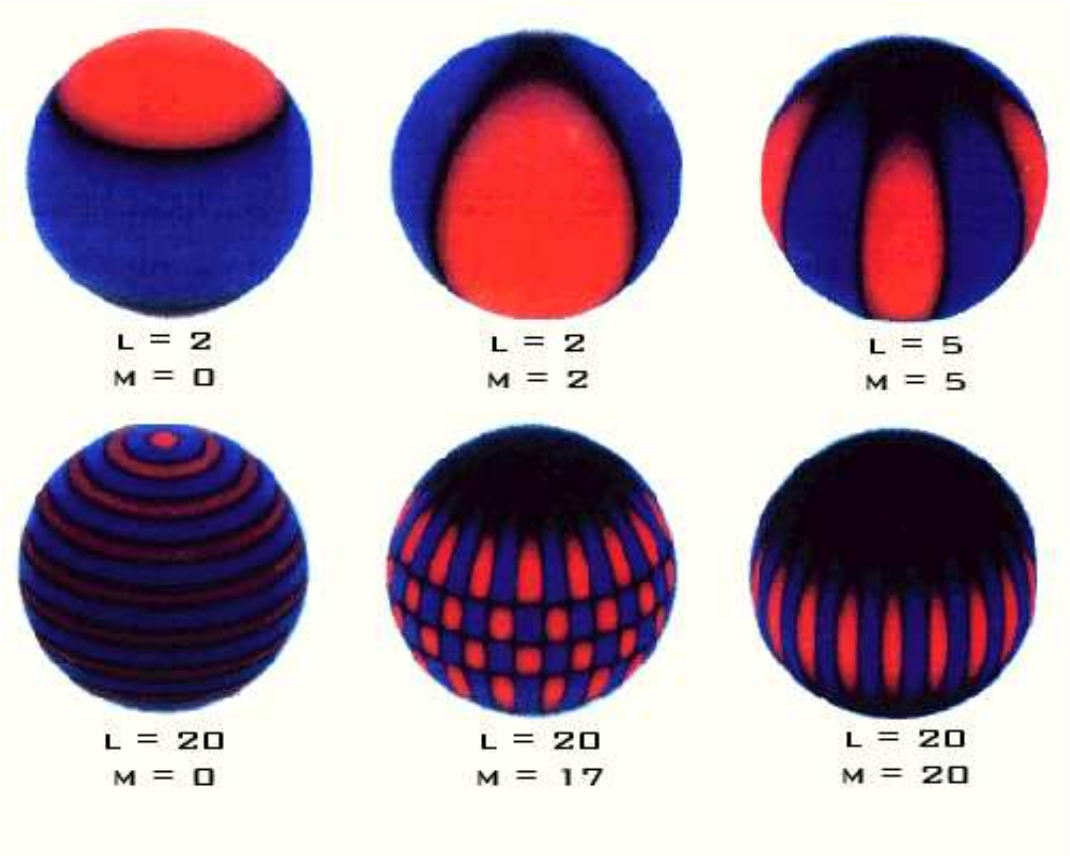

Figure 1.2: Example of surface displacements due to different modes of oscillation [Hale, 2012]. Spheres are orientated to show their north polar region.

vertically displaced so that the bubble is denser than its surroundings. This bubble will be pulled back to its original position by gravity, and the bubble begins to oscillate around its original position.

This occurs in regions where the main form of energy transportation is by radiation. In convective zones a displaced bubble of gas will continue to either rise or fall, so gravity waves do no propagate in these regions and become evanescent. Stars on the lower half of the main sequence have a central radiative zone, with a convective envelope, and so g-modes are trapped in the central region of the star and only have a very small amplitude on the stellar surface.

The modes of oscillations can be described via spherical harmonics, which are parameterised by the angular degree, l and azimuthal number, m. The angular degree, l, represents the total number of nodes across the surface of the star, while the azimuthal number, m, gives the number of nodes around the equator. The radial order,

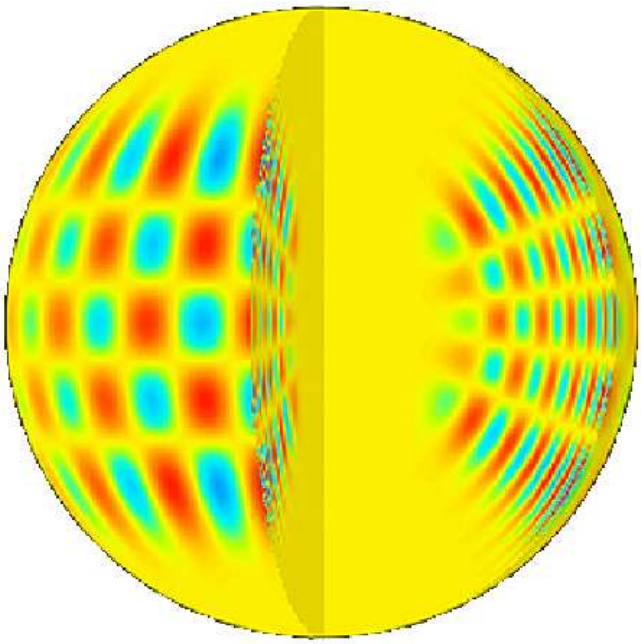

Figure 1.3: Cross-section of star showing the number of nodes in the radial direction, n [Baldwin, 2012].

n, represents the number of nodes seen in the radial direction.

The simplest modes are denoted by l=0, and are often referred to as radial modes as the wave travels straight through the centre of the star. Different values of l and m give rise to a variety of mode patterns that can be observed on the stellar surface. The lower l values are where the waves travel deepest into the interior, while the higher l values are constrained to shallower regions. A sample selection of l and m modes is presented in Figure 1.2, while a diagram showing the cross-section of a star to demonstrate radial nodes is presented in Figure 1.3.

The rotation of the star can affect the modes observed. For non-radial pulsations this means that prograde modes, travelling in the direction of rotation, will have slightly lower frequencies and retrograde modes, travelling against rotation, will have slightly higher frequencies. This results in modes being split into $2l + 1$ components with $m = -l, +l$ and is known as *rotational splitting*. The importance for this in asteroseismology is that if the l and m modes can be identified then the splittings can be used to measure the rotation rate of the star. If several splittings are observed, then it is possible to gather information about the variation in rotation in the interior of the star [Aerts

et al., 2010].

1.2 A little on asteroseismology

The discovery of the first pulsating star was made in 1596 by David Fabricius. While undertaking some planetary observations, Fabricius used the star o Ceti as a fixed point to determine the position of what he believed to be Mercury. During his observations he recorded that the brightness of o Ceti had increased from a magnitude of 3 to a magnitude of 2. Over the next few months the brightness of the star seemed to fade and disappear completely. Initially Fabricius concluded that the star was a nova (up until this point in time any recorded variability in a star was due to novae). However, Fabricius had to reject his original conclusion when he observed the star again in 1609 and determined that the brightness of the star was variable in nature [Hoffleit, 1997].

It was not until 1638 that Johann Holwarda determined the period of o Ceti to be 11 months. Further observations of the star confirmed the presence of a periodic variability, and the star was later called Mira, meaning *The Wonderful*.

This was the first piece of evidence that stars are variable, and not constant and unchanging as previously believed. Over the next few centuries several other variable stars were detected. However it was not until the use of photographic plates, where images of the sky could be easily compared, that the discovery of variable stars really accelerated.

With increasing numbers of variable stars being detected it was suggested that associations should be created whereby amateur astronomers could contribute to astronomical projects to aid professional astronomers in their work. In 1890 the BAA (British Astronomical Association) was founded and in 1911 the AAVSO (American Associations of Variable Star Observers).

One star that has been constantly studied is our Sun. The observations of sunspots have been recorded as far back as two to three thousand years, and an 11 year solar cycle has been well established. However the discovery that the Sun pulsates was only made

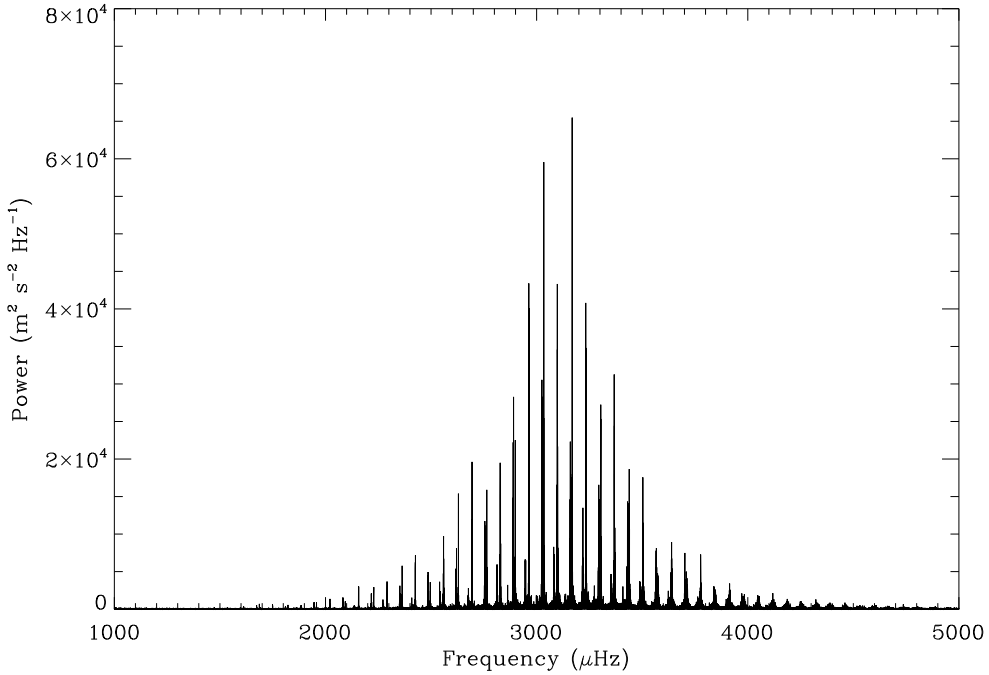

Figure 1.4: *BiSON* power spectrum constructed from 365 days worth of data. Courtesy of the *BiSON* team.

recently by Leighton et al. [1962], whereby a 5-minute periodic oscillation was detected. With an increasing number of ground-based observatories, 24-hour observations of the Sun were obtained.

One such network is *BiSON* (Birmingham Solar Oscillations Network), which has been in operation since 1975. It consists of six observatories located around the world for near continuous observations of the Sun. These observations are then used to generate power spectra to identify oscillations within the Sun, an example of which is shown in Figure 1.4.

Figure 1.4 shows a comb like structure of almost equally spaced frequencies observed in the Sun. These frequencies show the different modes, with overtone values of roughly 20 at the peak of the power spectrum. Figure 1.5 shows an expanded view of the power spectrum, where the spacings between the frequencies are shown more clearly. The large separation is the frequency difference between adjacent modes of the same angular degree. This is labelled as $\Delta\nu$ on Figure 1.5 and provides information about the mean density and the acoustic radius of the star.

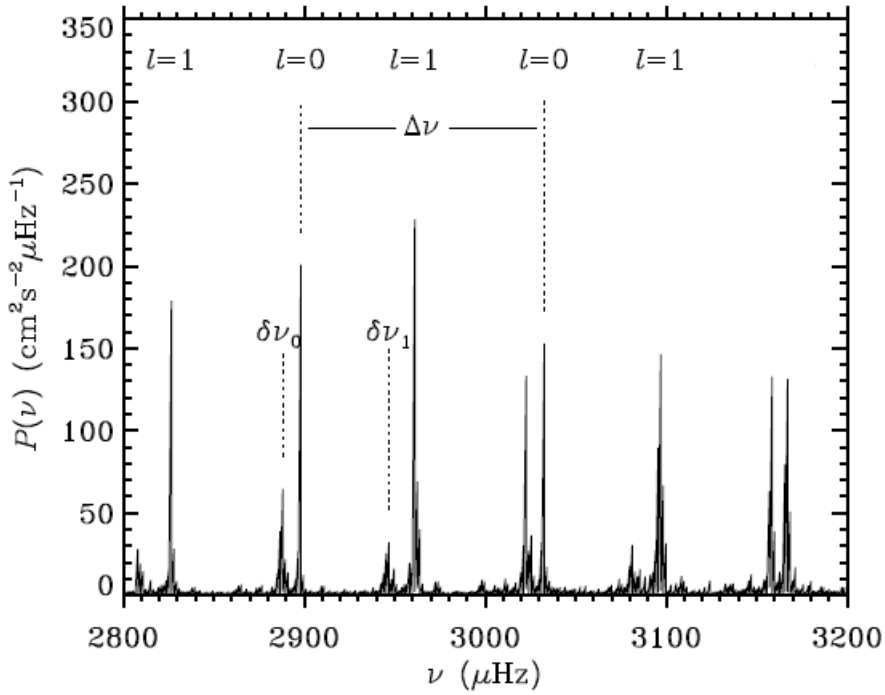

Figure 1.5: Expanded view of the *BiSON* power spectrum which clearly show the large separation labelled $\Delta\nu$ and small separations labelled $\delta\nu$ [Christensen-Dalsgaard, 1998].

On closer inspection the power spectrum also shows that there are frequencies that lie closer together. This is called the small separation, labelled $\delta\nu$ on Figure 1.5 and provides information about the sound-speed gradient in the central parts of the star. Although only $l = 0$ and $l = 1$ are labelled on Figure 1.5, modes $l = 2$ and $l = 3$ can also be clearly seen (to the left respectively of each $l = 0$ and $l = 1$ mode).

In solar-like stars the average values of the large and small separations can be used to place the star on a diagram (assuming the stellar composition is known from independent observations) to determine properties of the star (see below). If the S/N is high enough that the individual frequency values can be accurately determined then this provides more detailed information on the stellar properties and also in the internal structure.

Figure 1.6 shows a diagram of the small separation, $\delta\nu$, as a function of the large separation, $\Delta\nu$ [Christensen-Dalsgaard, 1993]. The solid near vertical lines marked on Figure 1.6 are lines of constant mass and indicate how the large separation varies with the mass of the star. These lines are predicted from stellar evolutionary models

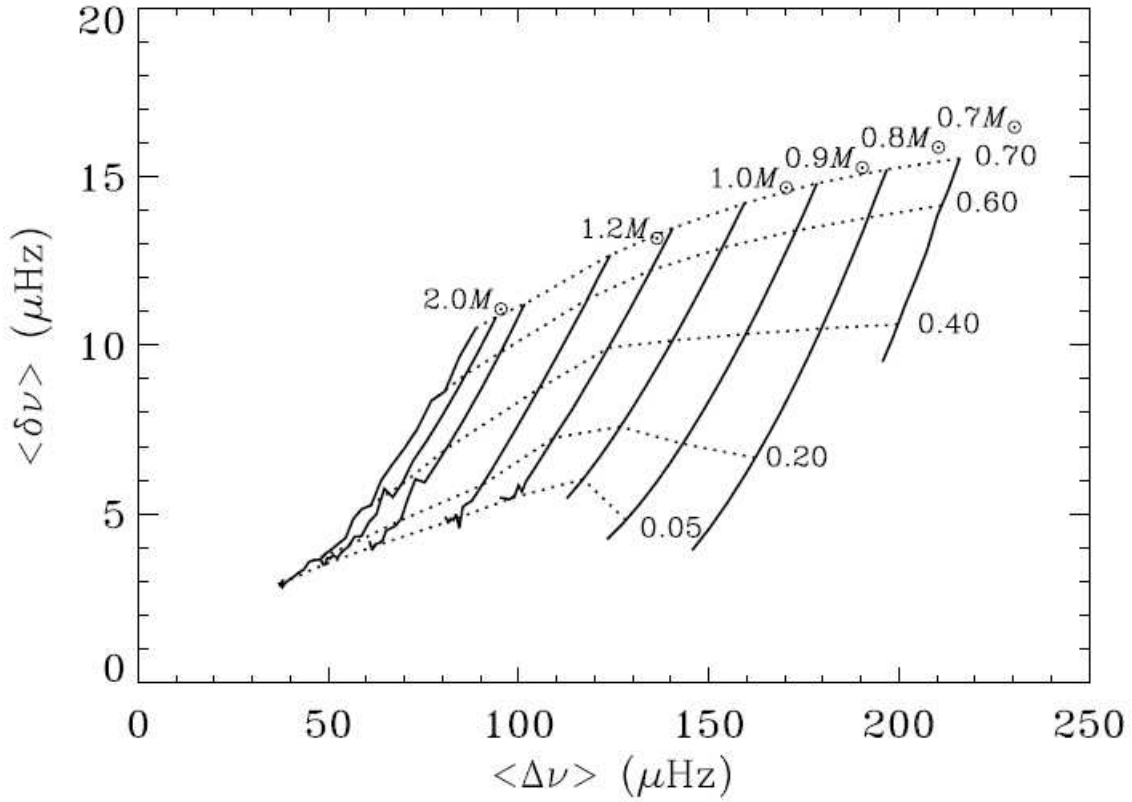

Figure 1.6: The near solid vertical lines represent constant mass, while the dotted near horizontal lines represent constant hydrogen fraction in the core at values specified [Christensen-Dalsgaard, 1993].

of known chemical composition. The small separation provides information about the sound speed gradient in the solar core, which can be modelled to determine the fractional content of hydrogen left in the solar interior. The hydrogen content in the core is a guide to the age of the star: the more hydrogen that has been burnt, the older the star will be. The dotted horizontal lines marked on Figure 1.6 are lines of constant fractional hydrogen content and show how this content varies when modelled against the small separation.

It is now thought that the majority of stars exhibit some sort of variability, even if only small. With higher precision ground- and space-based observations, using photometric and spectroscopic measurements, asteroseismologists are revealing more frequencies in stars covering the entire HR-diagram.

1.3 A little stellar evolution

The Hertzsprung-Russell diagram (HR diagram) is used to show the evolution of stars. It is a scatter plot of stars showing the relationship between their luminosity or absolute magnitude and effective temperature ($T_{\rm eff}$). Spectral class may also be defined on some HR diagrams. An example HR diagram is shown in Figure 1.7, which shows 22,000 stars from the Hipparcos catalogue, along with another 1,000 stars from the Gliese catalogue of nearby stars [Powell, 2012].

Stars vary greatly in their effective temperature and luminosity. The most striking feature of the HR diagram is the diagonal swathe of stars that goes from the top left-hand to the bottom right-hand corners. This swathe is where most of the stars lie and is called the *main sequence*. The stars in the top left-hand corner are massive stars (greater than $16M_{\odot}$) which have high luminosities and effective temperatures up to 50,000K. As one travels along the main sequence to the bottom right-hand corner, the stars become smaller and their luminosities and effective temperatures fall. The stars at the very bottom of the main sequence have masses below $0.5M_{\odot}$ and approximate effective temperatures of 3,700 K.

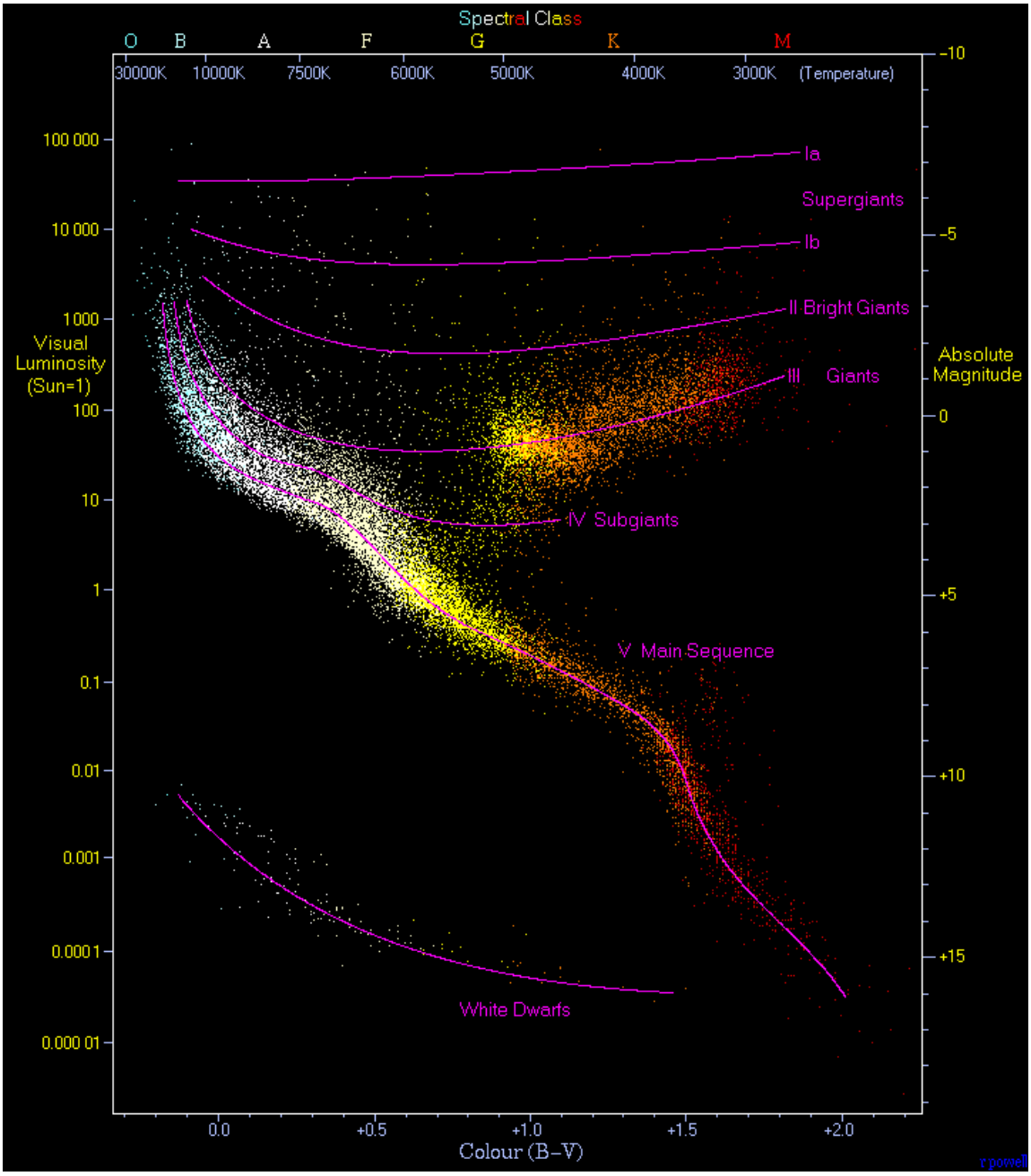

Figure 1.7: Hertzsprung-Russell diagram created using 22,000 stars from the Hipparcos Catalogue and 1,000 stars from the Gliese Catalogue of nearby stars [Powell, 2012].

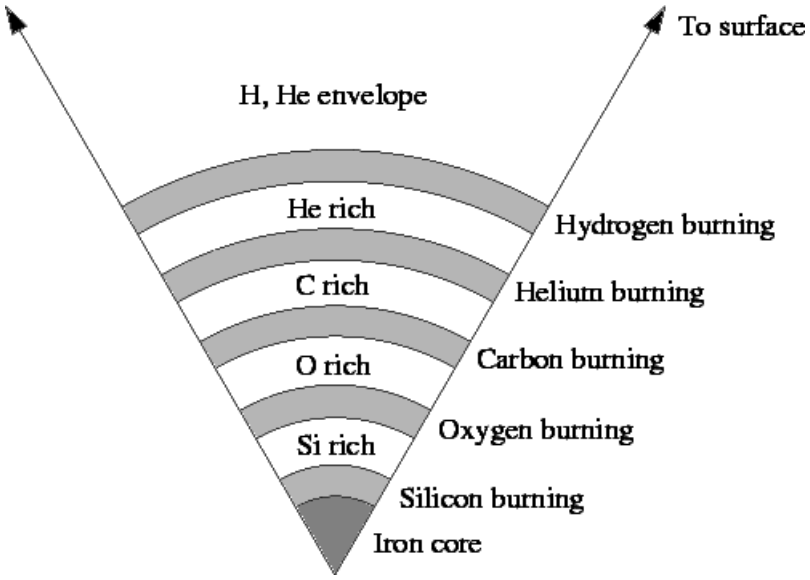

Figure 1.8: Onion-like structure of nuclear burning in larger stars [Mihos, 2012].

As mentioned above, Figure 1.7 is mainly composed of stars from the Hipparcos Catalogue. This catalogue only consists of stars brighter than 12.3 magnitudes and all stars are observed down to 7.3 magnitudes [Perryman, 1997]. Because of this observing constraint, this means that the catalogue is biased towards the brighter stars in the sky, which are often the largest stars. This has resulted in a greater number of stars shown on the upper main sequence in Figure 1.7 than there would have been if the sample were unbiased. It is estimated that approximately 90% of all stars lie on the main sequence and that most of these stars are similar to that of our Sun or smaller, therefore lying towards the bottom right-hand corner of the HR diagram.

The top right-hand corner of Figure 1.7 shows the positions of giant stars. These are stars that have evolved from the main sequence and now burn heavier elements. In massive stars the helium burning in the core is succeeded by carbon burning and an "onion" structure of nuclear burning is built up of the different burning elements with the heaviest element at the core (iron) to the lightest element (hydrogen) at the edge of the burning envelope. This onion-like structure is demonstrated in Figure 1.8.

In the bottom left-hand corner are compact objects, such as white dwarfs and neutron stars. As the name suggests these are small stars which have come to the end of their life.

It is now thought that most stars show some sort of variability. By collating observations on their variability it is possible to modify the HR diagram and group the stars by their oscillation characteristics, as shown in Figure 1.9 [Christensen-Dalsgaard, 2004]. The stars are grouped by the mechanism that drives their oscillations.

The main sequence in Figure 1.9 is still clearly shown, going diagonally from the top left-hand corner to the bottom right-hand corner. The ZAMS (zero-age main sequence) is represented by the dashed line, and is defined as the location of stars that have just started hydrogen burning. By following the ZAMS there are six types of classical pulsator that lie along the main sequence, from solar-like to β Cephei. The oval shapes represent their position on the HR diagram, whilst the hatching represents the excitation mechanism for the stars. Horizontal hatching represents stochastically excited oscillations, an example of which is our Sun which lies at the lower end of the main sequence in solar-like pulsators. Up-left hatching represents opacity driven p-modes, an example of which are β Cephei stars circled at the top of the main sequence. In contrast, SPB stars which lie just below β Cephei stars on the main sequence have oscillations which are opacity driven g-modes and are represented by up-right hatching. The opacity driving mechanism (known as the κ-mechanism) will be described in more detail in Section 1.5 of this chapter.

Figure 1.9 shows that it is not only main sequence stars that pulsate but stars throughout the HR diagram. The continuous lines show selected evolutionary tracks at 1, 2, 3, 4, 7, 12 and 20 $M_{\odot}$ respectively. By following these tracks it is shown that many evolved stars that lie off the main sequence pulsate. For example, Mira variables, the longest known periodic variables (mentioned in Section 1.2), are giant stars in the late stages of their stellar evolution, where their variability is characterised by large amplitudes (several magnitudes) and large periods (hundreds of days) [Lebzelter, 2011]. Also Cepheid variables are supergiant stars which pulsate due to the κ mechanism [Turner, 1998].

The continuous dotted line on Figure 1.9 represents the white dwarf cooling curve,

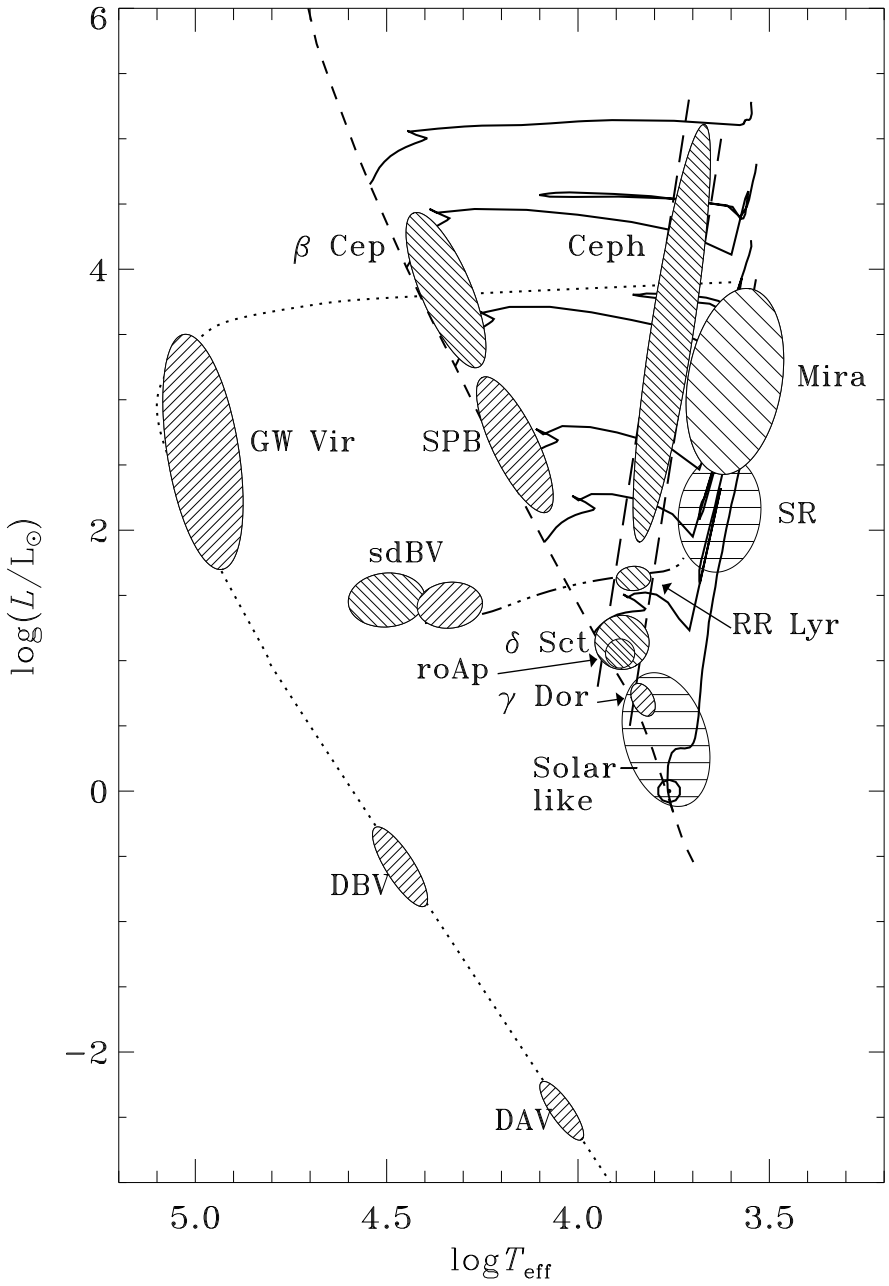

Figure 1.9: Locations of classically pulsating stars on the HR diagram. The dashed line represents the ZAMS (zero-age main sequence), whilst continuous lines represent evolutionary tracks at masses 1, 2, 3, 4, 7, 12 and 20 $M_\odot$ respectively. The dotted-dashed line represents the horizontal branch and the dotted line represents the white dwarf cooling curve. The different types of hatching represent the type of excitation mechanism for each group of stars: horizontal hatching for stochastically excited modes, up-right for opacity driven internal g-modes and up-left for opacity driven p-modes [Christensen-Dalsgaard, 2004].

Table 1.1: The Harvard Spectral classification system. Effective temperature (T_{eff}) obtained from Giridhar [2010] and *Mass* and *Radii* obtained from Habets and Heintze [1981].

Spectral Class	T_{eff} (K)	*Mass* ($M_\odot$)	*Radii* ($R_\odot$)
O	28,000 - 50,000	above 16	above 6.6
B	10,000 - 28,000	2.1 - 16	1.8 - 6.6
A	7,500 - 10,000	1.4 - 2.1	1.4 - 1.8
F	6,000 - 7,500	1.04 - 1.4	1.15 - 1.4
G	4,900 - 6,000	0.8 - 1.04	0.96 - 1.15
K	3,500 - 4,900	0.45 - 0.8	0.7 - 0.96
M	2,000 - 3,000	below 0.45	below 0.7
L	1,300 - 2,500		
T	below 1,400		

the final stages of stellar evolution. Even in the white dwarf region, groups of stars have been detected which continue to pulsate.

The stars of interest in this thesis are β Cephei type pulsators and Be type stars. These are both B-type stars that lie along the main sequence. B-type stars lie further along the main sequence than the Sun and also include Slowly Pulsating B stars (SPB). Dwarf (DBV) stars and subdwarf B (sdBV) stars are also included in the B-type spectral category, but do not lie on the main sequence.

Table 1.1 shows the Harvard Spectral Classification system, whereby stars are categorized by their spectral type. When using the table to compare between other spectral types B-type stars are amongst some of the largest and hottest stars in the sky, with effective temperatures between 10,000 and 28,000 K (our Sun lies at approximately 5,800 K), stellar radii of 1.8 to 6.6 $R_\odot$ and masses ranging from approximately 2 $M_\odot$ to 16 $M_\odot$.

The Sun has a radiative core and a convective outer zone. However the structure of large stars along the main sequence is different, with B-type stars having a convective core and a radiative outer zone.

The difference in size and location of convective and radiative zones in stars is shown in Figure 1.10. The x-axis shows the total stellar mass of a star on the main sequence. The y-axis shows the fractional mass of the star going from the centre to the

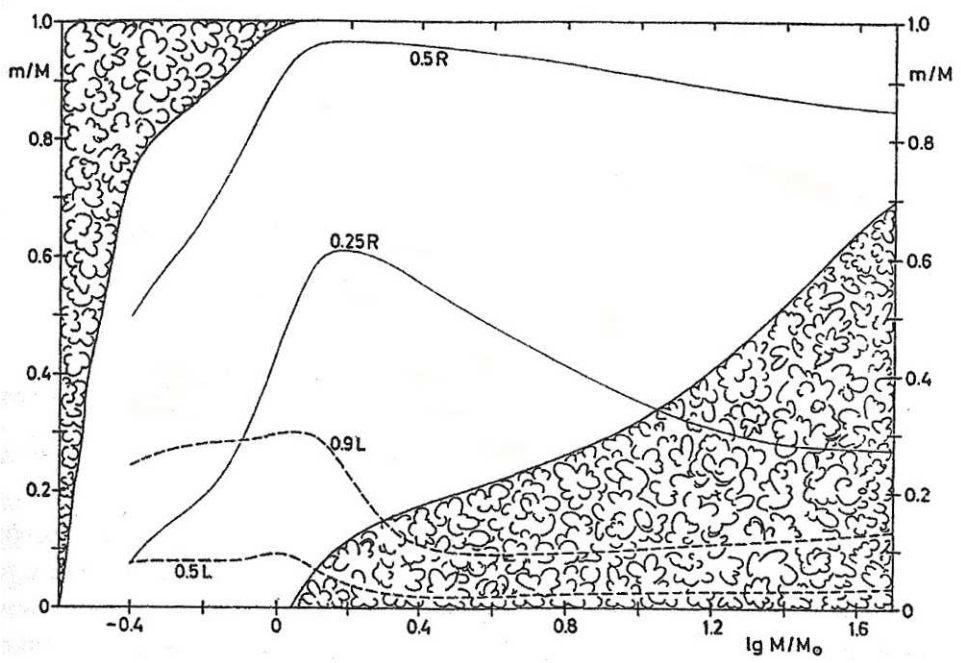

Figure 1.10: The mass values (m) from the centre of the star to the surface are plotted against the total stellar mass (M), for ZAMS (zero-age main sequence) models. The cloudy areas indicate the convection zones inside the stars, whilst blank areas represent radiative zones. The solid lines give the mass values of the star at 1/4 and 1/2 of the total radius (R) of the star. The dashed lines shown the mass values inside which 50 per cent and 90 per cent of the total luminosity (L) are produced [Kippenhahn and Weigert, 1990].

stellar surface. The cloudy areas of Figure 1.10 represent convective zones whilst blank areas represent radiative zones. Two solid lines are plotted on the chart, representing the mass values of the star where the radius of the star is 1/4 and 1/2 of the total radius (R). The dashed lines represent the mass values inside which 50 per cent and 90 per cent of the total luminosity (L) is produced [Kippenhahn and Weigert, 1990].

We know that B stars range from 2 $M_\odot$ up to 16 $M_\odot$, translating to a log $M/M_\odot$ of 0.3 and 1.2 respectively. By selecting these values on the x-axis in Figure 1.10, it is seen that these stars have a convective core, which increases in size with increasing stellar mass along the main sequence, and a radiative outer zone.

As shown in Figure 1.10 the change between a radiative core and convective outer zone to a convective core and radiative outer zone occurs gradually. The transition occurs around late A-type to early F-type stars (see Table 1.1), with stars just a little higher in mass than our Sun at approximately 1.4 $M_\odot$.

To determine why there is a change in the convection and radiative zones of a star we must first consider why these different methods of energy transfer take place.

Let us consider the criteria for convection. Consider a bubble of gas that has been displaced upwards. We will assume that the bubble moves fast enough that it does not exchange heat with the surrounding environment (the bubble acts adiabatically) and slow enough that the internal pressure of the bubble adjusts to remain in pressure equilibrium with its surroundings.

For this bubble to continue to rise and convection to occur the bubble of gas must remain lighter than its surroundings, whereby the density of the bubble remains smaller than the external density. Equation 1.3 shows the perfect gas law, where P is the pressure of the gas, ρ is the density of the gas, T is the temperature, μ is the mean molecular weight per particle and $\Re$ is the gas constant

$$P = \frac{\rho \Re T}{\mu}. \tag{1.3}$$

Equation 1.3 shows that if the convective bubble is to remain in pressure equilibrium

with its surroundings then the temperature of the bubble will need to be higher than its surroundings for the bubble to continue to rise. This requires that the temperature gradient of the surrounding gas, with respect to r (stellar radius), be steeper than that of the temperature gradient of the convective bubble. Therefore the condition for convective instability is given by

$$\left|\left(\frac{dT}{dr}\right)_{gas}\right| > \left|\left(\frac{dT}{dr}\right)_{ad}\right|. \tag{1.4}$$

It is more conventional in stellar physics to express this in terms of pressure, and so the following notations are introduced (a full derivation of which may be found in Christensen-Dalsgaard [1991]):

$$\nabla = \frac{dlnT}{dlnP}, \nabla_{ad} = \left(\frac{\partial lnT}{\partial lnP}\right)_{ad}. \tag{1.5}$$

Therefore the condition for convective instability can now be written as

$$\nabla > \nabla_{ad}. \tag{1.6}$$

The convective stability criteria (Equation 1.6) depends on the conditions in the surrounding gas, which relies on

$$\nabla \propto \frac{\kappa}{\mu}\frac{L(r)}{m(r)}\frac{\rho}{T^3}, \tag{1.7}$$

where κ is the opacity, $L(r)$ is the luminosity generated within a radius r and $m(r)$ is the mass of the star within a radius r.

For the case of the interiors of massive stars convection occurs because $L(r)/m(r)$ is large and therefore increases ∇ so that it is greater in magnitude than ∇_{ad}. The energy generation in massive stars increases as a function of temperature and so is strongly concentrated towards the centre of the star, hence the average rate of energy generation per unit mass within a given radius is large. This is why massive stars have convective cores.

Table 1.2: Overview of pulsating B-type stars: [1] Handler [2008], [2] Rivinius et al. [2003].

	Spectral type	Mass ($M_\odot$)	Oscillation period
β Cephei[1]	B0 - B3	8 - 18	2 - 8 (hours)
SPB[1]	B3 - B9	2 - 7	0.6 - 6 days
Be[2]	late O - early A	2 - 20	0.5 - 2 days

1.4 β Cephei, Be and SPB overview

There are two main pulsating B-type stars on the main sequence: β Cephei and SPB (Slowly Pulsating B-type)

β Cephei stars are the larger stars of the B-type pulsators and lie at the top of the main sequence for B-type stars (see Figure 1.9), with spectral types typically ranging from B0 to B3. Their masses lie in the region of 12 $M_\odot$ but can range between 8 $M_\odot$ and 18 $M_\odot$.

β Cephei stars oscillate with low order p and g modes with periods ranging between 2 and 8 hours, corresponding to frequencies in the range of 3 d^{-1} (cycles per day) to 12 d^{-1}, with the peak of the distribution of the periods occurring at 4 hours (6 d^{-1}).

SPB stars are the smallest of the B-type pulsators. As shown in Figure 1.9 they lie below β Cephei stars on the main sequence. Their spectral type is typically between B3 to B9 with masses ranging from 2 $M_\odot$ to 7 $M_\odot$ with photometric and radial velocity variations of the order of a few days [Handler, 2008]. This information is summarised in Table 1.2.

Be stars are B-type stars which show, or have previously shown, emission lines in the Balmer series (B for B-type stars, e for emission). The emission in the Balmer line series is due to the presence of a circumstellar disc. This will be explained in more detail in Chapter 4.

Although Be stars are mainly B-type stars, they do range from late O to early A. As a result Be stars show pulsations which have characteristics of both β Cephei and SPB type stars, depending on their position on the main sequence. Since the pulsation behaviour can be different in Be stars, they do not have a specific place on the asteroseismic HR-diagram. However, the presence of the circumstellar disc and the

nature of its formation is still unanswered and they are therefore interesting stars to study. Again this is explained in more detail in Chapter 4.

The pulsations that occur in B-type stars are driven by the κ-mechanism, which is explained in Section 1.5 below.

1.5 Excitation mechanism - The κ-mechanism

The mechanism that drives the pulsations in β Cephei and SPB stars is due to the opacity in ionisation zones and is called the κ-mechanism.

Usually the opacity of the star decreases when the star contracts, according to Kramer's law [Schönberg and Chandrasekhar, 1942].

$$\kappa = \kappa_o \rho T^{-3.5} \tag{1.8}$$

Here κ is the average opacity, κ_0 is a parameter which takes into account the abundances within the star (X, Y and Z), ρ is the stellar density and T is the stellar temperature.

In the ionisation zones of stars the opacity of the layer increases as the star contracts. When the star is compressed the temperature should increase, but in the case of the κ-mechanism some of the energy is used to ionise the material. As a result the opacity of the layer increases and photons are prevented from being lost from the star so readily and the pressure begins to increase beneath the layer. Finally over pressure causes the layer to expand, overshooting its equilibrium position. When the star is fully expanded, the ions release energy when they recombine with electrons. As a result the opacity is reduced allowing the trapped photons to escape. The pressure beneath the layer therefore drops and the radius of the star falls inwards, undershooting its equilibrium position. The cycle then repeats and results in an overstable oscillation. This process is known as the κ-mechanism.

In β Cephei and SPB stars the κ-mechanism acts on the iron ionisation zone where

the temperature is approximately 2×10^5 K [Dziembowski and Pamiatnykh, 1993]. This can cause the opacity at this depth to increase by a factor of 3 [Pamyatnykh, 1999]. Originally, stellar models were unable to explain unstable modes with periods that were found in β Cephei and SPB stars. This was due to the fact that the calculations for the opacities using OPAL [Rogers and Iglesias, 1992] and OP (Opacity Project) computations [Seaton et al., 1992] were the first to include the transitions in heavy-element ions. Revised models which include these transitions found a better agreement with the observed oscillations of variable B-type stars, although they do not account for all frequencies observed.

In order for an excitation to occur within the star there are two requirements that must be made, the first regarding the shape of the pressure eigenfunction and the second requirement regarding the ratio of the oscillation period, P, to the thermal time-scale in the ionisation layer, τ_{th}.

The first condition requires that the pressure eigenfunction ($\delta p/p$) is large and varies slowly with the stellar radius, r, within the driving zone, where δ is the Lagrangian perturbation.

The second condition requires that the ratio between the oscillation period and the locally defined thermal time-scale, τ_{th}/P, must not be much less than unity. τ_{th} must be either comparable or longer than the oscillation period, P, otherwise, the potential driving layer remains in thermal equilibrium during the pulsation cycle. The equation for the local thermal time-scale is defined by

$$\tau_{th} = \int_{r_1}^{r_2} \frac{c_p T}{L} dm \tag{1.9}$$

where c_p is the specific heat capacity of the gas at constant pressure, T is the local mean temperature, L is the local mean luminosity and r_1 and r_2 represent the boundaries between which the local thermal time-scale is being considered.

In β Cephei star models the iron opacity bump is located in a relatively shallow layer where the thermal time-scale, τ_{th}, is well below 1 d.

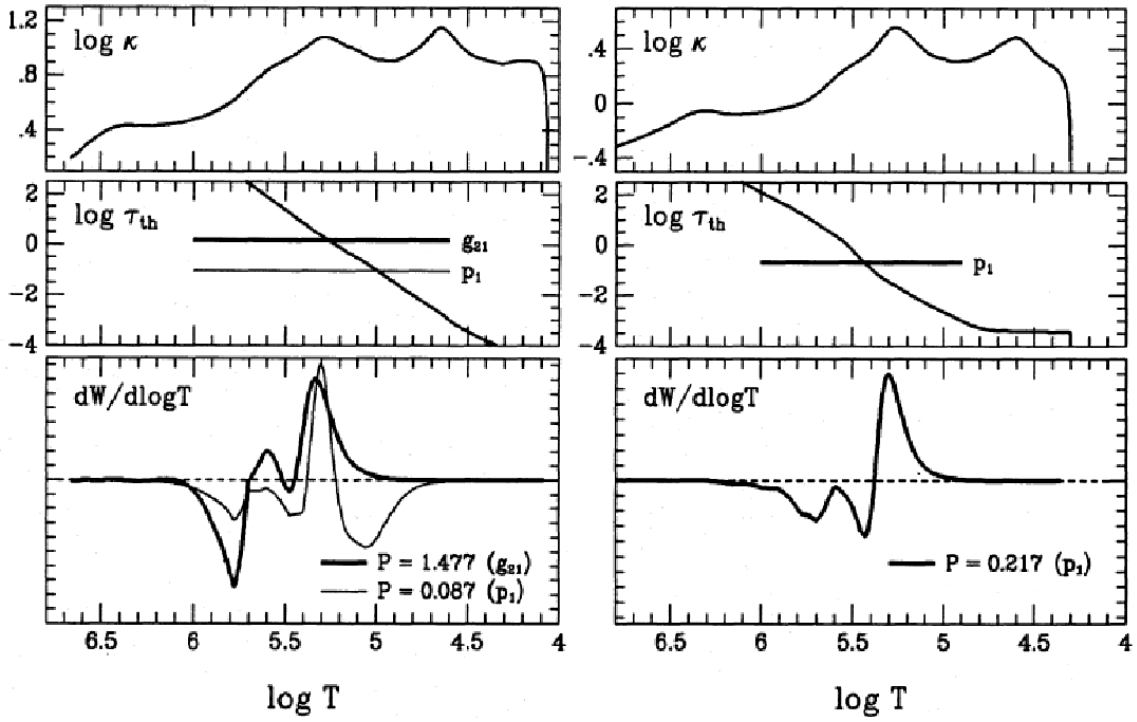

Figure 1.11: Opacity κ, thermal timescale τ_{th} and differential work integral for selected pulsation modes plotted against temperature. Left hand-side shows an SPB star model of $4M_{\odot}$, $\log(L/L_{\odot})$=2.51 and $\log T_{\rm eff}$=4.142. Right hand side shows a β Cephei star model of $12M_{\odot}$, $\log(L/L_{\odot})$=4.27 and $\log T_{\rm eff}$=4.378. Both models have compositions X=0.7 and Z=0.02. Taken from Dziembowski et al. [1993].

In less massive stellar models the iron opacity bump is located deeper in the star. Since SPB stars are cooler than β Cephei stars (see Table 1.2 for comparison) their iron opacity bump is located in deeper layers where the temperature is high enough for the ionisation of iron to occur. As a result low frequency modes can be driven.

Figure 1.11 is taken from Dziembowski et al. [1993] and shows the similarities and differences in the κ-mechanism between SPB and β Cephei stars. The left-hand side shows a model for an SPB star with a stellar mass of 4 $M_{\odot}$, $\log T_{\rm eff}$ of 4.142 and $\log(L/L_{\odot})$ of 2.51. The right-hand side shows the model for a β Cephei star with a stellar mass of 12 $M_{\odot}$, $\log T_{\rm eff}$ of 4.378 and $\log(L/L_{\odot})$ of 4.27.

The top panel of Figure 1.11 shows how the opacity, κ, changes as a function of temperature, T. In both panels there are two peaks in opacity which occur at the same temperatures. The first peak is associated with the iron ionisation bump which occurs at 200 000 K ($\log T = 5.3$), the second occurs at the He_{II} ionisation bump which occurs

at 40 000 K ($\log T = 4.6$).

The middle panel shows how the thermal timescale changes as a function of temperature. By comparison of the SPB model to the β Cephei model it can be shown that τ_{th} at the iron ionisation zone is larger in the SPB model than it is in the β Cephei model. This demonstrates that excited oscillations tend to have longer periods in SPB stars than β Cephei stars.

The lower panel shows the work integral for the p- and g-modes in the model of the SPB and β Cephei star. The SPB model shows that p-mode oscillations are not excited. The layer between the iron ionisation zone and He_{II} ionisation zone acts as a damping layer for short period oscillations. This gives a large negative contribution to the work integral causing short period modes to stabilize.

Further detail on the κ-mechanism inside B-type stars can be found in Dziembowski and Pamiatnykh [1993] and Dziembowski et al. [1993].

The theoretical pulsations in β Cephei stars have not always agreed with what is observed. A known example of this is the β Cephei star 12 Lacertae where low order p-modes were present with higher frequencies than predicted by models, along with the presence of g-mode oscillations. These observations have made researchers rethink the input parameters that go into the models, for example, altering the percentages of iron that need to be included in the stellar composition [Miglio et al., 2007b].

Figure 1.12 shows the theoretical location of β Cephei and SPB stars on the HR diagram with different metallicities using OPAL and OP computations. From Figure 1.12 it is clearly shown that a decrease in metallicity (Z) reduces the number of stars which theoretically pulsate. This is due to the κ mechanism being dependent on the abundance of iron in the star. An increase in the metallicity increases the number of stars that pulsate by shifting their position along the main sequence, with β Cephei stars pulsating at lower temperatures and luminosities, and SPB stars pulsating at higher temperatures and luminosities. It is shown on the left-hand side of Figure 1.12 that at Z=0.02 the SPB and β Cephei stars overlap on the HR diagram. As a

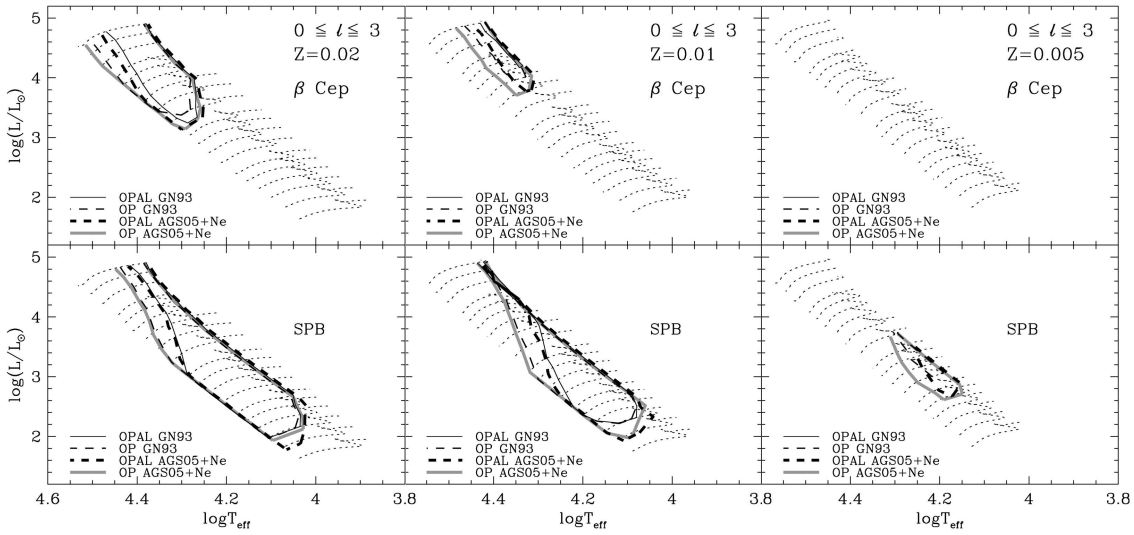

Figure 1.12: β Cephei and SPB pulsation instability strips on the HR diagram for Z=0.02, Z=0.01 and Z=0.005. The dotted lines represent stellar evolutionary tracks. Taken from [Miglio et al., 2007b]

consequence the number of stars which are expected to show both SPB and β Cephei like pulsations increases. Further details on this work can be found in Miglio et al. [2007b] and references therein.

However not all B-type stars are expected to pulsate. This is because the pulsation mechanism depends highly on the abundance of iron, and so whether or not they pulsate will depend on the metallicity of the stellar environment the star was formed in. For example Diago et al. [2010] comment that the number of β Cephei and SPB stars expected in the Magellanic Clouds and Small Magellanic Cloud should be low due to the low metallicity.

1.6 Observations

The study of pulsations in stars can be accomplished by either photometric or spectroscopic observations.

The first photometric data to show stellar variability were made very early on, as explained in Section 1.2. However, these magnitude changes were on very large scales. It is only in the last 50 years, where high quality photometric observations could be

obtained, that some of the most interesting observations have been made.

Photometric data on stars were initially collected using ground-based instrumentation. However ground-based instruments have several disadvantages, for example, they suffer with not only having to observe at night but also bad weather can hinder an observing session. This means that observing periods with a single telescope are not usually more than approximately 10 hours in length, and gaps between observing periods can be up to 12 hours or more. To overcome this problem, multi site campaigns were set up to make more continuous photometric observations of variable stars and are explained in more detail below.

Data from ground-based telescopes also suffer from atmospheric scintillation, caused by small fluctuations in the air density which increases the overall level in noise. This means that oscillations of low amplitude are unlikely to be seen in stars that are observed from the ground. Results from Appourchaux et al. [1995] proved that it was possible to detect solar oscillations from the ground, using photometric data from the *LOI* prototype. However, in general it is difficult to detect solar-like oscillations using ground-based photometric data.

In 1986 a network of collaborating astronomical observatories was set up to obtain nearly uninterrupted light curves of variable stars in order to resolve multi-periodic oscillations. This network is now known as *WET* (the Whole Earth Telescope) and is run as a single astronomical instrument [Nather et al., 1990]. *WET* currently consists of 25 observatories across the globe and has obtained one of the highest precision ground-based photometric studies [Kurtz et al., 2005] of the star HR 1217.

Other well known multi site campaigns include The Delta Scuti Network [Zima, 1997] and *STEPHI* [Michel et al., 1992], both of which are focused on detecting oscillations in δ Scuti stars, but do study other variable stars as well such as γ Doradus stars. Examples of photometric data from other multi-site campaigns for β Cephei stars can be found in Handler et al. [2006].

Although there may be large gaps in photometric data provided by space-based

telescopes, a continuous set of data on a star can be collected over several years.

The first space-based instrument to gather photometric data on oscillating stars was *WIRE*, using the on board star tracker. This was followed by instruments such as *MOST*, *SMEI*, *Kepler* and *CoRoT*. In this thesis, space-based observations obtained from the *SMEI*, *WIRE* and *MOST* instruments are used to study the oscillations in B-type stars. These instruments are discussed in more detail in Chapter 2.

Launched on 27^{th} December 2006, *CoRoT* was the first mission capable of detecting rocky extrasolar planets, several times the size of the Earth. *Kepler* was then launched on the 6^{th} March 2009 and has confirmed the presence of 61 planets using the transit method, with a further 2,000 planetary candidates. The high quality photometric data collected from both of these instruments have also been used to perform asteroseismology to which significant results have been obtained in the understanding of stellar structure and evolution (De Ridder et al. [2009]; Bedding et al. [2011]; Chaplin et al. [2010]; Chaplin et al. [2011]; Gilliland et al. [2010]). Due to the success of the *Kepler* mission, NASA have agreed to extend the mission and continue to fund the program until 2016 [Atkinson, 2012].

PLATO is the next generation planet finder from *ESA*. It will be designed to perform high precision photometry on hundreds of thousands of stars to detect planetary transits and also perform asteroseismology [Rauer and Catala, 2011]. The targets of the mission are similar to that of *Kepler*, however *PLATO* will observe a larger number of stars over the mission. However, *PLATO* is currently competing with other missions for funding and so the mission has yet to be approved.

Oscillations can also be detected by analysing ground-based radial velocity measurements. These measurements are made using spectroscopy, whereby the Doppler shift of spectral lines are detected. The use of spectroscopic observations is the main way that solar-like oscillations are detected from the ground. Since spectroscopy is completed on the ground there are several multi-site campaigns to enable 24 hours observations. For example the MUlti-SIte COntinuous Spectroscopy *(MUSICOS)* which

undertook major multi site campaigns in spectroscopy in 1989, 1992, 1994, 1996, 1998 and 2001 [Foing et al., 1999].

Future spectroscopic multi site campaigns are currently under development, an example of which is the Stellar Observations Network Group *(SONG)*. This will consist of up to 8 observing sites, observing oscillations in solar like stars [Grundahl et al., 2008]. *SONG* will also be focused on detecting extrasolar planets in the habitable zone around solar-like stars using the microlensing technique, with the aid of photometric data.

1.7 Thesis synopsis

This thesis is focused on analysing photometric data on main sequence B-type stars collected using the Solar Mass Ejection Imager *(SMEI)*. The analysis is aimed at not only detecting stellar oscillations but, due to the long times series provided by *SMEI*, amplitude variations in the oscillations can be detected over the observational period.

Details of the instruments from which data have been used in this thesis are given in Chapter 2. The chapter begins with an introduction to the space borne Solar Mass Ejection Imager and the pipeline developed to extract photometric data. The chapter then goes on to explain the characteristics of the light curves obtained and any pre-analysis required on the light curves before analysis can begin on stellar oscillations.

Although the Solar Mass Ejection Imager was the main source of photometric data for this thesis, data from the satellite instruments *MOST* and *WIRE* were used in the analysis of one particular star, ζ Oph, to provide complimentary results. These instruments are summarised at the end of Chapter 2.

The results on all β Cephei stars analysed in this thesis are presented in Chapter 3. The chapter begins with an introduction to β Cephei stars and their known characteristics. The second part of the chapter then presents the results on the oscillations of 27 confirmed β Cephei stars observed with the Solar Mass Ejection Imager. The final section of Chapter 3 presents the results on the survey to search for new β Cephei stars

observed with the Solar Mass Ejection Imager. The survey includes an analysis of the stellar characteristics of the stars in the survey as well as the results on individual stars which may be β Cephei like.

The results on all Be stars analysed in this thesis are presented in Chapter 4. An introduction to Be stars and their characteristics are given in the first section. The second part of this chapter presents the results on the Be star Achernar, while the final section presents the results on ζ Oph. The analysis on both of these stars have not only included the identification of oscillations within the stars, but also how the amplitudes of these oscillations vary with time and the significance of these variations.

Finally an overview of the thesis is presented in a conclusion in Chapter 5. Here the advantages of using the Solar Mass Ejection Imager as an instrument to collect photometric data on stars are given and prospects for future work involving amplitude and phase variations in oscillations are discussed.

Chapter 2

Instrumentation

The asteroseismic results reported in this thesis were obtained from photometric data provided by the Solar Mass Ejection Imager *(SMEI)*.

An introduction to the *SMEI* instrument and the data analysis pipeline used to generate light curves is presented in Sections 2.1.1 and 2.1.2. Section 2.1.3 describes the characteristics of the *SMEI* data and outlines the data analysis required to generate amplitude spectra.

In the case of the Oe star, ζ Oph, further photometric data were obtained from the *MOST* and *WIRE* instruments. These instruments are described in Sections 2.2 and 2.3 respectively.

2.1 The Solar Mass Ejection Imager - *SMEI*

2.1.1 Introduction

The Solar Mass Ejection Imager *(SMEI)* was built by the University of Birmingham, UK, and the University of California, San Diego. Launched on 6^{th} January 2003 on board the *Coriolis* satellite, *SMEI* was designed to primarily study coronal mass ejections (CMEs) moving towards the Earth.

CMEs are large ejections of material from the solar corona consisting of high-energy

particles. The high-energy particles can interact with the Earth's atmosphere and result in some of the more spectacular light display in the sky known as the Aurora Borealis and Aurora Australis. These high-energy particles can also be more disruptive, for example, high-energy particles caused surges in transmission lines in Quebec in 1989, causing the circuit breakers on the power grid to trip and leaving millions of people without power. In space, these charged particles can cause damage to satellites and an increase in radiation also means that they are also hazardous to astronauts. Given the disruption and danger posed by CMEs it is useful to know when such events are likely to take place. *SMEI* was designed to detect and forecast CMEs moving towards the Earth. During the quiet phase of the Sun's 11 year solar cycle, *SMEI* will detect CMEs at a rate of one every three days.

Although *SMEI* was primarily designed to study CMEs, due to its position above the atmosphere, a by-product of its observations are the light curves of some of the brightest stars in sky. *SMEI* has collected data on these stars since its launch in 2003. An archive of over 12,000 stellar light curves has been processed for the first 3 years of data, with more data readily available for processing for time periods of nearly 6 years.

With a regular cadence and a large number of bright stars observed, these light curves have been previously used to study stellar oscillations, for example: Arcturus [Tarrant et al., 2007], Shedir [George et al., 2009], Polaris [Spreckley and Stevens, 2008], β Ursae Minoris [Tarrant et al., 2008a], γ Doradus [Tarrant et al., 2008b] in addition to Novae [Hounsell et al., 2010] and Cepheid variables [Berdnikov and Stevens, 2010]. In this thesis *SMEI* will be used to study stellar oscillations of B-type stars, in particular β Cephei and Be stars.

2.1.2 The *SMEI* Instrument

SMEI is in a Sun-synchronous polar orbit 840km above the Earth's surface. It consists of three cameras, each with a field of view of $60^\circ \times 3^\circ$, which are sensitive over the optical waveband. Figure 2.1 shows where the cameras are positioned on the instru-

Figure 2.1: An illustration of the *SMEI* instrument onboard the Coriolis satellite. The three *SMEI* cameras point away from the Earth and from left to right are Camera 3, Camera 2 and Camera 1, respectively [Webb et al., 2006].

ment. The three cameras point away from the Earth and are mounted such that the combined field of view approximates a fan shape covering an area of approximately $170^\circ \times 3^\circ$. Figure 2.2 shows an example frame of the field of view from one of the cameras. This image is a negative, so stars appear black and the background is light.

SMEI can scan most of the sky every 101 minutes. Figure 2.3 shows an all-sky image produced from one orbit of the *SMEI* data. The notional Nyquist frequency for the *SMEI* data is therefore 7.08 d^{-1} (cycles per day), although in some stars it is possible to find evidence of frequencies higher than this. Figure 2.3 shows that there are two patches of sky that the cameras do not cover. The first and largest region covers a circular area approximately 20° in diameter directly towards the Sun. This is shown in the centre of the all-sky image in Figure 2.3. This region was purposefully excluded from the image as direct light from the Sun will saturate the cameras. The

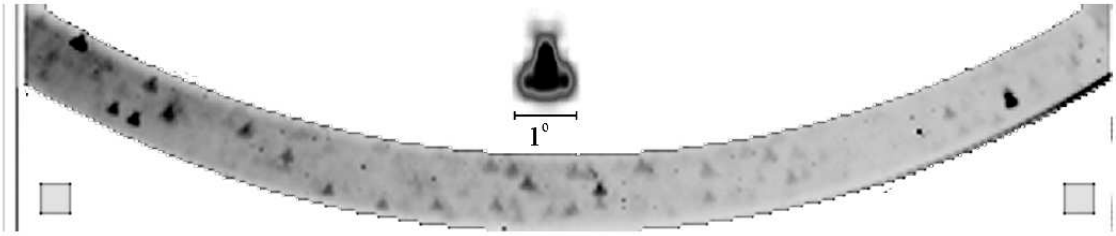

Figure 2.2: A single frame taken from one of the *SMEI* cameras. The image presented here is a photographic negative, so the stars appear as dark points and the background is light. Above the frame is an illustration of the 'nose-shaped' PSF [Tarrant, 2010].

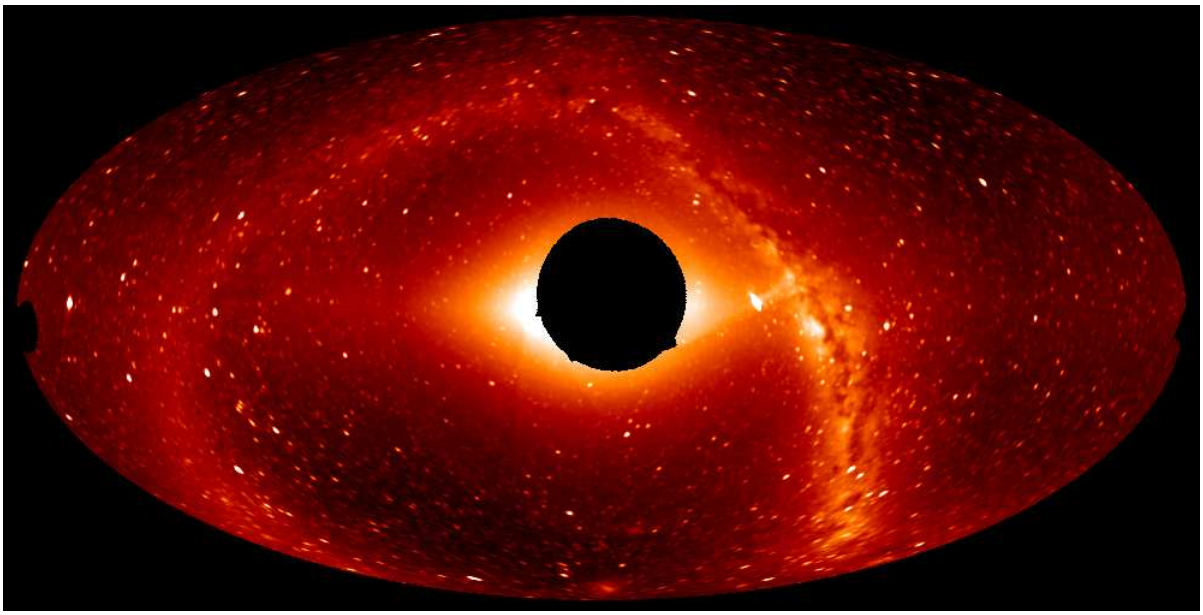

Figure 2.3: An all-sky image produced from 1 orbit of the *SMEI* instrument. The blank sections are regions of missing data, the main region occurs directly towards the Sun and a small region is also unobserved in the anti-solar direction (far left of image). The Galactic Plane and solar corona are also clearly visible in the image [Webb et al., 2006].

second is a smaller region in the anti-solar direction, seen on the far left of Figure 2.3.

Of the three cameras positioned on the *SMEI* instrument, only Camera 1 and Camera 2 are used in the analysis of stellar variability. Camera 3 is not used in the analysis due to a problem with the cooling mechanism. The CCDs in Camera 1 and Camera 2 are cooled to less than -30°C, whilst the CCD in Camera 3 tends to operate at around -5°C. This has led to problems with a large number of hot pixels appearing in the images, therefore it was decided that the data obtained from Camera 3 would not be used for generating stellar light curves.

A data reduction pipeline was used to generate the light curves analysed in this thesis. The data analysis pipeline was developed by Dr. S. A. Spreckley as part of his PhD, the details of which can be found in Spreckley [2008]. The pipeline is able to check if data are available for a star based on its HD and HIP number. The pipeline then prepares the *SMEI* data and outputs the data to a file which gives the time (in JD) and flux of the star over the available time period. The method used to complete this process is outlined below:

1. Checks were performed on the frames from the *SMEI* instrument to determine any bad frames that need to be rejected. A bad frame is one in which no data were collected. This circumstance usually occurs when the image was taken but the camera shutter was closed, or when the internal LED (which is used to check the flat-field of the CCD) was turned off.

2. Poor-quality frames were also removed from the remaining frames. Poor-quality frames are usually a result of the CCD temperature being too high and therefore a large number of hot pixels appear on these frames. The ideal temperature range for CCD operation is -60^{o}C to -24^{o}C, which was determined from the typical temperature variations seen during the first year of operation.

3. The pipeline then determines which stars will be in each frame, or if searching for a particular star which frames that star will be in, a process known as

position tagging ie *astrometry*. The frames generated by *SMEI* are unusual in terms of the shape of their field of view. An example of the *SMEI* field of view was shown in Figure 2.2 where it can be seen that the frames have an arc-like shape. Along with the continuous scanning of the sky by the instrument, this makes the process of position tagging quite complicated, as no two frames will have the same astrometric solution. The identification of the star is therefore established by determining the right ascension and declination of the *SMEI* instrument and rotation of the cameras at the time of exposure.

4. Each image is then prepared before photometry can take place. The dark current within the CCD is a source of noise and must be removed. This is completed by taking a number of exposures where no light is incident on the CCD to create a master dark current map. The removal of cosmic-rays from each frame is also a standard part of the preparation procedure. This is accomplished by comparing multiple images of the same area of sky to detect spuriously high values. It was discovered after launch that the baffle and optics design put in place to reduce stray-light did not reach the standard required in some situations. Therefore maps showing the distribution of stray-light were created so that the stray-light or glare in anyone frame could be accounted for. Finally, a flat-field image is applied to remove any artifacts from an imperfectly smooth mirror.

5. Photometry of the data can then be accomplished using aperture photometry, whereby the counts within an aperture placed on a region of the CCD image are summed.

6. Finally the light curves produced by the data analysis pipeline described above contain instrumental effects which need to be accounted for. These effects are removed before producing the final light curve. The post-processing corrections account for long term degradation of the CCDs (high levels of radiation when the instrument regularly pass through the SAA and general build up of dust cause

the efficiency of CCDs to decrease). This is corrected by estimating the rate at which the sensitivity of the CCDs was falling, which was estimated to be 1.5% per year. Secondly, although the shape of the PSF is always fairly 'nose-like' (see Figure 2.2), its orientation and size differ depending on where the star is situated in the field of view. Corrections for the size and orientation of the PSF were modelled and applied to the post-processing corrections.

The cadence of the *SMEI* instrument is 101 minutes, and therefore has a notional Nyquist frequency of 7.08 d^{-1} which is suited to studying transiting planets, eclipsing binaries and stellar oscillations. However, each datum point is made up from several short exposures, each 4 seconds in length, which means that it is possible to observe oscillations with a frequency higher than 7.08 d^{-1}.

As *SMEI* was not initially designed to study stellar oscillations in stars, it is only capable of detecting photometric variations in the brightest stars in the sky, stars brighter than magnitude 6.5. The size of the pixels on the cameras are large and means that *SMEI* suffers from *stellar blending* (light from different stars collected on the same pixel), especially stars near the Galactic Plane where the density of stars is the highest. As a result only stars that are further than 10° from the Galactic Plane are observed, unless they are very bright stars (brighter than magnitude 3), so that the light from these stars would dominate the light curve.

During April 2006 the *SMEI* instrument failed for over one month. This left a notable gap in the light curves of all the stars observed at this time. This gap is shown in Figure 2.5 between 700 and 800 days.

In 2008 it was decided that new *SMEI* data would no longer be archived at the University of Birmingham. Therefore the longest light curves available are approximately 5 years and 9 months (≈2000 days).

Further details and technical specifications regarding the *SMEI* instrument may be found in Eyles et al. [2003].

2.1.3 Data Analysis

Figure 2.4 shows an example of a *SMEI* light curve produced by the data analysis pipeline. This specific example is of the Oe star ζ Oph. As stated above in Chapter 2.1.2 only Camera 1 and Camera 2 were used in the analysis. Red points show data collected by Camera 1 and blue points by Camera 2. There are pronounced u-shapes in the light curve which are an effect of the *SMEI* instrument and not intrinsic to the star. These u-shapes can be removed from the light curve by calculating a smooth trend along the light curve using a boxcar length of 10 days. The smooth fit can then be subtracted leaving a flatter light curve to analyse. Various values of the boxcar length were tried and tested and it was found that the choice of smoothing did not significantly affect the amplitudes or frequencies being analysed. The frequencies analysed in this thesis typically range from 0.5 to 7.08 d^{-1}, with amplitudes varying between 0.001 and 0.05 mag. The error on the smoothing was also not significant enough to be included in the error analysis.

The data were then converted from flux into magnitudes for analysis. An example of a converted light curve is shown in Figure 2.5. The data collected by Camera 1 are shown by the red points and Camera 2 are shown by the blue points.

A typical duty cycle (number of data collected from the instrument against the total number of data that could have been collected in that time) for an entire *SMEI* light curve is approximately 40%. From Figure 2.5, this low duty cycle is mainly due to gaps from the absence of Camera 3 and gaps where the *SMEI* instrument was not recording because the star was inaccessible to other cameras. A duty cycle lower than this is often due to the light curve containing bad sections of data due to high levels of scatter, and therefore these sections were removed in the data reduction pipeline described earlier in Section 2.1.2. However, there are some stars that have a duty cycle considerably higher, up to 70%. This is mainly due to their large declination angle in the sky. These stars are near polar and are viewed exclusively with Camera 2. Figure 2.6 zooms in on a sample section of a light curve obtained by *SMEI*. This particular example is 30 days

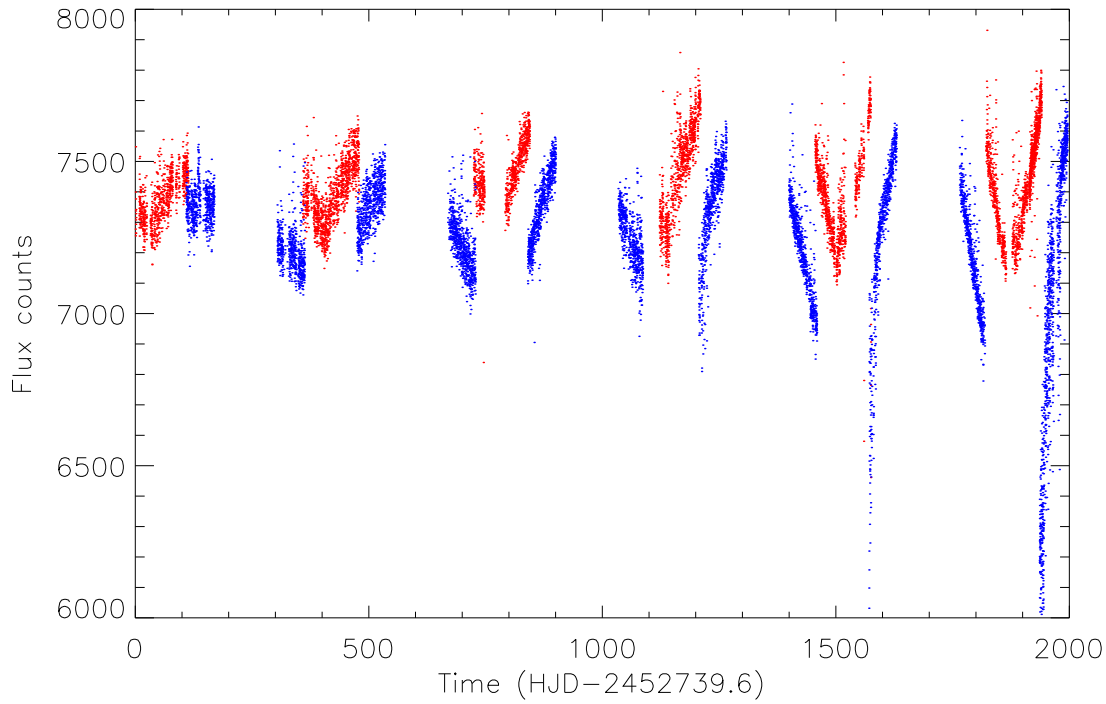

Figure 2.4: 5-year light curve of ζ Oph data before a running mean was subtracted, showing flux count against time. The red points show the data collected by Camera 1 and the blue points by Camera 2.

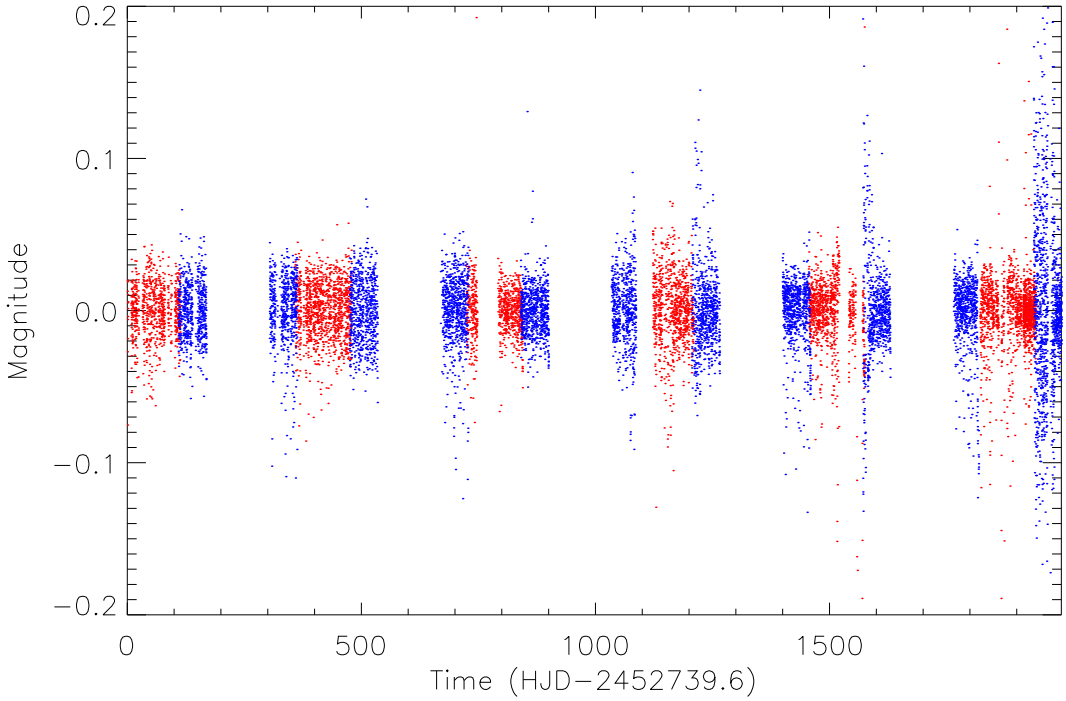

Figure 2.5: 5-year light curve of ζ Oph data after running mean was subtracted and flux count have been converted into magnitude. The red points show the data collected by Camera 1 and the blue points by Camera 2.

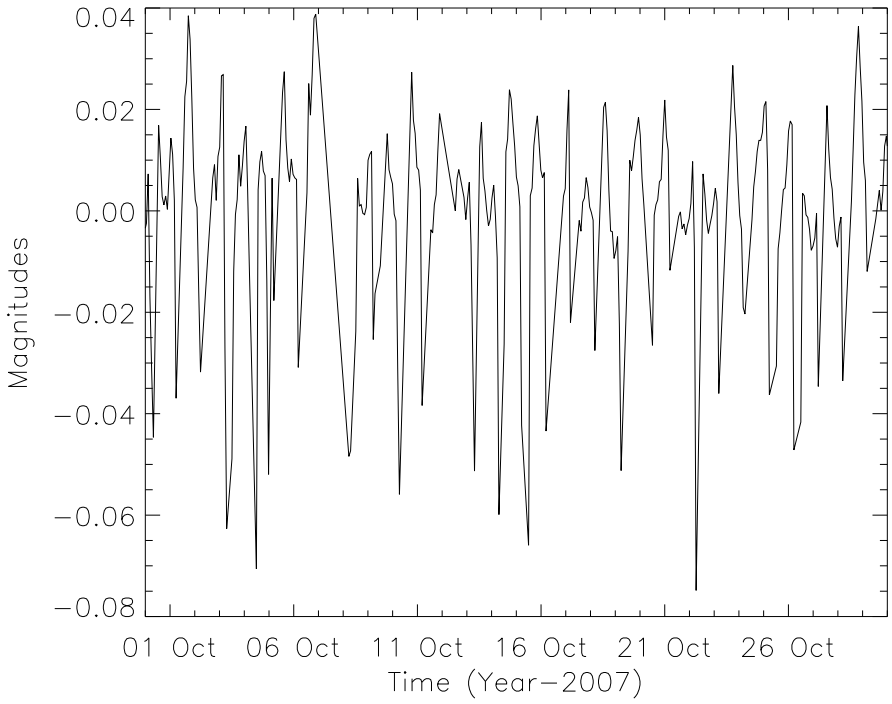

Figure 2.6: 30 day sample section of the light curve of Achernar obtained with *SMEI*.

in length and shows variations in the light curve of Achernar.

Once the smooth fit is removed and the data have been converted into magnitudes the light curve is ready for frequency analysis. An example amplitude spectrum is presented in Figure 2.7 (the spectrum is that of HIP 66657 using 3 years worth of collected data). The spectrum shows that alias frequencies are present in the data and are marked on Figure 2.7 with red arrows. These frequencies are effects of the orbit of the *SMEI* instrument and occur at 1 d^{-1}, and multiples thereof, due to the Sun-synchronous orbit of the satellite around the Earth. Therefore, any genuine oscillations from the star, at frequencies that are in the vicinity of 1 d^{-1} and multiples thereof, cannot be distinguished from those caused by the satellite and are therefore disregarded in the data analysis.

With regards to the detection of stellar variability, *SMEI* is capable of detecting millimagnitude brightness changes on objects brighter than 6.5 magnitudes. With a cadence of 101 minutes and data covering almost 6 years, *SMEI* is capable of detecting more frequencies with lower amplitudes than many other ground-based telescopes.

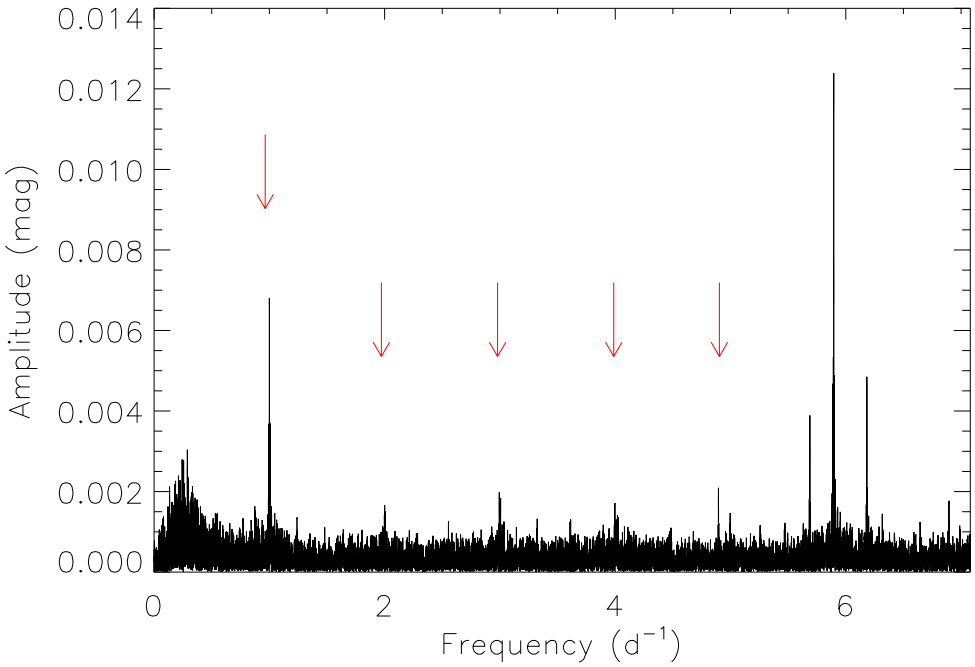

Figure 2.7: Amplitude spectrum of HIP 66657. Alias frequencies, due to the satellite orbit, occurring at 1 d^{-1} and multiples thereof, are marked by red arrows.

2.2 Microvariability and Oscillations of STars - *MOST*

MOST (Microvariability and Oscillations of STars) is a Canadian satellite and was the first satellite dedicated to asteroseismology. It was successfully launched on 30^{th} June 2003 and is returning data on variable stars. *MOST* was primarily designed to detect and characterise stellar oscillations, in particular acoustic oscillations from bright solar-like stars, metal poor stars and magnetic stars. *MOST* has also been used to detect reflected light from giant extrasolar planets orbiting closely round their parent star (to determine their physical size and atmospheric composition) [Walker et al., 2003].

MOST was launched into a low-Earth polar orbit and lies at an altitude of approximately 820km. It is in a Sun-synchronous orbit about the Earth with an orbital period of 101.4 minutes. Further information on the *MOST* instrument can be found in Matthews et al. [2000] and Walker et al. [2003].

MOST has previously been used to study stellar variations in: γ Equulei [Gruberbauer et al., 2008], κ^1 Ceti [Walker et al., 2007] and τ Bootis [Walker et al.,

Table 2.1: Overview of observational data received from *MOST*, *WIRE* and *SMEI* instruments while observing ζ Oph.

Satellite	Observational Period	Nos. data	RMS (mmag)
WIRE	18/02/04 - 27/02/04	6663	6.1
MOST	18/05/04 - 11/06/04	9084	6.1
WIRE	28/08/05 - 30/09/05	40730	4.8
WIRE	08/08/06 - 09/09/06	28113	7.8
SMEI	10/02/03 - 25/09/03	1467	17
SMEI	07/02/04 - 25/09/04	2473	20
SMEI	06/02/05 - 25/05/05	2255	18
SMEI	06/02/06 - 26/09/06	2194	24
SMEI	07/02/07 - 25/09/07	2340	24
SMEI	07/02/08 - 27/09/08	2123	22

2008] amongst many others as well as detecting and studying extrasolar planets in: HD 209458 [Rowe et al., 2008], HD 189733 [Miller-Ricci et al., 2008b] and searching for additional planets around HD 209458 [Miller-Ricci et al., 2008a].

In this thesis the data from the *MOST* instrument are only used to study the Oe star ζ Oph. *MOST* observed ζ Oph continuously for 23 days, in May and June of 2004, as summarised in Table 2.1. A sample section of the *MOST* light curve is shown in the bottom panel of Figure 2.8, alongside sample sections from the *SMEI* and *WIRE* instruments. A detailed comparison of the data collected by the different instruments is made at the end of Section 2.3.

The photometric data from the *MOST* instrument were previously processed and converted into magnitudes ready for analysis. It should be noted that these data were previously analysed and published by Walker et al. [2005]. The data have only been reanalysed here so that the results from the *MOST* instrument can easily be compared to the results from the *SMEI* and *WIRE* instruments i.e. the same procedure was used to analyse the *MOST* light curve as the *SMEI* and *WIRE* light curves.

2.3 Wide-field InfraRed Explorer - *WIRE*

Launched on 4^{th} March 1999, the Wide-field InfraRed Explorer (*WIRE*) was primarily designed to conduct a four-month infrared survey to study the evolution of galaxies,

in particular starburst galaxies (where rapid star formation is taking place) and protogalaxies (very young galaxies). The satellite was launched into a Sun-synchronous orbit about the Earth at an altitude of 540 km and has an orbital period of 93 minutes.

A failure during its launch into orbit caused the coolant in the main camera to leak and the primary instruments could no longer be used for the original mission. However the on board star tracker remained functional and was used to study stellar variability in bright stars.

The *WIRE* star tracker has previously been used to study: Arcturus [Retter et al., 2003], α Circini [Bruntt et al., 2009], K Giants [Stello et al., 2008] and eclipsing binaries [Southworth et al., 2007] amongst many others. See Buzasi et al. [2000] for an overview of *WIRE* instrument and examples of it being used to analyse oscillations from stars. The *WIRE* satellite re-entered the Earth's atmosphere on 10^{th} May 2011.

The photometric data from the *WIRE* instrument had previously been processed and converted into magnitudes ready for analysis when I received them. This analysis was accomplished by H. Bruntt using a pipeline specifically developed to optimally extract a light curve from the *WIRE* instrument. The pipeline binned the data such that the cadence of the light curve was 15.5 seconds. Further information on the *WIRE* pipeline can be found in Bruntt et al. [2005].

In this thesis the data from the *WIRE* instrument are only used to study the Oe star ζ Oph. *WIRE* was used to observe ζ Oph during three separate observing runs. The observational period of a *WIRE* target star can be up to 40 minutes for each 93 minute orbit. However in the case of ζ Oph the observational period is between 14 to 25 minutes per orbit. This information is summarised in Table 2.1 for both the *MOST* and *WIRE* satellites along with information about the number of data collected and the RMS (root mean squared) of the data.

Figure 2.8 shows how the *SMEI*, *MOST* and *WIRE* light curves compare to each other over a 20 day time period. As shown in the figure, it is clear that *SMEI* (top panel) has a lower cadence compared to the *WIRE* and *MOST* instruments (middle

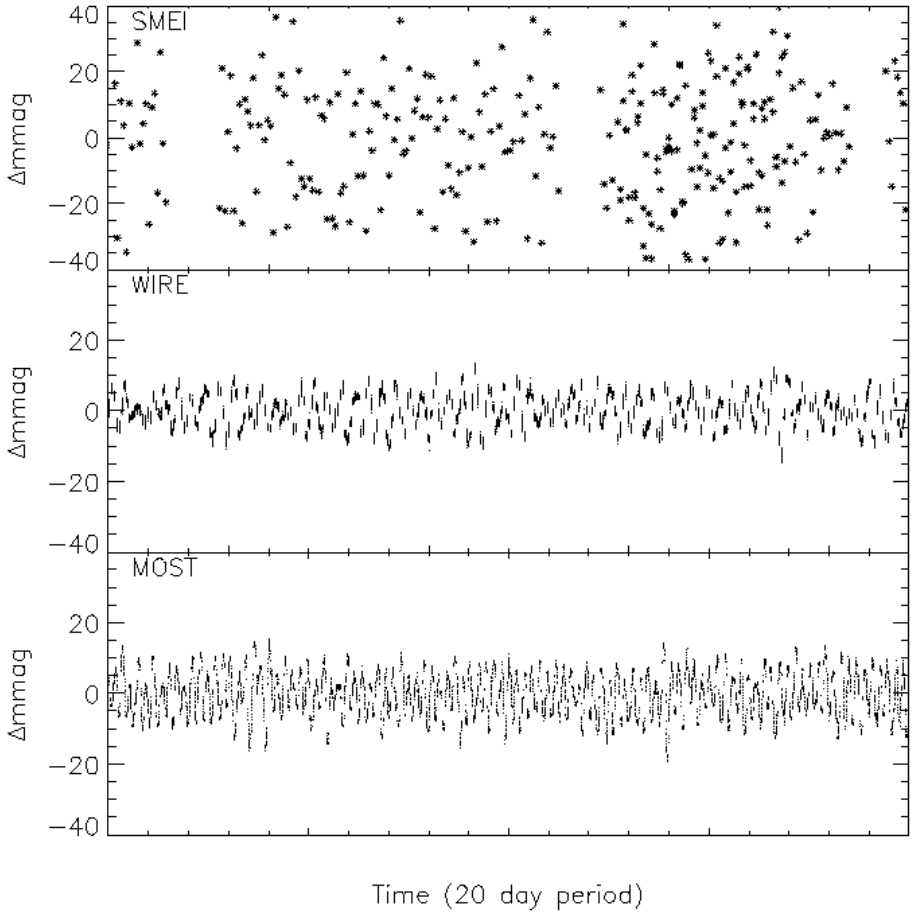

Figure 2.8: 20 day sample sections of ζ Oph light curve observed with *SMEI*, *WIRE* and *MOST*, zeroed at JD 2453201, JD 2453612 and JD 2453145 respectively.

and bottom panels respectively) and suffers more with noise. The quality of the data is also shown by the RMS values in Table 2.1. The RMS for both the *MOST* and *WIRE* data are significantly lower when compared to the RMS of the *SMEI* data. However *SMEI* does have the advantage of obtaining more continuous and much longer light curves in comparison to the *MOST* and *WIRE* instruments. The maximum length of a *SMEI* light curve is almost 6 years with approximately 40% coverage over that time period, while the *MOST* and *WIRE* instruments can only observe a star continuously for one month out of the year.

Chapter 3

β Cephei stars

This chapter is dedicated to β Cephei stars. An introduction to β Cephei stars, along with details of their characteristics, is provided in Section 3.1.

In Sections 3.2 and 3.3 of this chapter, results are presented on the oscillations observed in β Cephei using data provided by SMEI. The study of stellar oscillations in β Cephei stars can be used to determine information about the interior structure of some of the largest stars on the main sequence, and hence improve our general understanding of stellar formation and evolution.

The analysis initially focused on analysing known β Cephei stars. This was not only to detect further oscillations in these stars, which could be used by other researchers in modelling, but also to refine information on previously detected frequencies. These results are presented in Section 3.2.

Finally Section 3.3 describes the analysis and results on the search for further β Cephei stars observed with the SMEI instrument. 213 stars, selected using specific criteria, were analysed to search for frequencies in the β Cephei range. The results of the survey are analysed, and attention is made to individual stars which may possibly be β Cephei like.

3.1 An Introduction to β Cephei stars

Variability in the star β Cephei was first discovered by Frost [1902]. A few years later when enough data were available Frost [1906] published a radial velocity curve of β Cephei, calculating a radial velocity variation period of approximately four and a half hours (5.3 d^{-1}). This variability was confirmed a few years later, when light variations of the same period were identified by Guthnick, 1913 [Stankov and Handler, 2005]. The pulsation driving mechanism was finally determined to be the κ mechanism by Dziembowski and Pamiatnykh [1993], which has been explained in detail in Chapter 1.5.

Stankov and Handler [2005] made a review of all stars classed as β Cephei up until that point, 231 in total. As a result they found that known definitions made it very difficult to classify variable B-type stars. In an extensive review paper of β Cephei stars by Lesh and Aizenman [1978] the first definition of β Cephei stars was given as follows:

> These stars have the same short period for their light variations and radial velocity variation.

However, when classifying stars, overlaps often occurred between the different groups of variable stars. For example, the star β Cephei has been classified as a Be star and a magnetic Bp star [Hadrava and Harmanec, 1996]. Therefore Stankov and Handler [2005] suggested that the following definition for β Cephei variables should be used:

> The β Cephei stars are massive non-supergiant variable stars with spectral type O or B whose light, radial velocity and/or line profile variations are caused by low-order pressure and gravity mode pulsations.

This definition is appropriate as the classification is based upon the pulsation behaviour of the star. Each class of star should be driven by the same pulsation behaviour

and should have oscillations that are different and separable to those from other stellar classes. The position of β Cephei stars on the Asteroseismology HR-diagram is at the top of the main sequence and is clearly shown in Figure 1.9.

After refining the definition of a β Cephei star, any star that had previously been claimed to be a β Cephei star, or candidate, were re-evaluated individually to check whether they were consistent with the new definition. The results of the analysis split the stars into the three following categories:

1. Of the 231 stars, 93 were *confirmed* to be β Cephei stars, whereby the pulsations and known physical properties fit those of β Cephei stars.

2. Stars were classed as *candidate* β Cephei stars, where observational evidence was not conclusive either due to poor quality or lack of data. A total of 77 stars were classed as candidate β Cephei stars.

3. *Rejected* β Cephei stars, where observational evidence was found that they were not β Cephei pulsators, for example variability was disproved or was found to be due to other effects such as rotation. A total of 61 stars were classed as rejected β Cephei stars.

3.1.1 Properties of β Cephei stars

By using the 93 confirmed β Cephei stars, Stankov and Handler [2005] were able to identify and constrain physical and pulsation properties of β Cephei stars. Some of these properties were previously outlined in Chapter 1.4, but more detail is given in the following sections. All of the confirmed β Cephei stars lay between spectral types B0 and B2.5.

The stellar mass distribution of confirmed β Cephei stars can be seen in Figure 3.1. The figure shows that β Cephei stars have masses between 8 and 18 $M_{\odot}$, the distribution of which peaks sharply at about 12 $M_{\odot}$. In comparison, a histogram of the candidate β Cephei stars showed a similar maximum, at $12M_{\odot}$, but with a wider mass range,

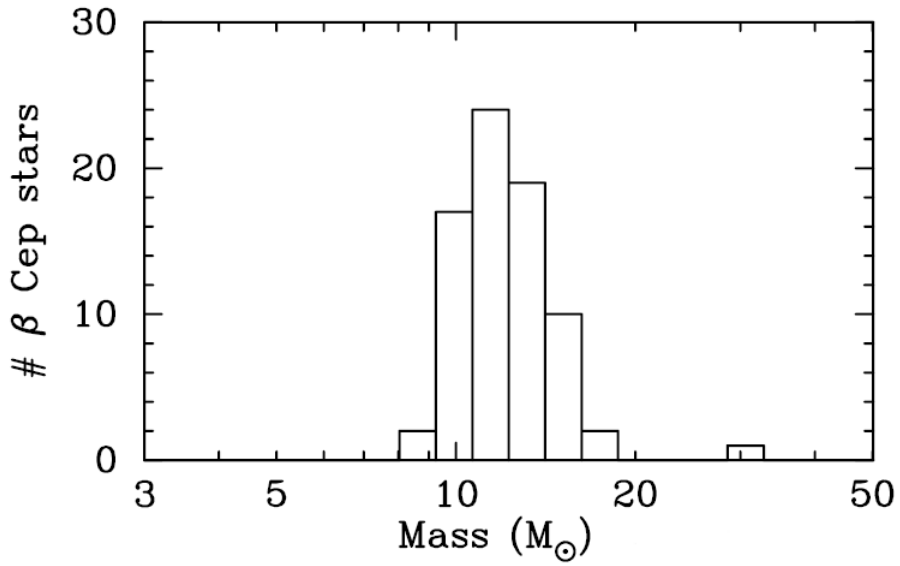

Figure 3.1: Stellar mass distribution of confirmed β Cephei stars [Stankov and Handler, 2005].

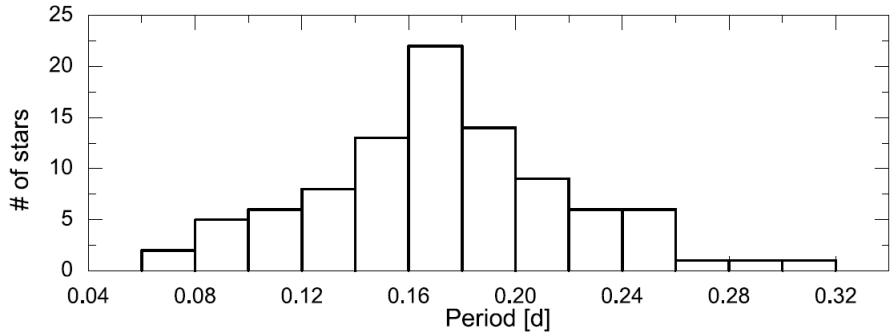

Figure 3.2: Pulsation period distribution of confirmed β Cephei stars [Stankov and Handler, 2005].

possibly indicating the presence of some β Cephei stars within the category, but perhaps not all. A histogram of the rejected β Cephei stars did not show any significant features or peaks.

The distribution of the known β Cephei pulsation periods is shown in Figure 3.2. The pulsation periods range between 0.0667 and 0.319 days (3.13 to 14.99 d^{-1}) peaking at a period of approximately 0.17 days (4 hrs).

Most β Cephei stars seem to be rather slow rotators, with an average $v \sin i$ in the 100 km s^{-1} range. This does not include β Cephei stars which also show Be characteristics (please see Section 4.1.1 for a more detailed explanation). It is possible

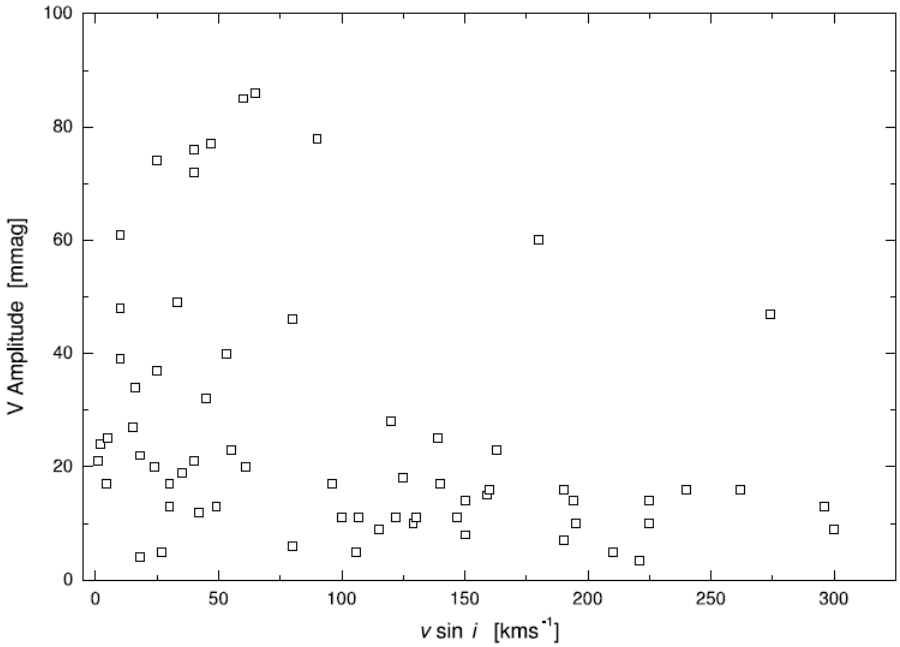

Figure 3.3: Comparison of $v \sin i$ and pulsation amplitude of confirmed β Cephei stars [Stankov and Handler, 2005].

that this characteristic is a selection effect, so that the highest amplitude pulsators are slowly rotating stars, and are hence more easily detected. This is supported by a comparison of pulsation amplitudes versus rotation rate by Stankov and Handler [2005], and is shown in Figure 3.3. With the exception of two stars, Figure 3.3 shows that stars with a $v \sin i$ less than 90 km s^{-1} show pulsation amplitudes larger than 25 mmag.

As mentioned in Chapter 1.5, the mechanism which drives the pulsations in β Cephei and SPB stars is the κ-mechanism acting on the iron ionisation zones. As shown in Figure 1.12, the β Cephei and SPB instability strips are dependent on the metallicity of the star. This is due to the κ-mechanism being dependent on the abundance of iron in the star, so B stars that are formed in a low metallicity environment are less likely to contain enough iron for the stars to pulsate. In regions where the metallicity is high enough, for example Z=0.02, the number of stars expected to pulsate with β Cephei and SPB frequencies is expected to increases, and as shown in Figure 1.12, the regions on the HR diagram where β Cephei and SPB like pulsations occur overlaps and stars are expected which show both types of pulsations.

γ Peg was the first hybrid pulsator where a sufficiently large number of high-order g-modes and low-order p-modes had been detected which could be used in seismic modelling. Because β Cephei and SPB oscillations are sensitive to physics conditions in different parts of the stellar interior, hybrid pulsators are able to provide a more complete picture of the physics inside B type stars using asteroseismology [Handler et al., 2009].

3.1.2 modelling β Cephei stars

As mentioned in Chapter 1, observed oscillations of stars are used to constrain global parameters and also help improve existing stellar models.

It was not until 1992 that the pulsation mechanism for β Cephei stars was found to be due to the κ mechanism. This process is explained in more detail in Chapter 1.5. This discovery was a huge step forward in understanding and modelling these stars. In particular the Rosseland mean opacity was increased in the OPAL opacity tables, providing a significant improvement in the discrepancies between observed frequencies and theoretical frequencies. Further alterations on the opacity calculations led to further improvements in the OPAL and OP opacity tables and for observations made up until the late 1990s theoretical models were able to explain most of the oscillations observed in β Cephei and SPB stars.

The increase in the number of space-based observations in the last 10 years has not only increased the number of stars observed but the accuracy at which they can be observed. β Cephei and SPB type stars have been found in low metallicity environments where no or few of these stars were expected [Kołaczkowski et al., 2006]. The number of observed oscillations in β Cephei stars has increased, where some frequencies are falling outside of regions where they are expected to be, causing new discrepancies between theoretical models and observed pulsations. For example, the β Cephei stars ν Eri [Jerzykiewicz et al., 2005] and 12 Lac [Handler et al., 2006] were found to have frequencies higher than those predicted by the pulsation models, as well as oscillations

that were characteristic of SPB type oscillations.

As discussed in Miglio et al. [2007a] this discrepancy may be due to an underestimation of iron in the metal opacity bump. Miglio et al. [2007a] found that uncertainties in the metal mixture and opacity calculations used in OPAL and OP have a considerable effect on the modes excited in β Cephei and SPB stars and could explain the difference between theoretical and observational pulsations. Recent research suggests that an increase in the Nickel contribution to the opacity may explain the observations in low metallicity environments. However, current OPAL and OP computations on stellar opacities in Nickel are not obtained from scratch, but are instead extrapolated from the Iron opacity calculations. It has therefore been suggested that the opacity calculations for Nickel be recalculated separately, so that a more accurate stellar model can be created [Salmon et al., 2012].

Although modelling is a crucial part of asteroseismology, it is the observational data that we concentrate on in this thesis. However a star observed in the β Cephei survey (HIP 30122, see Chapter 3.3.3) showed frequencies that were in both the β Cephei and SPB frequency range. With the aid of Andrea Miglio a model was found for this star which could account for the frequencies observed. This is be discussed in more detail in Chapter 3.3.3.

3.2 Confirmed β Cephei stars with SMEI

The purpose of analysing stars known to be β Cephei type is to identify pulsation frequencies that have previously been undetected. We are also able to refine our knowledge on known pulsations, as the long *SMEI* light curves enable a more precise determination of pulsation periods than has previously been achieved using ground based instrumentation.

As mentioned in the previous section (Chapter 3.1) Stankov and Handler [2005] presented an extensive catalogue of all claimed β Cephei stars to date. Stankov and Handler [2005] re-evaluated each star that was classified as a β Cephei star, or suspected to be a β Cephei star, to redetermine whether their physical and pulsation properties fit with that of a β Cephei star.

The list of 93 confirmed β Cephei stars provided by Stankov and Handler [2005] was used to provide an initial target list of β Cephei stars to be analysed. Restrictions of the *SMEI* instrument meant that only certain stars were able to be analysed. The criteria for this selection of stars was as follows:

1. Stars were only included if they have an apparent magnitude of 6.5 or brighter. At fainter magnitudes noise levels increase significantly above the millimagnitude level.

2. Stars were only included if they lie further than 10° from the Galactic Plane due to crowding issues. Observations close to or on the Galactic Plane risk being contaminated by light from other stars.

3. There is one exception to the above criterion whereby stars that have an apparent magnitude of 3 or brighter were included wherever they lie on the Galactic Plane. This decision was made on the basis that the light from these stars will dominate the light curve and will not be contaminated by light from other nearby stars.

The final target list of β Cephei stars to be analysed using the *SMEI* instrument contained 27 stars, which are listed in Table 3.1. Those targets which have a star

by them ($\star$) are those which I analysed in this investigation and whose results are presented in this thesis. The remaining stars were analysed by Dr. I. R. Stevens and these results will be collated to be presented in a paper.

Table 3.1 also shows some of the stellar parameters of the β Cephei stars being analysed in this thesis. The parameters were obtained from SIMBAD [Wenger et al., 2000] and include: alternative names in other catalogues, Right Ascension (RA), Declination (Dec), spectral type and apparent magnitude (m_v). Notice that the spectral types range between B0 and B3, a characteristic that belongs to most known β Cephei stars as mentioned in Section 3.1.

3.2.1 Analysis using Period04

The β Cephei stars targeted for analysis are listed in Table 3.1. These were collected using the *SMEI* instrument onboard the *Coriolis* satellite and prepared for analysis, as described in Chapter 2.1. At the time of analysis only 3 years worth of *SMEI* data were available.

The β Cephei light curves were analysed using Period04 [Lenz and Breger, 2005]. Period04 is a software package that has been designed to statistically analyse astronomical light curves. The Fourier analysis is based on a discrete Fourier transform algorithm and is capable of extracting individual frequencies from a light curve containing multiple frequencies and is also able to perform multiple frequency fits.

First, the light curve is entered into the package where spurious points can be determined and removed before continuing with further analysis. These points were detected by visually analysing the light curves to remove any points that looked obviously out of place that were not removed in the pipeline. For example, sometimes at the start or end of an observing session with the *SMEI* cameras, points are present which are obviously not related to the stellar observations. Period04 then uses a discrete Fourier transform (DFT) algorithm to create an amplitude spectrum of the light curve. This is accomplished by fitting a sine wave to the data at a set frequency

Table 3.1: Target list of β Cephei stars (as confirmed by Stankov and Handler [2005]) analysed with *SMEI*. Stellar parameters of β Cephei stars analysed taken from *SIMBAD* [Wenger et al., 2000]. Those targets which have a star by them ($\star$) are those which I analysed in this investigation.

	HD	HIP	Alt. Name	RA	Dec	Spectral Type	m_v
	886	1067	γ Peg	00 13 14	+15 11 00	B2IV	2.83
	16582	12387	δ Cet	02 39 26	+00 19 42	B2IV	4.07
	24760	18532	ϵ Per	03 57 51	+40 00 36	B0.5V	2.901
	29248	21444	ν Eri	04 36 19	−03 21 08	B2III	3.920
	35411	25281	η Ori	05 24 29	−02 23 50	B0.5V	3.38
	35715	25473	ψ Ori	05 26 50	+03 05 44	B2IV	4.595
	44743	30324	β CMa	06 22 41	−17 57 21	B1II-III	2.0
	46328	31125	ξ CMa	06 31 51	−23 25 06	B0.7IV	4.33
	50707	33092	EY CMa	06 53 32	−20 13 27	B1I	4.806
	56014	34981	EW CMa	07 14 15	−26 21 09	B3III	4.65
	64722	38438	V372 Car	07 52 29	−54 22 01	B1.5IV	5.680
	111123	62434	β Cru	12 47 43	−59 41 19	B0.5IV	1.297
$\star$	116658	65474	α Vir, Spica	13 25 11	−11 09 40	B1III	1.04
$\star$	118716	66657	ϵ Cen	13 39 53	−53 27 59	B1III	2.265
$\star$	122451	68702	β Cen	14 03 49	−60 22 22	B1III	0.60
$\star$	126341	70574	τ Lup	14 26 08	−45 13 17	B2IV	4.546
$\star$	129056	71860	α Lup	14 41 55	−47 23 17	B1.5III	2.276
$\star$	136298	75141	δ Lup	15 21 22	−40 38 51	B1.5IV	3.203
$\star$	144470	78933	ω Sco	16 06 48	−20 40 09	B1V	3.946
$\star$	147165	80112	σ Sco	16 21 11	−25 35 34	B1III	2.912
	157056	84970	θ Oph	17 22 01	−24 59 58	B2IV	3.248
$\star$	158926	85927	λ Sco	17 33 36	−37 06 13	B2IV	1.62
	160578	86670	κ Sco	17 42 29	−39 01 48	B1.5III	2.375
$\star$	163472	87812	V2052 Oph	17 56 18	+00 40 13	B2IV	5.834
$\star$	205021	106032	β Cep	21 28 39	+70 33 38	B2III	3.216
$\star$	214993	112031	DD Lac	22 41 28	+40 13 31	B2III	5.228
	216916	113281	EN Lac	22 56 24	+41 36 14	B2IV	5.584

and determining the amplitude and phase of the fitted sine wave at that frequency. The frequency is then incremented, the step rate of which is determined by the user, and the same process is repeated. This process continues until the desired frequency range, also determined by the user, has been covered and the results are plotted in an amplitude spectrum.

As mentioned, PERIOD04 is capable of identifying significant frequencies within the data. This is accomplished by assuming that the light curve consists of a single sine wave, calculating the best-fitting frequency, amplitude and phase. This frequency can then be removed from the data to search for further significant frequencies. This process can be repeated until all significant frequencies have been calculated and removed from the data.

A frequency is classified as significant if the S/N (ratio of signal amplitude to mean noise) is greater than four. This criterion provides a useful check on determining the reality of a peak due to pulsation rather than a peak produced by noise, and was first suggested by Breger et al. [1993] and later on confirmed theoretically by Kuschnig et al. [1997].

The S/N was also calculated using PERIOD04. The frequency for which a S/N is to be calculated is selected, the amplitude of which is stored and then removed from the data. The mean local amplitude of the remaining signal (the box size of which is determined by the user) is then calculated. For the β Cephei stars analysed here, the box size was chosen to be 0.1 d^{-1}. The calculated value of the mean amplitude in this box is taken to be the background noise. The S/N can then be determined by dividing the amplitude of the selected frequency by the calculated background noise.

Errors on frequency, amplitude and phase were calculated in PERIOD04 by using Monte Carlo simulations supplied with the package.

An overview of the observational data collected of the confirmed β Cephei stars is shown in Table 3.2. The table shows the durations over which the stars were observed, the number of points collected during the observational period and the duty cycle (the

Table 3.2: An overview of the observational data collected by *SMEI* on the β Cephei stars.

HIP	Observational dates	Nos. days	Nos. data	Duty cycle (%)
65474	10/04/03 - 21/03/06	1077	5693	37.08
66657	10/04/03 - 21/03/06	1077	6116	39.83
68702	10/04/03 - 21/03/06	1077	6074	39.56
70574	10/04/03 - 21/03/06	1077	6646	43.28
71860	10/04/03 - 21/03/06	1077	6499	42.32
75141	10/04/03 - 21/03/06	1077	6378	41.54
78933	10/04/03 - 18/03/06	1074	5308	34.66
80112	10/04/03 - 18/03/06	1074	5211	34.03
85927	10/04/03 - 21/03/06	1077	5896	38.40
87812	10/04/03 - 21/03/06	1077	6775	44.12
106032	10/04/03 - 21/03/06	1077	10989	71.57
112031	18/04/03 - 15/01/06	1002	7335	51.33

percentage of data points collected against the total number of possible data points that could have been collected). As shown in Table 3.2 the typical duty cycle for a stellar observation is approximately 40%, but as shown with HIP 106032 this value can be as high as 70%. This is explained in further detail in Chapter 2.1.3.

3.2.2 Results of confirmed β Cephei stars

The results of the 12 β Cephei stars analysed in this thesis can be found on the following pages. For each star the amplitude spectrum is shown, along with a table of significant frequencies (if necessary) and an explanation as the frequencies observed. Frequencies which were not found in the literature are indicated by a star ($\star$) in the tables.

HD 116658; HIP 65474; α Vir: Spica

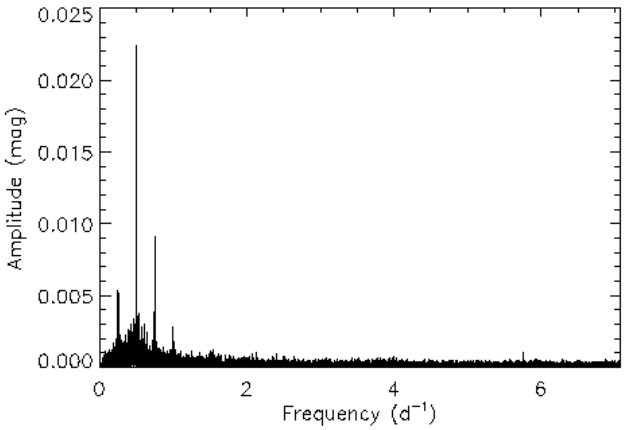

	Freq (d^{-1})	Amp (mmag)	S/N
f_1	0.498241(4)	23.0(2)	72.6
f_2	0.74729(1)	8.9(2)	30.1
f_3	0.24911(2)	5.6(2)	16.1
$f_4^\star$	2.40265(8)	1.2(2)	6.3
f_5	5.75430(9)	1.1(2)	7.0
$f_6^\star$	1.54009(9)	1.0(2)	4.7

Figure 3.4: Spectrum of α Vir, Spica (HD 116658, HIP 65474)

Table 3.3: Significant frequencies found in α Vir, Spica (HD 116658, HIP 65474)

α Vir is the primary star in a binary system with an eccentricity of 0.146. It has an orbital period of 4.01 days (0.24938 d^{-1}) [Aerts and De Cat, 2003] which corresponds to the frequency detected at f_3 (Table 3.3). Frequencies f_1 and f_2 are multiples of the orbital frequency. Lomb [1978] reported a frequency of 5.754 d^{-1}, which is confirmed in the *SMEI* data in f_5 (see Table 3.3). Lomb [1978] reported that the amplitude of this frequency decreased to a level which was undetectable and has not been observed since (see Smith [1985a]). It is possible that the frequency detected in f_5 is the pulsation which was suspected to have dropped to an undetectable level or ceased altogether. In addition, two new frequencies were detected in the *SMEI* data at 2.40265 d^{-1} and 1.54009 d^{-1} (f_4 and f_6 in Table 3.3).

Smith published additional frequencies of 0.498 d^{-1}, 3.681 d^{-1}, 7.500 d^{-1} [Smith, 1985a] and 2.99 d^{-1} [Smith, 1985b], none of which have been confirmed in the *SMEI* data. Stankov and Handler [2005] and Aerts and De Cat [2003] suggest that further spectroscopic data would need to be analysed before these frequencies are confirmed.

HD 118716; HIP 66657; ϵ Cen

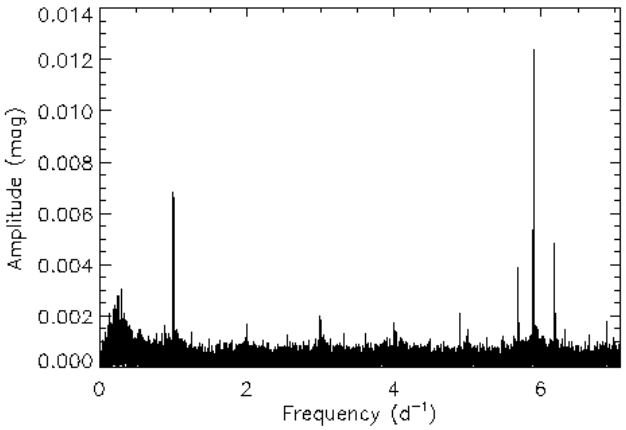

	Freq (d^{-1})	Amp (mmag)	S/N
f_1	5.89523(1)	12.3(3)	38.5
f_2	6.18273(2)	4.8(3)	14.2
f_3	5.68836(4)	3.9(3)	11.6
$f_4^\star$	6.3165(1)	1.5(3)	4.3

Figure 3.5: Spectrum of ϵ Cen (HD 118716, HIP 66657)

Table 3.4: Significant frequencies found in ϵ Cen (HD 118716, HIP 66657)

Shobbrook [1972] reported periods of 0.169608 days and 0.17696 days, corresponding to frequencies of 5.8959 d^{-1} and 5.650995 d^{-1} respectively. These oscillations are shown in the light curve as frequencies f_1 and f_3 respectively in Table 3.4. Schrijvers et al. [2004] later on found additional oscillations of 6.183 d^{-1}, 7.378 d^{-1} and 7.645 d^{-1}.

The first oscillation is confirmed in the *SMEI* data in f_2, while the later are above the Nyquist frequency and no evidence of them is observed in the light curve. In addition a new frequency of 6.316562 d^{-1} was observed (see f_4, Table 3.4).

HD 122451; HIP 68702; β Cen

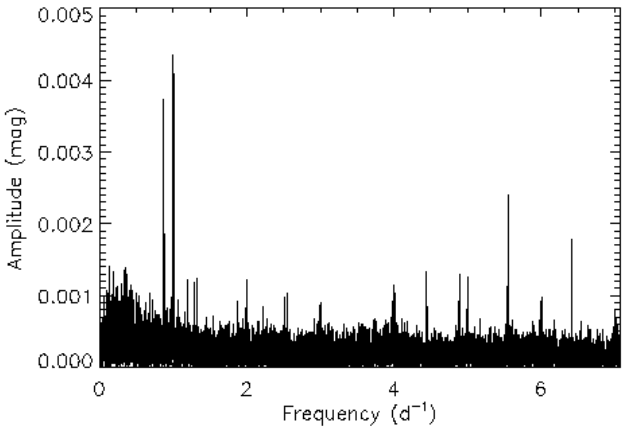

	Freq (d^{-1})	Amp (mmag)	S/N
$f_1^\star$	0.86796(3)	3.6(2)	14.7
$f_2^\star$	5.54508(5)	2.3(2)	13.0
f_3	6.41313(6)	1.9(2)	12.1
$f_4^\star$	4.88538(8)	1.4(2)	7.2
$f_5^\star$	1.19941(8)	1.3(2)	6.2
$f_6^\star$	4.44438(8)	1.3(2)	8.3
$f_7^\star$	1.28907(9)	1.2(2)	6.0
$f_8^\star$	2.55313(9)	1.1(2)	5.7
$f_9^\star$	1.3203(1)	1.1(2)	5.3
$f_{10}^\star$	2.51893(7)	1.1(2)	5.5

Figure 3.6: Spectrum of β Cen (HD 122451, HIP 68702)

Table 3.5: Significant frequencies found in β Cen (HD 122451, HIP 68702)

β Cen is a spectroscopic binary system with an orbital period of 357 days and eccentricity of 0.81 [Ausseloos et al., 2002]. The two components of the binary system are of similar mass: $M_1 = 10.7 \pm 0.1 M_\odot$ and $M_2 = 10.3 \pm 0.1 M_\odot$ [Ausseloos et al., 2006]. Both components of the system are β Cephei like stars. β Cen is multi-periodic with the most dominant oscillation at 0.1535 days (6.51466 d^{-1}) [Stankov and Handler, 2005].

Ausseloos et al. [2002] reported frequencies of 6.51481 d^{-1}, 6.41356 d^{-1} and 6.49521 d^{-1} in the primary component of β Cen. The first and third frequencies are not seen in the *SMEI* data, but the second frequency is observed as shown in f_3 in Table 3.5.

Ausseloos et al. [2006] reported oscillations in the primary star of the β Cen system of 7.415 d^{-1} and 4.542 d^{-1}. The first oscillation is above the Nyquist frequency for *SMEI* so cannot be observed directly, and no evidence of it appears in the spectrum. There is also no evidence for the second frequency in the data. However, we do find several other new frequencies (see Table 3.5), many of which are below 3 d^{-1}.

HD 126341; HIP 70574; τ Lup

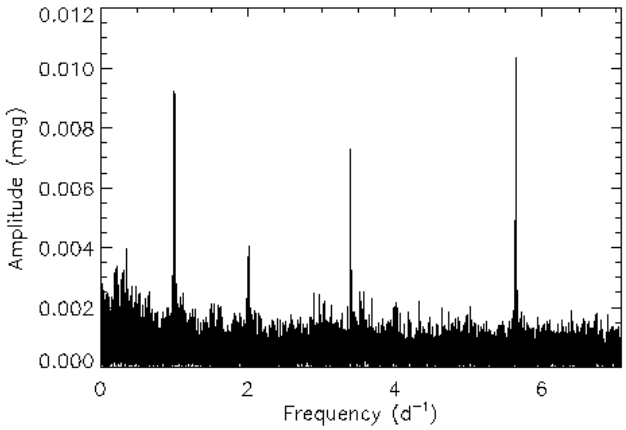

	Freq (d^{-1})	Amp (mmag)	S/N
f_1	5.63784(3)	10.4(6)	18.2
$f_2^\star$	3.39701(4)	7.3(6)	11.0

Figure 3.7: Spectrum of τ Lup (HD 126341, HIP 70574)

Table 3.6: Significant frequencies found in τ Lup (HD 126341, HIP 70574)

τ Lup has previously been reported as a mono-periodic β Cephei star of spectral type B2IV. Cuypers [1987] report a single oscillation with a period of 0.17736934 days (5.637953 d^{-1}). This frequency can be seen in f_1, Table 3.6 and Figure 3.7.

An additional frequency of 3.397008 d^{-1} has also been identified with the *SMEI* data, (see f_2, Table 3.6), which has not been previously reported in the literature.

HD 129056; HIP 71860; α Lup

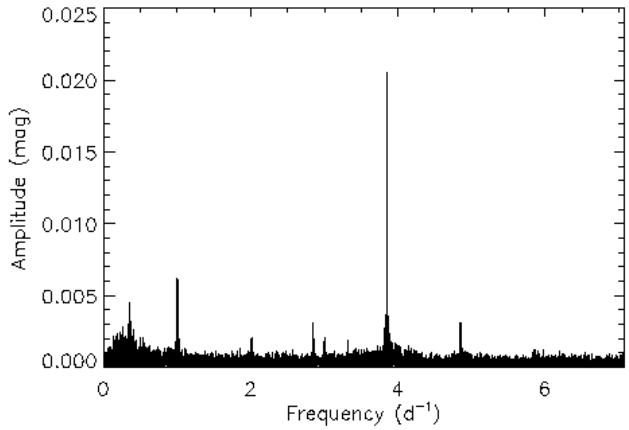

	Freq (d^{-1})	Amp (mmag)	S/N
f_1	3.848403(9)	19.8(3)	58.0
$f_2^\star$	0.35030(3)	4.4(3)	6.1
$f_3^\star$	3.31796(9)	1.8(3)	5.3

Figure 3.8: Spectrum of α Lup (HD 129056, HIP 71860)

Table 3.7: Significant frequencies found in α Lup (HD 129056, HIP 71860)

Heynderickx [1992] reported frequencies of 3.84842 d^{-1} and 4.22297 d^{-1} using the Walvern photometer at La Silla Observatory. Results from Mathias et al. [1994a] verified the first frequency, but since their data only covered three nights, they stated that it would be 'fairly reckless' to search for the second frequency. The first frequency is shown in f_1 (see Table 3.7), but the second frequency was not detected with *SMEI*.

In addition, two further frequencies were detected using *SMEI*: 0.350297 d^{-1} and 3.317959 d^{-1}, which are shown as f_2 and f_3 in Table 3.7 respectively. It is possible that a combination of the 0.350297 d^{-1} and 3.84842 d^{-1} frequencies result in the second frequency (4.22297 d^{-1}) that Heynderickx [1992] reports.

HD 136298; HIP 75141; δ Lup

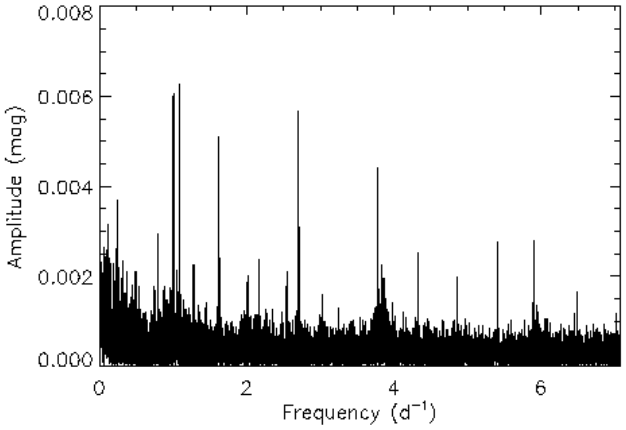

	Freq (d^{-1})	Amp (mmag)	S/N
$f_1^\star$	1.08131(3)	6.2(3)	12.4
f_2	2.70331(3)	5.6(3)	15.5
$f_3^\star$	1.62196(3)	5.1(3)	12.9
f_4	3.78459(3)	4.6(3)	7.7
f_5	5.40656(6)	2.9(3)	9.2
f_6	5.90218(6)	2.8(3)	7.7
$f_7^\star$	0.78374(6)	2.8(3)	5.0
f_8	4.32525(6)	2.6(3)	7.8
f_9	2.16259(7)	2.4(3)	5.9
$f_{10}^\star$	1.27512(7)	2.4(3)	5.3
f_{11}	4.86585(8)	2.1(3)	6.8
f_{12}	2.54005(8)	2.1(3)	6.4
f_{13}	6.48790(9)	1.8(3)	5.6

Figure 3.9: Spectrum of δ Lup (HD 136298, HIP 75141)

Table 3.8: Significant frequencies found in δ Lup (HD 136298, HIP 75141)

δ Lup is part of a binary system, with an orbital period between 16 and 19 days [Lloyd and Pike, 1988]. Two frequency detections for δ Lup are claimed in the literature; a photometric frequency of 6.05 d^{-1} [Shobbrook, 1972] and a spectroscopic frequency of 5.04 d^{-1} [Lloyd and Pike, 1988]. Stankov and Handler [2005] comment that the photometric period is likely an alias of the spectroscopic period.

However, neither of these frequencies are observed with the *SMEI* data. As shown in Figure 3.9, the spectrum shows many frequencies that have not been recorded before. Six of these frequencies lie above 3 d^{-1}, and seven below 3 d^{-1}. However, only four of theses are new frequencies that have been detected; 1.08131 d^{-1}, 1.62196 d^{-1}, 0.78374 d^{-1} and 1.27512 d^{-1} shown in f_1, f_3, f_7 and f_{10} in Table 3.8 respectively. The remaining frequencies stated in Table 3.8 are harmonics of these four frequencies.

HD 144470; HIP 78933; ω Sco

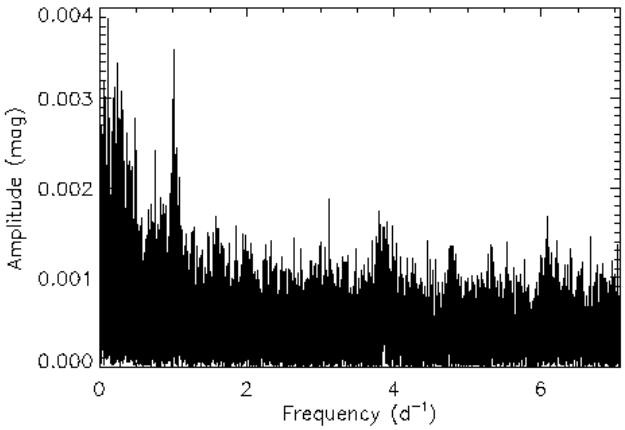

Figure 3.10: Spectrum of ω Sco (HD 144470, HIP 78933)

ω Sco is a B1V star that has been reported to be a β Cephei star on the basis of spectroscopic observations. Telting and Schrijvers [1998] analysed a set of 30 spectra for ω Sco. Their results found the absorption lines of the SiIII triplet to be variable with a frequency of 15.0 d^{-1}. This frequency is above the Nyquist frequency for *SMEI*, so cannot be observed directly. There is also unclear evidence for its detection in the reflection of the Nyquist frequency, as there are no definite peaks in the spectrum that could be attributed to this frequency (see Figure 3.10).

HD 147165; HIP 80122; σ Sco

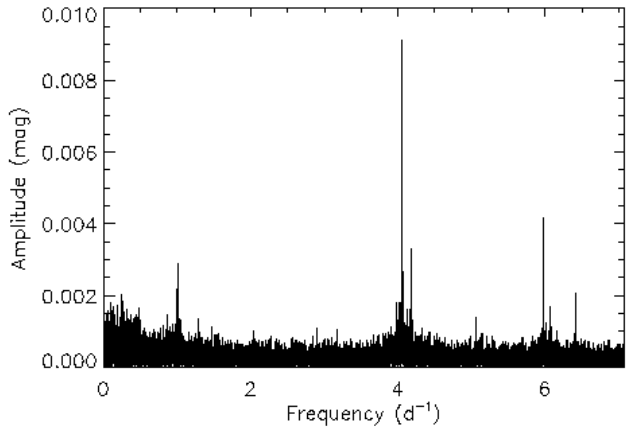

	Freq (d^{-1})	Amp (mmag)	S/N
f_1	4.05169(2)	8.3(3)	27.4
$f_2^\star$	5.97201(4)	4.1(3)	13.9
f_3	4.17313(4)	3.9(3)	13.6
$f_4^\star$	6.40982(7)	2.2(3)	8.9
$f_5^\star$	6.06756(9)	1.8(3)	5.8

Figure 3.11: Spectrum of λ Sco (HD 158926, HIP 85927)

Table 3.9: Significant frequencies found in σ Sco (HD 147165, HIP 80112)

σ Scorpii is a quadruple system with the primary component identified as a β Cephei type star in a spectroscopic binary with an orbital period of 33.0114 days (North et al. 2007 and Chapellier and Valtier [1992]).

Chapellier and Valtier [1992] analysed all available spectroscopic data of σ Scorpii to date and found periods of 0.246829 days and 0.239661 days present, corresponding to frequencies of 4.051388 d^{-1} and 4.172560 d^{-1} respectively. These two frequencies were detected in the *SMEI* data in frequencies f_1 and f_3 respectively (see Table 3.9).

In addition, three new frequencies were detected with *SMEI*: f_2, f_4 and f_5 (see Table 3.9), where no previous evidence of them was found in the literature. The new frequencies that were found are highlighted with a star (*) in Table 3.9.

HD 158926; HIP 85927; λ Sco

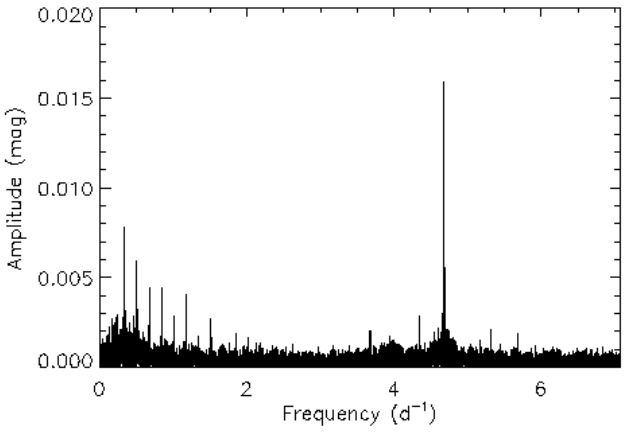

	Freq (d^{-1})	Amp (mmag)	S/N
f_1	4.67948(1)	16.7(4)	40.5
f_2	0.33606(2)	8.8(4)	12.8
f_3	0.67206(4)	5.7(4)	12.6
f_4	1.00816(6)	3.8(4)	9.0
$f_5^\star$	1.84816(9)	2.9(4)	9.1
f_6	1.34419(9)	2.9(4)	8.2
$f_7^\star$	4.34321(8)	2.2(4)	6.6
$f_8^\star$	5.3155(1)	2.2(4)	5.9
f_9	2.0161(1)	2.2(4)	5.6
$f_{10}^\star$	2.1842(1)	2.0(4)	5.3
f_{11}	2.3524(1)	1.8(4)	5.0

Figure 3.12: Spectrum of λ Sco (HD 158926, HIP 85927)

Table 3.10: Significant frequencies found in λ Sco (HD 158926, HIP 85927)

λ Sco is a spectroscopic triple system, with a B1.5IV star in orbit about a T Tauri star with an orbital period of 5.9525 days. The third component, a B2V star, moves about the orbit with an orbital period of 1082 days [Uytterhoeven et al., 2004a].

HD 158926 is the primary of this system with a variable dominant period of 0.2137 days, corresponding to a frequency of 4.6794 d^{-1} [Lomb and Shobbrook, 1975]. The dominant period was detected with the *SMEI* data, which is shown as frequency f_1 in Table 3.10.

Uytterhoeven et al. [2004b] report a period of 5.9525 days, corresponding to a frequency of 0.167997 d^{-1}. A frequency of 0.336 d^{-1} (see f_2, Table 3.10), and multiples of this frequency (see f_3, f_4, f_6, f_9 and f_{11} in Table 3.10), were also calculated and can be seen in Figure 3.12. These frequencies are all multiples of the frequency reported by Uytterhoeven et al. [2004b].

Uytterhoeven et al. [2004a] also report on three other significant frequencies at 3.899013 d^{-1}, 5.340978 d^{-1} and 9.726644 d^{-1}. These frequencies are not detected in the *SMEI* data. In addition, further frequencies were found at f_5, f_7, f_8 and f_{10} (Table 3.10).

HD 163472; HIP 87812; V2052 Oph

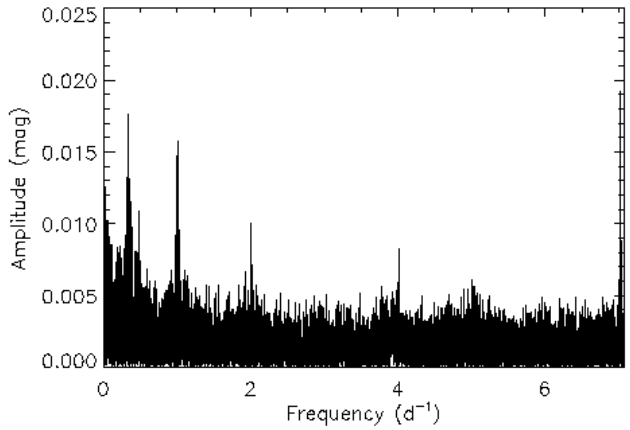

	Freq (d^{-1})	Amp (mmag)	S/N
f_1	7.02216(5)	17.1(2)	9.8

Figure 3.13: Spectrum of V2051 Oph (HD 163472, HIP 87812)

Table 3.11: Significant frequencies found in V2052 Oph (HD 163472, HIP 87812)

V2052 Oph has one of the shortest periods and lowest luminosities for a β Cephei variable.

Jerzykiewicz [1972] reported a period of 0.13989 days, corresponding to a frequency of 7.14847 d^{-1}. Since this frequency is above the Nyquist frequency for *SMEI*, we cannot detect this directly. However, it is reflected through the Nyquist showing a frequency at 7.022155 d^{-1} (f_1, Table 3.11), as shown in Figure 3.13.

Neiner et al. [2003a] confirm this frequency and also reported on two additional frequencies. The first frequency was detected at 6.82128 d^{-1} and the second frequency at 0.55 d^{-1}, corresponding to twice the rotational frequency at 0.27 d^{-1}. These two frequencies have recently been confirmed by Pollard et al. [2008] using the *HERCULES* spectrograph at the Mt John University Observatory in New Zealand. However, neither of these frequencies are found in the *SMEI* data.

A low frequency of 0.33105 d^{-1} appears to be prominent in the amplitude spectrum (Figure 3.13). However, upon analysis the S/N of this frequency falls below four and so was not found to be significant.

HD 205021; HIP 106032; β Cep

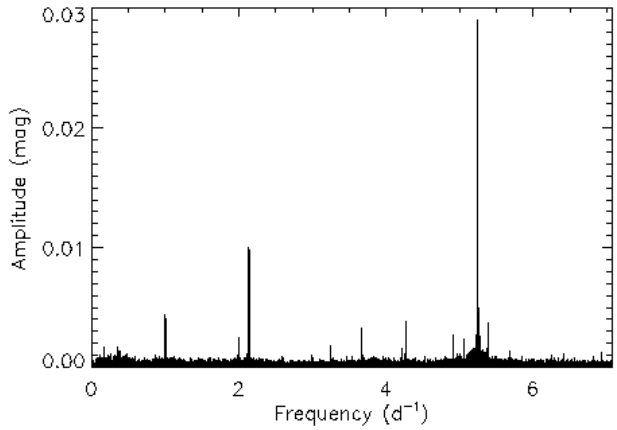

	Freq (d^{-1})	Amp (mmag)	S/N
f_1	5.249694(4)	29.1(2)	131.0
$f_2^\star$	2.13639(1)	10.0(2)	41.8
$f_3^\star$	4.27280(3)	3.7(2)	17.0
f_4	5.38584(3)	3.5(2)	17.3
f_5	5.05853(4)	2.5(2)	11.7
f_6	4.92034(5)	2.3(2)	11.4
$f_7^\star$	4.22128(7)	1.5(2)	6.7
$f_8^\star$	6.40906(8)	1.4(2)	7.0

Figure 3.14: Spectrum of β Cep (HD 205021, HIP 106032)

Table 3.12: Significant frequencies found in β Cep (HD 205021, HIP 106032)

The β Cep system consists of three stars. β Cep is the primary of a spectroscopic binary and there is also a distant visual tertiary component [Pigulski and Boratyn, 1992].

Aerts et al. [1994] reported frequencies of 5.2497 d^{-1}, 5.385 d^{-1} and 4.920 d^{-1}. These frequencies can be seen in the *SMEI* data in frequencies f_1, f_4 and f_6 respectively (see Table 3.12). Telting et al. [1997] confirmed the frequencies by Aerts et al. [1994] and also reported additional frequencies of 5.08388 d^{-1} and 5.41712 d^{-1}. The first is shown in f_5, Table 3.12, however the later is not detected in the *SMEI* data.

A frequency of 2.13639 d^{-1} (f_2, Table 3.12) and multiples thereof (f_3 and f_8, Table 3.12) are also detected in the *SMEI* data set, which have not been reported previously. A further frequency at 4.221280 d^{-1} was also detected with *SMEI* satellite (f_7, Table 3.12).

HD 214993; HIP 112031; DD Lac

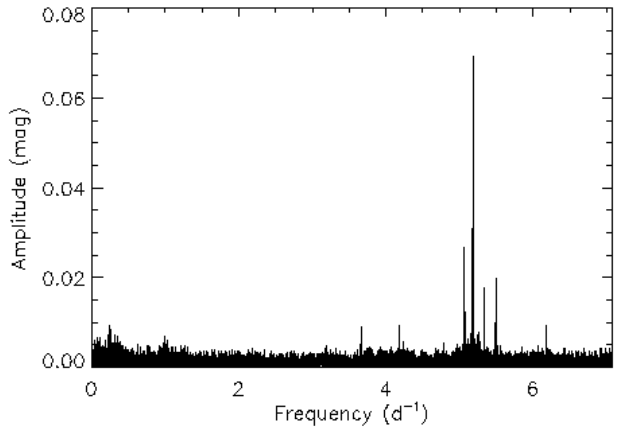

	Freq (d^{-1})	Amp (mmag)	S/N
f_1	5.178998(8)	72.0(1)	57.0
f_2	5.06637(2)	30.0(1)	22.5
f_3	5.49022(3)	21.0(1)	17.4
f_4	5.33427(3)	18.0(1)	14.5
$f_5^\star$	3.66038(6)	9.0(1)	6.7
f_6	0.35543(8)	8.0(1)	4.1
f_7	4.2409(1)	6.0(1)	4.5

Figure 3.15: Spectrum of DD Lac (HD 214993, HIP 112031)

Table 3.13: Significant frequencies found in DD Lac (HD 214993, HIP 112031)

DD Lac is a spectroscopic binary with a period of 0.1931 days, corresponding to a frequency of 5.17866 d^{-1}. Mathias et al. [1994b] reported frequencies of 5.06637 d^{-1}, 5.17893 d^{-1}, 5.33419 d^{-1} and 5.48998 d^{-1}, which can be seen in f_2, f_1, f_4 and f_3 respectively (see Table 3.13). The equally spaced frequencies of 5.17893 d^{-1}, 5.33419 d^{-1} and 5.48998 d^{-1} were previously suspected to be a rotationally split triplet, but this hypothesis was proved incorrect by work from Handler et al. [2006] and actually consists of three modes of different spherical degree.

Further to this Handler et al. [2006] confirmed all the frequencies that were reported in Mathias et al. [1994b], using photometric observations carried out at nine different observatories over a period of 190 nights. They also reported on the following additional frequencies below the *SMEI* Nyquist frequency: 0.35529 d^{-1}, 4.24034 d^{-1}, 5.21648 d^{-1}, 5.30786 d^{-1}, 5.8341 d^{-1}, 5.84454 d^{-1} and 6.7023 d^{-1}. Desmet et al. [2009] confirmed all the frequencies reported by Mathias et al. [1994b] and also Handler et al. [2006]. Of these frequencies, only 0.35529 d^{-1} and 4.24034 d^{-1} were confirmed in the *SMEI* data, which are shown in f_6 and f_7 respectively (see Table 3.13). The remaining frequencies were undetected. A further frequency of 3.66038 d^{-1}, f_5, was also detected in the *SMEI* data.

3.2.3 Conclusion

Analysis of the 12 stars presented in this thesis and those analysed by Stevens found that many of the new frequencies detected have lower amplitudes than those previously detected with ground based observations.

From the analysis of all 27 β Cephei stars, a total of 78 frequencies were detected in the β Cephei range (3 d^{-1} or higher), 26 of which had previously been undetected. These new frequencies were found in 14 of the 27 stars. 35 frequencies were detected where the frequencies fell below 3 d^{-1}, 20 of which had been previously undetected. The new lower pulsation frequencies were found in 7 of the 27 stars. Frequencies that lie below 3 d^{-1} fall into the SPB category, so it possible that the presence of these frequencies suggest that some of these stars maybe β Cephei-SPB hybrid stars.

Further significant frequencies were also observed in the β Cephei stars but these were the results of combinations of frequencies already detected or binary effects.

By analysing the light curves of the confirmed β Cephei stars we are able to improve the accuracy and precision of the frequencies that have already been confirmed. The detection of new frequencies has increased the overall number of known frequencies in individual stars. By obtaining a more complete picture of the frequencies present in an individual star we are able to use current stellar models to provide an accurate model of the star. These frequencies can also be used to help confirm and/or improve the current stellar models. For example, if a frequency is present in a star that is not predicted by the models, this may suggest that the stellar physics in the model is not completely accurate and needs refining. An improvement on the stellar models will hence improve our understanding of stellar structure and their evolution.

These frequencies could also be used in further analysis, along with previously detected frequencies, to determine any frequency changes that might be due to the stars evolution. However this requires an in-depth analysis of the stars individually.

3.3 Survey to search for β Cephei stars

The aim of the survey is to detect potentially new β Cephei stars using photometric data from the *SMEI* instrument. With observations of over 12,000 stars in the sky covering an observational period of over 5 years, *SMEI* has the potential to discover β Cephei stars which have previously remained undetected.

3.3.1 Analysis

Target selection

A list of target stars was created which were then analysed to determine if any of them showed β Cephei-like frequencies. This list was created using data from The Bright Star Catalogue [Hoffleit and Jaschek, 1991]. A set of three criteria were used to determine which stars from the catalogue would be analysed.

1. The spectral types of most of the known β Cephei stars are B0 to B3 [Stankov and Handler, 2005]. Therefore only stars which have been classified as B0 to B3 in The Bright Star Catalogue were selected for analysis.

2. *SMEI* can only detect millimagnitude brightness changes in stars brighter than 6.5 in magnitude, so only stars brighter than 6.5 were selected. At fainter magnitudes noise levels increase significantly above the millimagnitude level.

3. Only stars further than 10° from the Galactic Plane were selected. As the stellar density increases closer to the Galactic Plane, the overcrowding of stars close to or on the Galactic Plane is an issue with *SMEI*. Observations of stars close to the Galactic Plane risk being contaminated by the light from other stars.

The final target list from The Bright Star Catalogue comprised of 302 stars. This list was compared to the stars observed by *SMEI*. In total 213 stars out of the 302 stars from The Bright Star Catalogue were observed with *SMEI* and were analysed in this survey.

Data analysis pipeline

The light curves for each of the 213 stars were then converted into magnitudes for analysis (see Section 2.1.3) and analysed for β Cephei-like frequencies. The individual analysis of 213 light curves using Period04 would be very time consuming. Therefore a pipeline was developed incorporating the Least-squares spectrum [Frandsen et al., 1995]. The pipeline searches for the frequency with the highest amplitude in the amplitude spectra. Since β Cephei stars have frequencies that range between 3 and 15 d^{-1}, frequencies below 1 d^{-1} were not analysed to speed up the processing. The frequency with the highest amplitude is then recorded and cleaned from the light curve to search for the frequency with the next highest amplitude. This process is repeated until no more significant frequencies are left (see following section, Chapter 3.3.1, for information on what makes a frequency significant). The pipeline then moves on to the next star on list for analysis.

The 4.0 S/N test

Traditionally a frequency was classed as significant if the S/N (the ratio of the signal amplitude to mean noise) was greater than four (Breger et al. [1993]; Kuschnig et al. [1997]). This threshold corresponds to a low false-alarm probability when datasets of length typically used in ground-based observations are analysed. Work by Tarrant [Tarrant, 2010] found that data collected over longer durations, for example those from space-based telescopes, require a higher S/N criterion in order to keep the result significant. This is explained below.

The amplitude spectrum follows the χ distribution. The probability that a random variable X has a value higher than a given value of x is given by:

$$P(x < X) = \frac{\Gamma(n/2, x^2/2)}{\Gamma(n/2)}, \tag{3.1}$$

where $\Gamma(a, s)$ is the upper incomplete gamma function and is given by:

$$\Gamma(a,s) = \int_s^{+\infty} e^{-t} t^{a-1} dt. \tag{3.2}$$

For 2 degrees of freedom (d.o.f., n=2), the probability that a random variable X has a value higher than a given value of x simplifies to:

$$P(x < X) = \frac{\Gamma(1, x^2/2)}{\Gamma(1)} = e^{\frac{-x^2}{2}}. \tag{3.3}$$

The mean value of a χ distribution is given by:

$$\mu = \sqrt{2}\frac{\Gamma((n+1)/2)}{\Gamma(n/2)}. \tag{3.4}$$

For a value of x with 4 times this number at 2 d.o.f., $x = 4.0\mu = 4.0\sqrt{2}\Gamma(1.5)/\Gamma(1) \approx 5.01$. When entered into Equation 3.3, the probability of a random value X being greater than 5.01 is $p(S/N < X) = 3.48763 \times 10^{-6}$.

The probability of observing at least 1 spike greater than 5.01 across many bins is given by:

$$P = 1 - [1 - p(S/N < X)]^N, \tag{3.5}$$

where N is the number of bins and is calculated by $N = \Delta_f T$, where T is the total time observed and Δ_f is the frequency range analysed. Therefore with increasing observational periods the value of N increases. The *SMEI* instrument has been collecting data for over 5 years and as a result the number of bins in the analysis $\approx$ 13,000 or greater, over a frequency range of 0 to 7.08 d^{-1}. By substituting this into Equation 3.5 we find that there is a almost a 5% probability a random value could lie higher than the amplitude S/N ratio of 4.0.

To reduce this probability down to 1% the S/N criterion must be higher than 4.0. To work out the new value for the S/N the above calculations were worked through backwards to find what $p(S/N < X)$ should be for a 1% error. The results of this

find that $p(S/N < X) = 7.77 \times 10^{-7}$ and for this to occur the boundary for the S/N criterion needs to lie at 4.23. The error on the S/N is 0.13, where the S/N is marginal on a typical *SMEI* light curve. We therefore included frequencies for analysis where the S/N was greater than 4.10.

The noise level around a signal was determined by creating a histogram of the amplitudes in a ± 0.1 d^{-1} range of the signal frequency. A Gaussian was then fitted over the histogram. The calculated mean of the Gaussian was taken as the mean value of the noise. Calculating the mean noise using this method ensures that the large amplitude of the signal would lie so far away from the other amplitudes in the histogram that it would not be included in the Gaussian fit. Therefore the signal amplitude would not skew the calculated value of the mean noise.

1 day alias cutoff

As described in Chapter 2.1.3 frequencies that occur at 1 d^{-1} and multiples thereof are present in the light curves due to the Sun-synchronous orbit of the *SMEI* instrument about the Earth. These frequencies should not be included in the analysis as they are not genuine oscillations from the star. Therefore a cutoff frequency is required in the pipeline to determine at what point frequencies should be included in the analysis.

Figure 3.16 shows a graph of how the number of frequencies observed changed using different cutoff values. Obviously the larger the cutoff value the more frequencies are excluded from the analysis. If the frequencies were uniformly distributed then one would expect the number of frequencies to fall linearly with increasing cutoff value. However, because of the clustering of frequencies around the 1 d^{-1} aliases, larger numbers of frequencies are removed at 1 d^{-1} and multiples thereof.

Figure 3.16 shows that the frequencies start to fall linearly between 0.03 and 0.04 d^{-1}. Therefore a cutoff frequency of ± 0.04 d^{-1} either side of the 1 d^{-1} frequency and multiples thereof was adopted. This means that any genuine frequency from a star that fell within this range would not be included in the analysis.

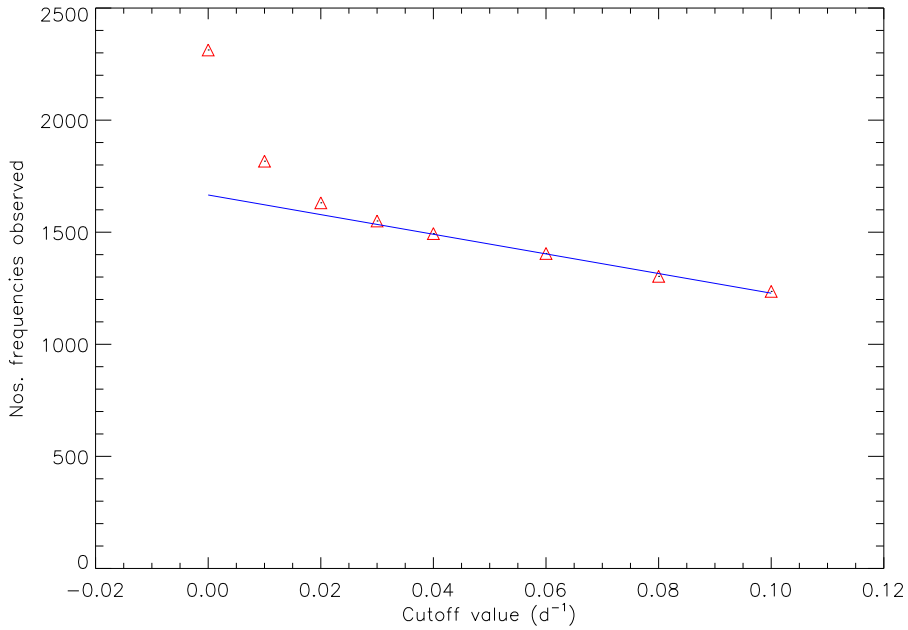

Figure 3.16: A graph to illustrate the number of frequencies observed with increasing cutoff values around with 1 day alias frequencies. The red triangles show the number of frequencies observed. The blue line is a fitted line to the final points.

Further research

Each of the stars in the survey were then checked to determine if they were part of a known binary system using the 9th Catalogue of Spectroscopic Binary Orbits [Pourbaix et al., 2004], although some binary periods were found using alternative sources. The periods of the binary systems were then compared to the periods found in the photometric data to determine if any of the frequencies found were due to binarity. Those frequencies that were found to be due to binarity were removed from the frequency list. Known binary periods are listed alongside their respective stars in Tables 3.15, 3.16 and 3.17.

The effective temperatures and bolometric corrections were calculated for the survey stars using equations provided by Balona [1984]. The Strömgren values required for these calculations were obtained from Hauck and Mermilliod [1997]. The bolometric corrections were used to calculate the luminosities of the stars. The effective temperatures and stellar luminosities are listed against their respective stars in Tables 3.15, 3.16 and 3.17. Those stars which do not have a value for their effective temperature

and luminosity are stars where Strömgren values from Hauck and Mermilliod [1997] could not be obtained. Strömgren values can be obtain from other sources but for consistency in the analysis these values were left blank. Right ascension, declination and magnitude are from The Bright Star Catalogue [Hoffleit and Jaschek, 1991].

Stars which were already confirmed as β Cephei stars in Stankov and Handler [2005] were not re-analysed in this project. These stars have previously been analysed, the results of which are presented in Chapter 3.2.

Individual analysis

Once frequencies due to instrumentation and binarity were removed from the analysis, the number of stars suspected to be β Cephei-like could be determined. Each of these stars were analysed in more detail using Period04, where frequencies were analysed between 0 and 7.08 d^{-1}. Uncertainties on the frequency, amplitude and phase were determined using Monte Carlo simulations provided by Period04. In total 13 stars showed frequencies above 3 d^{-1} which were not due to binarity or instrumentation effects, and which had not previously been confirmed as β Cephei stars.

A detailed literature review of each of the suspected β Cephei stars was also undertaken. This review was used to determine whether frequencies observed had been seen before, if any of the frequencies were due to other effects, for example, stellar rotation, and if the stars had any previous classifications. By obtaining values for the effective temperature (T) and stellar luminosity (L) the radius (R) of the star can be estimated using

$$\left(\frac{L}{L_\odot}\right) = \left(\frac{R}{R_\odot}\right)^2 \left(\frac{T}{T_\odot}\right)^4. \tag{3.6}$$

The lower limit for the rotational frequency can then be calculated if the $v\sin i$ of the star is known using the equation for angular velocity

$$v \sin i = 2\pi f R, \tag{3.7}$$

where f is the frequency of rotation of the star and R is the radius of the star.

The Roche model [Maeder, 2009] uses the mass of the star to calculate the angular velocity for the upper rotational frequency, i.e.

$$\Omega^2_{\max} = 0.7215\pi G\overline{\rho} \tag{3.8}$$

where Ω is the angular velocity and $\overline{\rho}$ is the mean density.

13 stars were found to have frequencies above 3 d^{-1}, which had not already been confirmed as β Cephei stars. The frequencies detected in two of these stars were found to be due to stellar rotation and five of the stars were already confirmed Be type stars. Therefore a total of six stars were found to have oscillations above 3 d^{-1} which could be β Cephei like in nature and have not previously been reported as β Cephei stars. An overview of the observational data collected on these stars is presented in Table 3.20 and results are presented in Section 3.3.3.

3.3.2 Survey Characteristics

213 stars were analysed in the survey to search for stellar frequencies which could possibly be related to β Cephei-like pulsations. Frequencies were searched for in the photometric data between 1 and 7.08 d^{-1} (as previously mentioned, frequencies below 1 d^{-1} were not searched for to speed up processing). Stars where a frequency was detected above 3 d^{-1} are listed in Table 3.15 along with their frequencies, of which there are 27 stars. Stars where a frequency was detected between 1 and 3 d^{-1} are listed in Table 3.16, for which there are 31 stars. 155 stars did not show evidence of a significant frequency between 1 and 7.08 d^{-1} and are listed in Table 3.17. This information is summarised in Table 3.14, along with information about how many of these stars are already confirmed as β Cephei stars [Stankov and Handler, 2005], those which are candidate β Cephei stars [Stankov and Handler, 2005] and those which have been confirmed as Be stars in Simbad [Wenger et al., 2000]. Stars of different classifications are listed under *Other*.

Table 3.14: A table to indicate the number of different star types within the survey. [1] as stated by Stankov and Handler [2005].

Type of star	Freq > 3 d^{-1}	1 d^{-1} $<$ Freq < 3 d^{-1}	No freq	**Total**
Confirmed β Cephei stars[1]	14	1	4	**19**
Candidate β Cephei stars[1]	0	2	20	**22**
Be stars	5	15	21	**41**
Other stars	8	13	110	**131**
Total	**27**	**31**	**155**	**213**

For the survey Kolmogorov-Smirnov tests were used to compare the effective temperatures and stellar luminosities of the stars that fell into the following groups:

- stars where a frequency, or frequencies, were detected above 3 d^{-1} (Freq > 3 d^{-1}),
- stars where a frequency, or frequencies, were detected between 1 and 3 d^{-1} (Freq < 3 d^{-1}),
- stars were no frequencies were detected (no Freq)

The first of these groups was then split into two, to determine difference between stars which had frequencies only greater than 3 d^{-1} and stars where frequencies were observed both greater than and less than 3 d^{-1}:

- stars where only a frequency, or frequencies, greater than 3 d^{-1} were detected (Freq ONLY > 3 d^{-1}) and
- stars where frequencies less than AND greater than 3 d^{-1} were detected (Freq > 3 d^{-1} AND Freq < 3 d^{-1}).

The Kolmogorov-Smirnov tests helped determine whether trends were present in the survey relating temperature and luminosity to the observed frequencies. The results of the Kolmogorov-Smirnov tests are presented in the following sections.

Table 3.15: Stars in the survey where a frequency above 3 d^{-1} was detected. The table shows the stars HIP number, right ascension (RA), declination (Dec), apparent magnitude (m_v), effective temperature (T_{eff}), luminosity ($\log(L/L_\odot)$), frequency, amplitude, signal-to-noise (S/N), known binary periods associated with the system according to: [1] Pourbaix et al. [2009], [2] Uytterhoeven et al. [2004b] and [3] Balona and Cuypers [1993], Simbad classification and β Cephei classification according to Stankov and Handler [2005].

HIP	HD	RA	Dec	m_v	T_{eff}	$\log(L/L_\odot)$	Freq (d^{-1})	Amp (mag)	S/N	Binary frequencies	Simbad classification	SH05
8068	10516	01 43 39	+50 41 19	3.98			1.931	0.0118	13.1516	[1] 0.0079 d^{-1}	Var. star with	
							1.899	0.0116	13.0100		rapid variations	
							1.851	0.0115	15.0764			
							3.396	0.0043	6.5702			
							2.090	0.0039	7.2564			
							1.872	0.0031	4.6361			
							3.626	0.0029	4.5071			
							1.803	0.0025	4.1424			
12387	16582	02 39 28	+00 19 42	4.01	20351	3.85	6.205	0.0292	7.2551		β Cep	Confirmed
18532	24760	03 57 51	+40 00 36	2.83	25699	4.50	5.898	0.0110	30.8560	[1] 0.4028 d^{-1}	β Cep,	Confirmed
							5.682	0.0033	10.5015		includes comps	
							6.256	0.0022	9.1821			
							4.873	0.0013	5.0984			
18724	25204	04 00 40	+12 29 25	3.38	16033	2.90	1.363	0.0096	5.5411	[1] Aa 0.2530 d^{-1}	Eclips. binary	
							3.506	0.0085	5.6762	[1] AB 0.0302 d^{-1}	of Algol type	
21444	29248	04 36 19	−03 21 08	3.87	21089	3.97	5.654	0.0367	17.5059		β Cep	Confirmed
							5.620	0.0368	16.4543			
							5.763	0.0369	22.6065			
							5.637	0.0244	37.7401			
							2.754	0.0065	7.5052			
23972	33328	05 09 08	−08 45 14	4.19	21186	4.15	1.425	0.0044	13.5363		Be star	Rejected
							4.835	0.0018	7.7109			
							1.309	0.0014	5.3193			
30122	44402	06 20 18	−30 03 48	2.95	17566	3.11	3.247	0.0029	12.1822	[1] 0.0015 d^{-1}	Cepheid var. star	
							1.080	0.0014	5.9160			
30324	44743	06 22 41	−17 57 21	1.89	23212	4.34	4.183	0.0027	13.7498		β Cep	Confirmed
31125	46328	06 31 51	−23 25 06	4.26	23678	4.49	4.769	0.0096	11.5421		β Cep	Confirmed
33558	52092	06 58 25	−34 06 42	5.02	16375	2.92	4.958	0.0045	4.6701		Star	
38438	64722	07 52 29	−54 22 01	5.68	22909	4.10	5.505	0.0135	4.7097		β Cep	Confirmed
59196	105435	12 08 05	−50 39 40	4.40			1.780	0.0030	7.1236		Be star	
							6.172	0.0025	7.5233			
60710	108257	12 26 31	−51 27 02	4.77	16279	2.98	4.804	0.0045	5.5927		In double system	
70574	126341	14 26 08	−45 13 17	4.51	19657	3.75	5.638	0.0086	13.0910		β Cep	Confirmed

Continued on Next Page...

Table 3.15: (continued)

HIP	HD	RA	Dec	m_v	T_{eff}	$\log(L/L_\odot)$	Freq (d^{-1})	Amp (mag)	S/N	Binary frequencies	Simbad classification	SH05
							3.397	0.0069	10.9924			
71860	129056	14 41 55	−47 23 17	2.23	20439	4.00	3.843	0.0056	8.7982		β Cep	Confirmed
							3.318	0.0024	7.6256			
75141	136298	15 21 22	−40 38 50	3.14	21158	3.91	1.622	0.0049	11.0236		β Cep	Confirmed
							2.703	0.0031	9.7283			
							1.275	0.0024	5.9866			
							5.902	0.0022	5.8257			
80112	147165	16 21 11	−25 35 33	2.92	23541	4.22	4.049	0.0032	7.8189	[1] 0.0292 d^{-1}	β Cep	Confirmed
							4.173	0.0031	7.1469			
85927	158926	17 33 36	−37 06 13	1.52	21127	3.94	4.685	0.0066	9.8026	[2] 0.1680 d^{-1}	β Cep,	Confirmed
							4.815	0.0019	5.8596	[2] 0.0009 d^{-1}	also binary	
							5.338	0.0015	5.4043			
88149	164284	18 00 15	+04 22 07	4.74			4.882	0.0118	13.2301		Be star	
							2.208	0.0055	7.1235			
							2.278	0.0042	10.6714			
89290	166596	18 13 12	−41 20 09	5.41	16255	4.53	3.335	0.0143	4.8418		Var. star	
92609	173948	18 52 13	−62 11 15	4.17	19044	4.44	1.638	0.0157	16.8971		Be star	
							1.476	0.0041	4.7792			
							1.162	0.0033	4.5394			
							3.162	0.0023	4.3665			
93808	178329	19 06 17	+41 24 49	6.45	16518	2.95	4.801	0.0063	4.2551	[1] 0.9700 d^{-1}	Spec. binary	
95408	182180	19 24 14	−27 50 41	6.04	17719	3.24	3.833	0.0308	10.4488		Star	
106032	205021	21 28 39	+70 33 38	3.14	23268	4.19	5.250	0.0129	20.0585	[1] 0.0918 d^{-1}	β Cep	Confirmed
							5.386	0.0026	8.1847			
							2.136	0.0023	8.9747			
							3.675	0.0019	10.3569			
							4.920	0.0012	5.5414			
111544	214168	22 35 52	+39 37 41	6.49	20952	3.56	5.176	0.0037	4.3100		In double system	
112031	214993	22 41 28	+40 13 31	5.20	21818	4.03	5.179	0.0500	63.4921		β Cep	Confirmed
							5.069	0.0239	6.4315			
							5.337	0.0179	4.1300			
							5.490	0.0149	4.7623			
113281	216916	22 56 23	+41 36 13	5.55	20992	3.76	5.853	0.0087	7.2415	[1] 0.0827 d^{-1}	β Cep	Confirmed
							5.504	0.0067	6.4467			

Table 3.16: Stars in the survey where a frequency between 1 d^{-1} and 3 d^{-1} was detected. The table shows the stars HIP number, right ascension (RA), declination (Dec), apparent magnitude (m_v), effective temperature (T_{eff}), luminosity ($\log(L/L_\odot)$), frequency, amplitude, signal-to-noise (S/N), known binary periods associated with the system according to: [1] Pourbaix et al. [2009], [2] Uytterhoeven et al. [2004b] and [3] Balona and Cuypers [1993], Simbad classification and β Cephei classification according to Stankov and Handler [2005].

HIP	HD	RA	Dec	m_v	T_{eff}	$\log(L/L_\odot)$	Freq (d^{-1})	Amp (mag)	S/N	Binary frequencies	Simbad classification	SH05
7588	10144	01 37 42	−57 14 11	0.42			1.449	0.0031	5.4012		Be star	
							1.370	0.0027	5.6485			
							1.550	0.0025	5.0946			
							1.775	0.0021	7.5030			
							1.727	0.0019	4.3439			
17448	23180	03 44 19	+32 17 17	3.86	20637	4.11	2.450	0.0021	5.0385	[1] 0.2263 d^{-1}	Ellips. var. star, includes comps	
20922	28497	04 29 06	−13 02 54	5.54			1.538	0.0169	4.9219		Be star	
25142	35149	05 22 50	+03 32 40	4.94	21708	3.89	1.317	0.0034	5.1291		Var. star	Candidate
25281	35411	05 24 28	−02 23 49	3.29	24334	4.23	2.317	0.0180	11.4802	[1] Aab 0.1252 d^{-1}	β Cep,	Confirmed
										[1] Ac 0.0003 d^{-1}	eclipsing comp.	
25302	35439	05 24 44	+01 50 47	4.82	20000	4.44	1.305	0.0158	5.5308		Be star	
							1.496	0.0104	5.5453			
							2.798	0.0101	5.0080			
							1.679	0.0088	6.8539			
26594	37490	05 38 59	+04 08 19	4.57	16383	4.36	1.053	0.0172	8.1460		Be star	
28744	41335	06 04 13	−06 42 32	5.22			1.418	0.0042	5.6994	[1] 0.0124 d^{-1}	Be star	
28756	41534	06 04 20	−32 10 21	5.58	18533	3.31	2.091	0.0046	4.2777		Double/multiple star,	
							1.277	0.0044	4.5881		includes comps	
28973	41814	06 06 51	−11 10 24	6.61	17238	3.02	2.502	0.0684	4.1073		Var. star	
30214	44458	06 21 24	−11 46 23	5.54			1.904	0.0110	18.0553		Be star,	
							1.083	0.0035	6.1636		includes comps	
32292	48917	06 44 28	−31 04 13	5.18			1.337	0.0076	7.6051		Be star	
32385	49131	06 45 31	−30 56 56	5.58	15998	5.40	1.337	0.0069	6.2474		Be star, includes comps	
32759	50013	06 49 31	−32 32 31	3.96			1.406	0.0095	9.3162		Be star	
							1.615	0.0085	10.4779			
							1.316	0.0081	6.2959			
							1.459	0.0076	7.9696			
							1.353	0.0064	4.7177			
							1.562	0.0047	4.8461			

Continued on Next Page...

Table 3.16: (continued)

HIP	HD	RA	Dec	m_v	T_{eff}	$\log(L/L_\odot)$	Freq (d^{-1})	Amp (mag)	S/N	Binary frequencies	Simbad classification	SH05
38500	64740	07 53 03	−49 36 47	4.54	23503	4.08	1.375	0.0085	7.4958		Star	
39225	66546	08 01 23	−54 30 55	6.11	17935	3.45	1.591	0.0079	6.9191		Eclipsing binary	
							1.193	0.0073	8.5856		of Algol type	
44626	78764	09 05 38	−70 32 18	4.61	14920	5.19	1.553	0.0117	6.2369		Be star	
65630	116862	13 27 20	−49 22 52	6.23	16716	3.66	1.248	0.0145	4.2763		Star	
71352	127972	14 35 30	−42 09 27	2.27			1.554	0.0290	7.6831		Be star	
							1.733	0.0082	4.2003			
73624	132955	15 02 59	−32 38 35	5.41	16577	2.87	1.155	0.0083	6.5581		In double system	
76013	137387	15 31 30	−73 23 22	5.35			1.615	0.0145	5.8161		Be star	
							1.210	0.0078	4.1789			
76600	139365	15 38 39	−29 46 39	3.60	17494	3.04	1.449	0.0029	5.7568	[1] 0.3039 d^{-1}	Spec. binary	
							1.739	0.0024	4.4649			
78168	142883	15 57 40	−20 58 58	5.85	16233	2.76	1.087	0.0251	11.3711	[1] 0.0995 d^{-1}	Cepheid var. star	Candidate
							1.522	0.0171	7.8088			
							1.739	0.0166	8.0626			
							2.826	0.0112	5.9315			
							2.386	0.0108	6.0393			
							1.951	0.0096	4.3497			
							1.307	0.0095	4.6594			
86768	161056	17 43 47	−07 04 46	6.37	18474	4.00	1.928	0.0118	4.1211		Star	
90422	169467	18 26 58	−45 58 05	3.42	16690	3.02	1.075	0.0034	4.5990		Star	
							1.212	0.0027	4.7026			
							1.403	0.0025	4.3706			
92855	175191	18 55 15	−26 17 47	2.01	18294	3.25	1.590	0.0021	5.6314		In double system	
95176	181615	19 21 43	−15 57 18	4.57			1.728	0.0065	5.9759	[1] 0.0072 d^{-1}	Be star	
105138	202904	21 17 55	+34 53 48	4.37			1.520	0.0078	8.2501		Be star	
							1.293	0.0071	4.7947			
							1.474	0.0065	6.3352			
106723	205637	21 37 04	−19 27 57	4.45	14373	4.53	1.829	0.0039	5.2931		Be star	
109332	210191	22 08 58	−18 31 10	5.75	17031	3.59	1.506	0.0040	4.2717		Star	
117315	223145	23 47 15	−50 13 35	5.12	16943	3.09	1.362	0.0032	6.8193		Star	

Table 3.17: Stars in the survey where non significant frequencies were detected. The table shows the stars HIP number, right ascension (RA), declination (Dec), apparent magnitude (m_v), effective temperature (T_{eff}), luminosity ($\log(L/L_\odot)$), known binary periods associated with the system according to: [1] Pourbaix et al. [2009], [2] Uytterhoeven et al. [2004b] and [3] Balona and Cuypers [1993], Simbad classification and β Cephei classification according to Stankov and Handler [2005].

HIP	HD	RA	Dec	m_v	T_{eff}	$\log(L/L_\odot)$	Binary frequencies	Simbad classification	SH05
5062	6300	01 04 46	+51 00 35	6.51	16139	2.99		Star	
12719	16908	02 43 27	+27 42 25	4.61	16421	2.99	[1] 0.0020 d^{-1}	Spec. binary	
14131	19400	03 02 15	−71 54 08	5.47	14300	2.69		Double/multiple star includes comps	
14514	19374	03 07 25	+17 52 47	6.09	21538	3.58		β Cep	Rejected
16518	21856	03 32 40	+35 27 42	5.88	23693	4.11		Var. star	Candidate
17563	23466	03 45 40	+06 03 00	5.31	16619	2.97	[1] 0.4153 d^{-1}	Spec. binary	
17771	23793	03 48 16	+11 08 36	5.03	16186	2.92		Var. star, includes comps	
18081	24131	03 51 53	+34 21 32	5.78	22319	3.94		In double system	
18246	24398	03 54 07	+31 53 01	2.90	20412	4.63		Var. star	
18434	24640	03 56 28	+35 04 51	5.48	20304	3.56		Cepheid var. star	Rejected
19860	26912	04 15 32	+08 53 32	4.27	15494	3.07		Star	
20533	27778	04 23 57	+24 18 13	6.36	15535	2.93		In double system	
21060	28873	04 30 50	−44 57 13	5.00	19107	3.40		Star	
21881	29763	04 42 14	+22 57 25	4.24	16030	2.77	[1] 0.3382 d^{-1}	Spec. binary, includes comps	
22024	30076	04 44 05	−08 30 12	5.76				Be star	
22549	30836	04 51 12	+05 36 18	3.62	19075	3.90	[1] 0.1050 d^{-1}	Spec. binary	
22797	31237	04 54 15	+02 26 26	3.65	18958	3.93	[1] 0.2702 d^{-1}	Ellips. var. star	
23060	31726	04 57 44	−14 13 54	6.08	22258	3.82		Star	
23364	32249	05 01 26	−07 10 26	4.73	18101	3.29		Star	
23551	32612	05 03 52	−14 22 12	6.35	18962	3.34		Star	
23734	32343	05 06 08	+58 58 20	5.20	11881	6.16		Be star	
23883	32991	05 07 55	+21 42 17	5.87				Be star	
24845	34816	05 19 34	−13 10 36	4.20	27059	4.49		Star	
24847	34748	05 19 35	−01 24 42	6.30	19279	3.57		Star	
25028	35007	05 21 31	−00 24 59	5.63	17113	3.06		In double system	
25041	34989	05 21 43	+08 25 42	5.74	24205	4.12		Star in nebula	
25044	35039	05 21 45	−00 22 57	4.72	18747	3.65	[1] 0.0034 d^{-1}	Spec. binary	
25202	35337	05 23 30	−13 55 38	5.16	21942	3.84		Star	
25336	35468	05 25 07	+06 20 59	1.55	19996	3.86		Var. star	Rejected
25473	35715	05 26 50	+03 05 44	4.51	22802	4.00	[1] 0.3959 d^{-1}	β Cep,	Confirmed
25582	35912	05 28 01	+01 17 53	6.34	18482	3.28		Star	

Continued on Next Page...

Table 3.17: (continued)

HIP	HD	RA	Dec	m_v	T_{eff}	$\log(L/L_\odot)$	Binary frequencies	Simbad classification	SH05
25751	36166	05 29 54	+01 47 21	5.70	20884	3.65		Var. star	Candidate
25861	36351	05 31 05	+03 21 11	5.46	20337	3.62		Double/multiple star, includes comps	
25923	36512	05 31 55	−07 18 05	4.52	29507	4.72		Var. star	Candidate
26311	37128	05 36 12	−01 12 06	1.62	23539	5.36		Emission line star	
26821	37971	05 41 41	−16 43 33	6.17	15442	3.07		Be star	
27366	38771	05 47 45	−09 40 10	2.01	25774	4.98		Var. star	
27658	39291	05 51 21	−07 31 04	5.29	20705	3.65		Var star.	Candidate
27937	40200	05 54 41	−49 37 37	6.06	15990	3.06		Star	
28199	40494	05 57 32	−35 16 59	4.31	15713	3.29		Var. star	Candidate
29276	42933	06 10 17	−54 58 07	4.64	25810	4.47	[1] 0.5979 d^{-1}	Eclipsing binary of β Lyr type	
29488	42927	06 12 46	−17 45 47	6.46	17631	3.17		Pulsating var. star	
29941	43955	06 18 13	−19 58 01	5.45	17869	3.25		Star	
30073	44112	06 19 42	−07 49 22	5.20	18155	3.37		Var. star	Candidate
31037	46189	06 30 46	−27 46 10	5.87	16736	3.07		Star	
31068	46792	06 31 10	−61 52 46	6.10	16342	3.05	[1] 0.3364 d^{-1}	Spec. binary	
3300	3901	00 42 03	+50 30 45	4.77	15688	3.17	[1] 0.0011 d^{-1}	Spec. binary	
33330	51411	06 55 54	−31 47 24	6.31	15885	2.79		In double system	
33532	51925	06 58 07	−27 09 51	6.30	19352	3.57		Var. star, includes comps	
33579	52089	06 58 37	−28 58 19	1.42	22072	4.53		In double system, includes comps	
33591	52140	06 58 43	−30 59 52	6.36	16047	2.83		In double system	
34248	54031	07 06 00	−30 39 20	6.29	16516	2.95	[3] 0.1235 d^{-1}	Eclipsing binary	
34495	54893	07 08 51	−39 39 20	4.77	16878	3.26		Cepheid var. star	
37530	62758	07 42 10	−58 37 51	6.38	17213	2.99		Star	
38020	63578	07 47 31	−46 36 30	5.17	22841	3.92		Star	
38159	63949	07 49 12	−46 51 27	5.77	22757	4.04		β Cep	Candidate
38827	65575	07 56 46	−52 58 56	3.39	16419	3.21		β Cep	Rejected
38994	66194	07 58 22	−60 51 27	5.81	15597	4.90		Be star	
39138	66591	08 00 19	−63 34 03	4.76	16709	3.04		Star	
39530	67536	08 04 30	−62 50 26	6.30	18203	3.96		β Cep	Rejected
40932	70839	08 21 12	−57 58 23	5.94	21065	4.15		Var. star	Candidate
42129	73390	08 35 15	−58 13 29	5.21	16609	3.02		Star	
42568	74375	08 40 37	−59 45 39	4.28	20360	4.11		β Cep	Rejected
42799	74280	08 43 13	+03 23 55	4.23	17770	3.33		β Cep	Rejected
47868	84567	09 45 22	−30 12 09	6.40	24458	5.13		Star	
49220	87015	10 02 48	+21 56 57	5.61	17728	3.30		Var. star	
50684	89688	10 20 48	+02 21 03	6.66	16476	3.55		β Cep	Candidate

Continued on Next Page...

Table 3.17: (continued)

HIP	HD	RA	Dec	m_v	T_{eff}	$\log(L/L_\odot)$	Binary frequencies	Simbad classification	SH05
51624	91316	10 32 48	+09 18 23	3.80	21081	5.05		Var. star, includes comps	
52633	93845	10 45 16	−80 28 10	4.45	18131	3.14		Star	
58587	104337	12 00 51	−19 39 32	5.21	20665	3.95	[2] 0.3375 d^{-1}	Ellipsoidal var. star	Candidate
59232	105521	12 08 54	−41 13 53	5.49	15243	3.92		Be star	
59449	105937	12 11 39	−52 22 06	3.91	16590	2.83		Star	
60823	108483	12 28 02	−50 13 50	3.84	19477	3.41		Var. star	Candidate
64004	113791	13 06 54	−49 54 22	4.21	19696	3.43	[1] 0.1307 d^{-1}	Spec. binary	
65247	116084	13 22 16	−52 10 58	5.87	16499	5.16		Star	
65474	116658	13 25 11	−11 09 40	0.89	22920	4.16	[1] 0.2491 d^{-1}	β Cep	Confirmed
67301	120315	13 47 32	+49 18 47	1.80	17037	2.96		Var. star	
67464	120307	13 49 30	−41 41 15	3.32	21045	3.84	[1] 0.3809 d^{-1}	Ellipsoidal var. star	Candidate
67472	120324	13 49 37	−42 28 25	3.40	15506	6.29		Be star	
68002	121263	13 55 32	−47 17 17	2.44	21969	3.93	[1] 0.1246 d^{-1}	Spec. binary	
68245	121743	13 58 16	−42 06 02	3.74	19631	3.60		Var. star	Candidate
68282	121790	13 58 40	−44 48 12	3.79	19298	3.53		Var. star	Candidate
68862	122980	14 06 02	−41 10 46	4.29	19359	3.41		β Cep	Rejected
69996	125238	14 19 24	−46 03 29	3.48	17518	3.32		Var. star	
70270	125721	14 22 38	−48 19 11	6.06	23784	4.45		Ellipsoidal var., includes comps	
71865	129116	14 41 57	−37 47 36	3.94	17758	3.16		Star	
73273	132058	14 58 31	−43 08 01	2.60	20805	3.87		Var. star	
73334	132200	14 59 09	−42 06 14	3.07	18962	3.47		Var. star, includes comps	Candidate
74117	133955	15 08 50	−45 16 47	4.00	17420	3.05		Double/multiple star, includes comps	
74449	134687	15 12 49	−44 30 01	4.76	17454	3.05	[1] 1.1094 d^{-1}	Spec. binary	
74716	135348	15 16 10	−43 29 05	6.01	16410	3.17		Star	
75264	136504	15 22 40	−44 41 22	3.31	18312	3.33	[1] 0.2193 d^{-1}	Spec. binary, includes comps	Candidate
76297	138690	15 35 08	−41 10 00	2.70	19761	3.59	[1] 0.3561 d^{-1}	Spec. binary, includes comps	
77635	141637	15 50 58	−25 45 04	4.62	20166	3.62		Star	
77811	142096	15 53 20	−20 10 01	5.03	17288	2.93	[1] 0.0802 d^{-1} [1] 0.0690 d^{-1}	Ellipsoidal var. star	
77840	142114	15 53 36	−25 19 37	4.58	17979	3.12		Double/multiple system	
78104	142669	15 56 53	−29 12 50	3.81	19602	3.52	[1] 0.2498 d^{-1}	Spec. binary includes comps	Candidate
78265	143018	15 58 51	−26 06 50	2.83	22984	4.03	[1] 0.6369 d^{-1}	eclipsing binary	Candidate

Continued on Next Page...

Table 3.17: (continued)

HIP	HD	RA	Dec	m_v	T_{eff}	$\log(L/L_\odot)$	Binary frequencies	Simbad classification	SH05
								of β Lyr type	
78384	143118	16 00 07	−38 23 47	3.34	20319	3.79		In double system	
78401	143275	16 00 20	−22 37 17	2.26	24720	4.29	[1] 0.0003 d^{-1}	Be star	
78820	144217	16 05 26	−19 48 19	2.59	23411	4.12	[1] 0.1465 d^{-1}	Spec. binary, includes comps	
78821	144218	16 05 27	−19 48 07	4.92	19177	3.30		Var. star	
78918	144294	16 06 35	−36 48 07	4.16	17605	3.20		Star	
78933	144470	16 06 48	−20 40 08	3.93	23730	4.07		β Cep	Confirmed
79374	145502	16 11 59	−19 27 38	4.01	20091	3.35	[1] 0.1801 d^{-1}	Spec. binary, includes comps	Candidate
79404	145482	16 12 18	−27 55 34	4.53	18872	3.37	[1] 0.1730 d^{-1}	Spec. binary	
80473		16 25 35	−23 26 49	4.63				Double/multiple star, includes comps	
80569	148184	16 27 01	−18 27 22	4.29			[1] 0.0072 d^{-1}	Be star	
81266	149438	16 35 52	−28 12 57	2.74	29278	4.66		Star	
83323	153261	17 01 47	−58 57 29	6.22				Be star	
83635	154445	17 05 32	+00 53 31	5.67	20978	3.83		Star	
84573	156633	17 17 19	+33 06 00	4.74	18122	3.38	[1] 0.4876 d^{-1}	eclipsing binary of β Lyr type, includes comp	
85147	156838	17 23 41	−62 50 33	5.70	18538	3.67		Star	
86414	160762	17 39 27	+46 00 22	3.75	16970	3.19	[1] 0.0088 d^{-1}	β Cep	Rejected
87280	162732	17 50 03	+48 23 38	6.75	11918	3.09	[1] 0.0115 d^{-1}	Be star	
87812	163472	17 56 18	+00 40 13	5.85	19533	3.64		β Cep	Confirmed
88213	164432	18 00 52	+06 16 05	6.32	18948	3.79		Star	
88331	164852	18 02 23	+20 50 01	5.22	16812	3.00	[1] 0.0803 d^{-1}	Spec. binary	
88346	164900	18 02 30	+22 55 23	6.19	16364	3.08		Star	
88714	165024	18 06 37	−50 05 29	3.63	21614	4.43		Star	
88886	166182	18 08 45	+20 48 52	4.30	18692	3.80		In double system	
89605	167128	18 17 07	−56 01 23	5.35	15854	3.89		Be star	
90200	168905	18 24 18	−44 06 36	5.18	17418	3.16		Var. star	
90398	170111	18 26 29	+26 27 39	6.53	16193	2.89		In double system, includes comps	
90853	170523	18 32 01	−45 45 26	5.04	14849	3.00	[1] 0.0461 d^{-1}	Spec. binary	
91014	171034	18 33 57	−33 00 59	5.24	17299	3.50		Var. star	Candidate
91918	172910	18 44 19	−35 38 30	4.80	18482	3.21		In double system, includes comp	
92243	174179	18 47 57	+31 45 24	6.01	16848	3.19		Be star	
92728	175426	18 53 43	+36 58 18	5.54	16665	3.14	[1] 0.0113 d^{-1}	Spec. binary	

Continued on Next Page...

Table 3.17: (continued)

HIP	HD	RA	Dec	m_v	T_{eff}	$\log(L/L_\odot)$	Binary frequencies	Simbad classification	SH05
93299	177003	19 00 13	+50 32 00	5.33	17884	3.15		Var. star	
93996	178175	19 08 16	−19 17 25	5.54	14973	4.44		Be star	
94481	180163	19 13 45	+39 08 45	4.36	15658	3.41	[1] 0.0177 d^{-1}	Spec. binary	
94986	180885	19 19 39	−35 25 17	5.55	15207	2.97		Star	
95219	181858	19 22 20	−08 12 03	6.65	16076	2.90		Star	
96483	184915	19 36 53	−07 01 38	4.95	21806	4.82		Star	
97244	186660	19 45 52	−02 53 00	6.48	15745	3.23		Star	
97774	188252	19 52 07	+47 55 54	5.85				Var. star	
97845	188439	19 53 01	+47 48 27	6.26	23331	4.42		β Cep	Rejected
98412	189103	19 59 44	−35 16 34	4.31	16970	3.19	[1] 0.4750 d^{-1}	Spec. binary	
99234	191263	20 08 38	+10 43 33	6.30	16717	3.03		Star	
99457	191639	20 11 10	−08 50 32	6.45	22886	4.41		Be star	
100751	193924	20 25 38	−56 44 05	1.86	17317	3.22	[1] 0.0851 d^{-1}	Spec. binary	
101909	196775	20 39 04	+15 50 17	5.93	17769	3.21		In double system	
102771	198781	20 49 17	+64 02 32	6.47	21357	4.38		Star	
105268	203467	21 19 22	+64 52 18	5.18	12452	4.95		Be star	
108022	208057	21 53 03	+25 55 30	5.04	16747	3.08		Be star	
108612	209008	22 00 07	+06 43 02	5.96	15256	3.12		Star	
110386	212076	22 21 31	+12 12 18	4.80	17620	3.97		Be star	
110672	212571	22 25 16	+01 22 38	4.74			[1] 0.0119 d^{-1}	Be star	
110790	212883	22 26 45	+37 26 37	6.41	19027	3.39		In double system includes comps	
110849	212978	22 27 26	+39 48 36	6.11	18990	3.46		Double/multiple star	
111104	213420	22 30 29	+43 07 24	4.49	18345	3.62	[1] 0.0011 d^{-1}	Spec. binary	
112778	216200	22 50 21	+41 57 12	5.94	16019	3.42		Be star	
113371	217101	22 57 36	+39 23 19	6.18	20811	3.48		Star	
113640	217543	23 00 54	+38 42 28	6.53	17759	3.34		Be star	

Table 3.18: Kolmogorov-Smirnov test results relating to the effective temperature of the different frequency groups of stars in the survey.

Comparison of frequency groups	Probability
Freq > 3 d^{-1} vs. Freq < 3 d^{-1}	0.009
Freq > 3 d^{-1} vs. no Freq	0.008
Freq < 3 d^{-1} vs. no Freq	0.258
Freq ONLY > 3 d^{-1} vs. Freq > 3 d^{-1} AND Freq < 3 d^{-1}	0.838

Kolmogorov-Smirnov test: Temperature

Table 3.18 and the left-hand side of Figure 3.17 show the Kolmogorov-Smirnov results between the different frequency groups relating to the effective temperature.

The results of the Kolmogorov-Smirnov tests show that the two groups which are most likely to be from different distributions are stars where a frequency was found to be greater than 3 d^{-1} (Freq > 3 d^{-1}) and stars where the highest frequency was found to be less than 3 d^{-1} (Freq < 3 d^{-1}). The probability of these two frequency groups being from the same distribution is 0.009, as shown in Table 3.18. The difference between the two distributions is clearly shown when comparing their two cumulative frequency distributions in the top-left hand panel of Figure 3.17. The panel shows that the stars where a frequency was found to be greater than 3 d^{-1} tended to have higher effective temperatures, with two distinct temperature points where the cumulative frequency distribution rises sharply. These occur at $\log(T_{\rm eff}) = 4.21$ and 4.32 (and possibly a third rise at $\log(T_{\rm eff}) = 4.37$). In contrast, the stars where the highest frequency was found to be lower than 3 d^{-1} tend to have lower effective temperatures with a sharp rise in the cumulative frequency distribution at $\log(T_{\rm eff}) = 4.21$.

Stars where no frequencies were detected (No Freq) and those where a frequency was detected above 3 d^{-1} (Freq > 3 d^{-1}) are also likely to be from different distributions, with a probability of 0.008. The second panel down on the left-hand side of Figure 3.17 again shows that the stars where a frequency was found greater than 3 d^{-1} tend to have higher effective temperatures than other stars in the survey.

The groups of stars where a frequency was detected above 3 d^{-1} was split into two

Table 3.19: Kolmogorov-Smirnov test results relating to the stellar luminosity of the different frequency groups of stars in the survey.

Comparison of frequency groups	Probability
Freq > 3 d^{-1} vs. Freq < 3 d^{-1}	0.524
Freq > 3 d^{-1} vs. no Freq	0.007
Freq < 3 d^{-1} vs. no Freq	0.377
Freq ONLY > 3 d^{-1} vs. Freq > 3 d^{-1} AND Freq < 3 d^{-1}	0.838

further groups, those where only frequencies greater than 3 d^{-1} were detected (Freq ONLY > 3 d^{-1}) and those where frequencies both less than and greater than 3 d^{-1} were detected (Freq > 3 d^{-1} AND Freq < 3 d^{-1}). As shown in the bottom left-hand panel of Figure 3.17 these two groups have very similar cumulative frequency distributions, with a probability of the two groups coming from the same distribution being 0.838 (Table 3.18).

In summary the Kolmogorov-Smirnov results show that the stars where a frequency was detected in the β Cephei range tend to have higher effective temperatures when compared to other stars in the survey.

Kolmogorov-Smirnov test: Luminosity

Table 3.19 and the panels in the right-hand column of Figure 3.17 show the Kolmogorov-Smirnov results between the different frequency groups relating to their stellar luminosity.

The two groups which are most likely to come from different distributions are those where a frequency was detected greater than 3 d^{-1} (Freq > 3 d^{-1}) and stars where no frequencies were found (No Freq). The probability of these two groups being from the same distribution is 0.007 (Table 3.19). As shown in the second panel down on the right-hand side of Figure 3.17, stars where a frequency was detected greater than 3 d^{-1} tend to have higher luminosities than those where no frequencies were found.

The stars where the highest frequency detected was less than 3 d^{-1} and those where the frequency was greater than 3 d^{-1} show a more similar distribution in their luminosities than in their effective temperatures. The second panel down on Figure

Table 3.20: Overview of observational data collected by *SMEI* of possible β Cephei stars. RA and Dec were obtained using Simbad.

HIP	RA	Dec	Observational dates	Nos. days	Nos. data	Duty cycle (%)
18724	04 00 40	+12 29 25	25/07/03 - 11/11/08	1937	14637	53.01
30122	06 20 18	−30 03 48	10/04/03 - 26/11/08	2058	14932	50.89
33558	06 58 25	−34 06 42	10/04/03 - 26/11/08	2058	14026	47.80
60710	12 26 31	−51 27 02	10/04/03 - 20/07/08	1929	13175	47.91
93808	19 06 17	+41 24 49	11/04/03 - 20/09/08	1989	16169	57.01
111544	22 35 52	+39 37 41	18/04/03 - 01/11/08	2024	14710	50.98

3.17 shows that stars where a frequency was detected above 3 d^{-1} tend to have higher luminosities, with a sharp increase in the distribution at approximately $\log(L/L_{\odot}) = 3.8$.

As with the Kolmogorov-Smirnov tests relating to effective temperature, the stars where a frequency was detected at greater than 3 d^{-1} were split into two groups, those where only frequencies greater than 3 d^{-1} were detected and those where frequencies both less than and greater than 3 d^{-1} were detected. The probability of these frequency groups being from the same distribution is 0.838, and show very similar cumulative frequency distributions in the bottom right-hand panel of Figure 3.17.

In summary the results of the Kolmogorov-Smirnov tests show that stars where a frequency was detected in the β Cephei range tend to have higher luminosities when compared to other stars in the survey.

3.3.3 Results on individual survey stars

Of the 213 stars analysed in this survey, 27 stars were found to have a frequency greater than 3 d^{-1}. These stars are plotted on a HR diagram in Figure 3.18 according to their stellar classification. 14 of the stars have already been confirmed as β Cephei stars in Stankov and Handler [2005], and are shown as red stars in Figure 3.18. Some of the β Cephei stars were analysed previously in Chapter 3.2. Therefore these stars will not be analysed in any more detail in the analysis of this survey.

Five confirmed β Cephei stars did not show positive results in the survey. As

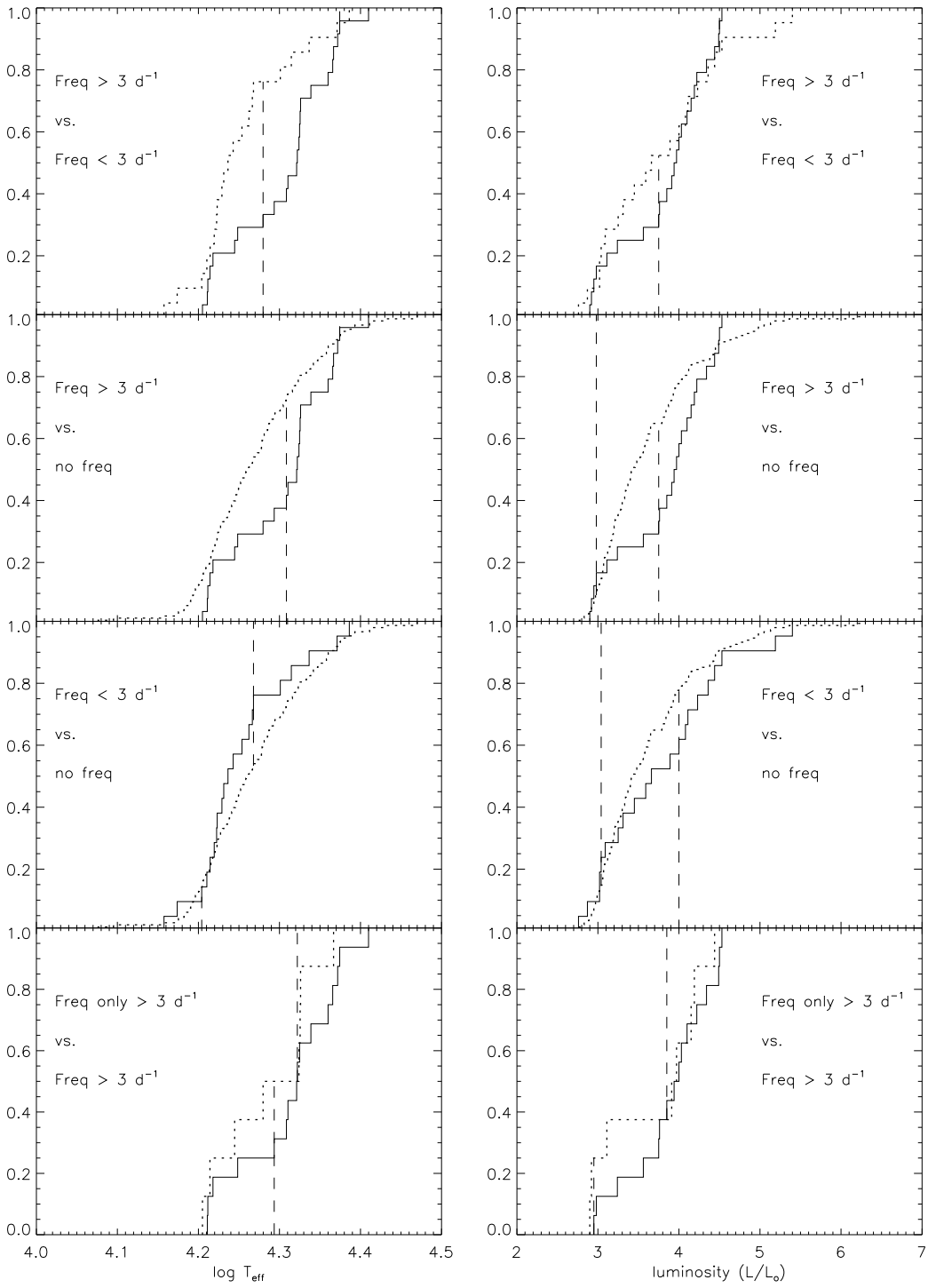

Figure 3.17: Normalised cumulative frequency distributions for Kolmogorov-Smirnov tests comparing different frequency groups. The left-hand side shows Kolmogorov-Smirnov results relating to effective temperature. The right-hand side shows the Kolmogorov-Smirnov results relating to stellar luminosity. The first frequency group stated in the title of the graph is shown by the solid line on the graph. The second frequency groups stated in the title of the graph is shown by the dotted line on the graph. The dashed lines represent point where there is the largest gap between the two distributions.

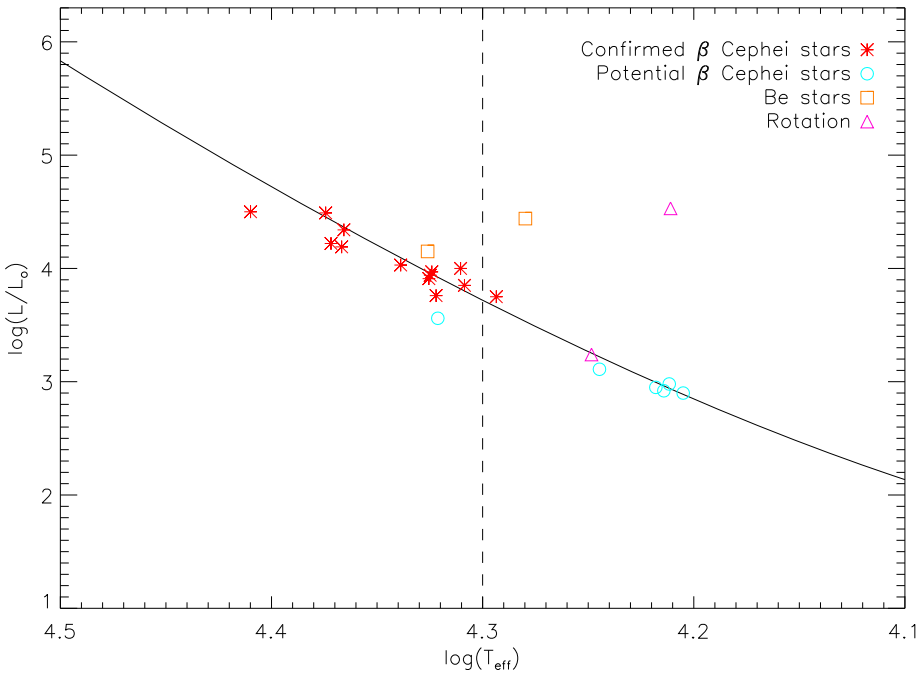

Figure 3.18: HR-diagram of stars in the survey which showed at least one significant frequency greater than 3 d^{-1}. Red stars show positions of confirmed β Cephei stars as published by Stankov and Handler [2005]. Orange squares show confirmed Be stars. Purple triangles show stars where the frequency present was due to stellar rotation. Blue circles show stars that have not been published as β Cephei stars but could potentially be β Cephei stars. The solid black line indicates the ZAMS, while the dashed line indicates the temperature boundary at approximately 20 000 K.

previously mentioned, the Nyquist frequency of the *SMEI* light curves is only 7.08 d^{-1}. Therefore β Cephei stars where the oscillations lie above this frequency will not be detected. The cutoff around the 1 day aliases means that some of the genuine stellar frequencies may not have been included in the analysis and also not all oscillations in confirmed β Cephei stars have been detected photometrically.

Of the remaining 13 stars, five have been confirmed as Be stars. These are shown as orange squares on the HR diagram in Figure 3.18. Note that only two Be stars are plotted on the HR-diagram (HIP 23972 and HIP 92609). This is because Strömgren values could not be obtained for three of the stars and hence their respective effective temperatures and stellar luminosities could not be calculated.

The frequencies from two of the 13 stars were found to be due to stellar rotation and are shown as purple triangles on the HR diagram.

The remaining six stars were analysed in more detail as suspected β Cephei candidates, and are shown as blue circles on the HR diagram. Table 3.20 gives more details on the *SMEI* data available for these stars, while Table 3.21 provides an overview of their stellar parameters.

The solid black line in Figure 3.18 represents the zero age main sequence (ZAMS) and is present to guide the eye along the main sequence. It is expected that all of these stars should lie above the ZAMS line within errors. As mentioned in Section 3.3.1, the effective temperatures and bolometric corrections were calculated using equation provided by Balona [1984], who report a standard deviation of 0.03 on $\log T_{\rm eff}$ and 0.11 mag on the magnitude. Most of the confirmed β Cephei stars have effective temperatures between 20 000 and 30 000 K [Degroote et al., 2009]. The vertical dashed line in the HR-diagram represents the lower end of the temperature boundary at 20 000 K (approximately $\log(L/L_{\odot}) = 4.3$). Most of the potentially new β Cephei candidates lie below 20 000 K, with only one star positioned above 20 000 K. However, the potential β Cephei stars do lie in the region where there are expected to be stars that oscillate with both SPB and β Cephei like pulsations. It is possible that the stars presented here

Table 3.21: Overview of stellar parameters of the six stars being investigated as potential β Cephei stars. [1] Hoffleit and Jaschek [1991], [2] Abt et al. [2002], [3] Glebocki and Gnacinski [2005], [4] Hohle et al. [2010] and [5] Tetzlaff et al. [2011].

HIP	T_{eff}	$\log(L/L_\odot)$	Spec type[1]	$v\sin i$ (km s^{-1})	Mass ($M_\odot$)	Simbad classification
18724	16033	2.90	B3V	50 [2]	7.94[4]	Eclipsing binary of Algol type
30122	17566	3.11	B2V	25 [2]	7.15[4]	Cepheid variable star
33558	16375	2.92	B3V	70 [3]	6.31[4]	Star
60710	16279	2.98	B3V	298 [3]	6.2[5]	In double system
93808	16518	2.95	B3V	15 [3]	6.31[4]	Spectroscopic binary
111544	20952	3.56	B2V	320 [3]	9.97[4]	In double system

may fall into this category. Therefore we proceeded in analysing the suspected β Cephei stars individually, the results of which are presented in the following subsections.

An overview of the stellar parameters of the suspected β Cephei stars is given in Table 3.21.

HD 25204; HIP 18724

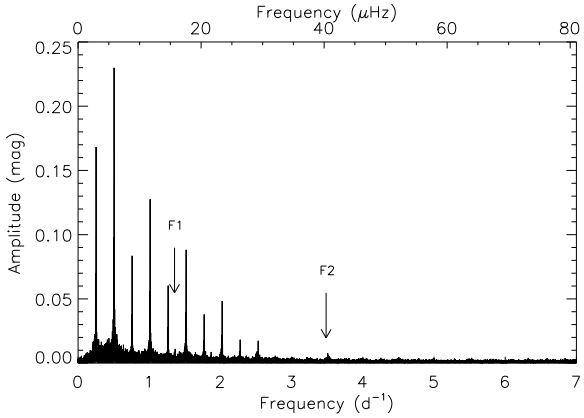

	Freq (d^{-1})	Amp (mag)	S/N
f_1	1.36318(7)	0.011(3)	4.213
f_2	3.50597(9)	0.008(3)	4.133

Figure 3.19: Amplitude spectrum of HIP 18724

Table 3.22: Significant frequencies identified in HIP 18724

HIP 18724 is an eclipsing binary of the Algol type. The binary period is 3.953 d (0.253 d^{-1}) long, the effects of which dominate the amplitude spectrum as shown in Figure 3.19. The system has an apparent magnitude of 3.408 and appears to be semi-detached. It consists of a B3V type star and an A4IV type star with masses of 7.18 $M_\odot$ and 1.89 $M_\odot$ respectively. The system was found to have an invisible third component with an orbital period of 33 days. With a mass of 0.7 $M_\odot$ it is speculated to be a K dwarf type star [Fekel and Tomkin, 1982].

Two frequencies which lie at 1.363 and 3.506 d^{-1} (as listed in Table 3.22) are present in the *SMEI* spectrum that do not appear to be related to the orbital periods. As shown in Table 3.22 the amplitudes of these frequencies are very small. No stellar frequencies have previously been published in the literature on this system. To increase the accuracy of the fitted frequencies the eclipses due to the binary system should be removed before the frequency analysis is completed on the light curve. However, this is not a simple process, and was not performed here.

Unfortunately we are unable to identify which frequency corresponds to which star, although we are fairly certain it is not a true oscillation from the K-type star as that star is much fainter, and so *SMEI* would unable to detect oscillations from it. K-type

stars also have much shorter periods and their amplitudes of oscillations are much lower, so would not be detected in the *SMEI* light curves. With a short binary period and the long cadence of the *SMEI* instrument, there are not enough data during the eclipses to determine whether the frequencies originate from the A or B type star.

The B star is the brightest star in the system, with a predicted magnitude difference between the A and B stars of 2.5 magnitudes [Fekel and Tomkin, 1982]. The secondary star could oscillate like a δ Scuti star, which have pulsation periods between 0.02 and 0.3 d (3.3 to 50 d^{-1}). This may account for the frequency at 3.50 d^{-1} but not the one at 1.36 d^{-1}. We therefore suggest that the 1.36 d^{-1} frequency is from the primary star, while the 3.50 d^{-1} frequency may be from either but is more likely to be from the primary star as it is the brighter component.

HD 44402; HIP 30122; ζ CMa

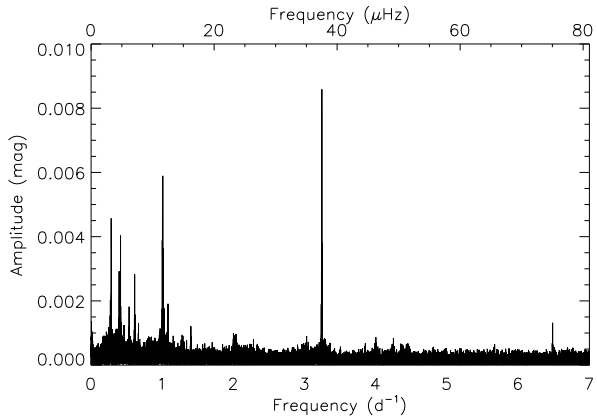

	Freq (d^{-1})	Amp (mag)	S/N
f_1	3.241573(6)	0.0086(2)	43.213
f_2	0.28245(1)	0.0046(2)	10.935
f_3	0.41338(1)	0.0040(2)	11.260
f_4	0.39365(2)	0.0029(2)	7.926
f_5	0.61196(2)	0.0028(2)	9.959
f_6	6.48317(4)	0.0019(2)	7.806
f_7	1.08021(3)	0.0019(2)	5.972
f_8	0.53390(3)	0.0018(2)	5.975
f_9	1.40163(5)	0.0011(2)	5.274

Figure 3.20: Amplitude spectrum of HIP 30122

Table 3.23: Significant frequencies identified in HIP 30122

HIP 30122 is a star with an apparent magnitude of 3.0. It is the primary star in a binary system with an orbital period of 675 days.

The secondary star in the binary orbit (HD 44380) has an apparent magnitude of 7.7. Since the *SMEI* instrument can only detect milli-magnitude brightness changes in stars down to 6.5 magnitude, it is safe to assume that the data presented here are dominated by the light from HIP 30122 and are not contaminated by light from the secondary component.

Observations of HIP 30122 in the literature have found that the star is a suspected β Cephei star [Telting et al., 2006].

As shown in Figure 3.20, several high amplitude oscillations are present in the light curve which are listed in Table 3.23. The most dominant frequency is at 3.24 d^{-1} (f_1) with a frequency at twice its value at 6.48 d^{-1} (f_6). The lower and upper rotation frequencies for the star were estimated to be around 0.126 d^{-1} and 2.541 d^{-1} and so this dominant frequency is unlikely to be due to stellar rotation or the binary period. Therefore we assume that f_1 is a true oscillation of HIP 30122 and that f_6 is a multiple of it.

Figure 3.20 also shows that several oscillations lie between 0 and 1.5 d^{-1}: f_2, f_3,

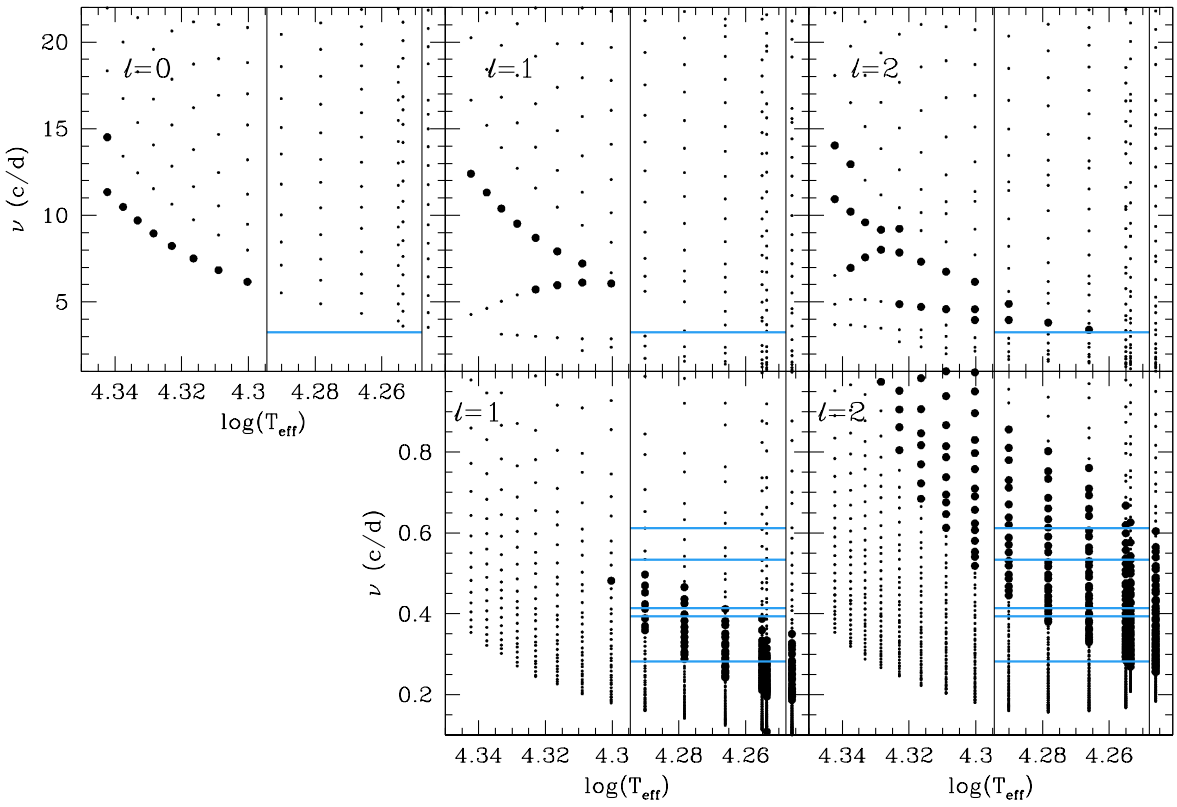

Figure 3.21: Frequencies of pulsation modes as a function of $\log T_{\rm eff}$ for main-sequence models of a 8 $M_{\odot}$, Z=0.02 star computed with overshooting ($\alpha_{\rm OV} = 0.2$) and X=0.7. Unstable modes are described by black dots. Lower panels show high-order g-modes. Vertical dashed lines delimit the 1-σ observational domain of $T_{\rm eff}$ and horizontal lines represent the observed frequencies.

f_4, f_5, f_7, f_8 and f_9 (as listed in Table 3.23). Oscillations with these frequencies are characteristic of SPB type stars. Along with the frequency detected in f_1, it is possible that this star is an SPB - β Cephei hybrid pulsator.

Degroote et al. [2010] report on the star HD 50230, B3V, which showed oscillations characteristic of both β Cephei and SPB nature. They observe hundreds of gravity modes with frequencies between 0.2 and 2 d^{-1}, and tens of acoustic modes with frequencies between 2.4 and 24 d^{-1}. Degroote et al. [2010] reported that the acoustic modes had considerably lower amplitudes than the gravity modes. This observation is not true for the data that we present here, where the high-frequency mode is the most dominant frequency in the light curve.

To check whether the detected frequencies are compatible with current predictions

of oscillation modes excited in B stars, we compared our findings with models in the grid of non-rotating main-sequence models described in Miglio et al. [2007b]. Stellar models were computed with CLÉS [Scuflaire et al., 2008a], adiabatic frequencies with LOSC [Scuflaire et al., 2008b], and the stability of modes of degree $l = 0, 1$, and 2 were investigated with the code MAD [Dupret et al., 2003]. All stellar models were computed with overshooting from the convective core ($\alpha_{\rm OV} = 0.2$). OP opacity tables [Badnell et al., 2005] with Asplund et al. [2005] metal mixture were also adopted. By searching in this grid, we find that the observed frequencies, as well as the observed $T_{\rm eff}$ and luminosity, are compatible with those of β Cephei and SPB type modes excited in $Z = 0.02$, 8 $M_{\odot}$ models. These models are shown clearly in Figure 3.21, which shows the frequencies of the pulsation modes as a function of $\log T_{\rm eff}$. The excited modes are shown by full black dots. Horizontal lines represent the frequencies observed with the *SMEI* data. The vertical lines show limits of the $T_{\rm eff}$ of the star between 17700K and 19700K.

HD 52092; HIP 33558

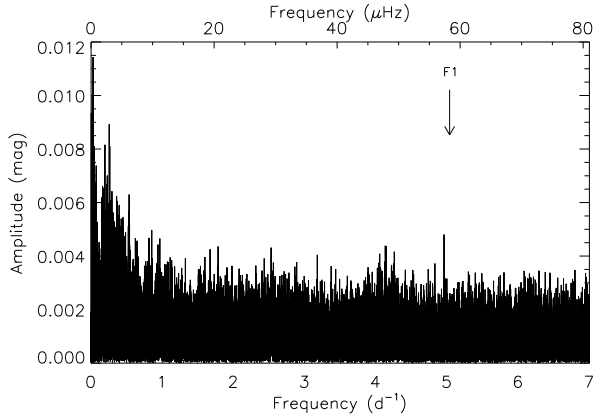

	Freq (d^{-1})	Amp (mag)	S/N
f_1	4.95790(6)	0.005(1)	4.32

Figure 3.22: Amplitude spectrum of HIP 33558

Table 3.24: Significant frequencies identified in HIP 33558

HIP 33558 (HD 52092) is a B3V star with an apparent magnitude of 5.1. A frequency of 4.958 d^{-1} (see f_1, Table 3.24) was observed in the *SMEI* light curve, which has not been previously published in the literature. The star was observed by Jaschek et al. [1964] and Balona et al. [1992] in surveys to search for Be stars. Neither of these papers reported any variability in the star or evidence of emission lines that would be found in a Be star. Estimations of the upper and lower stellar rotation limits do not provide evidence that this frequency is related to stellar rotation. Figure 3.22 and Table 3.24 shows that this frequency has a low amplitude, and hence low S/N, so it may have been too weak to have been detected in previous observations.

HD 108257; HIP 60710

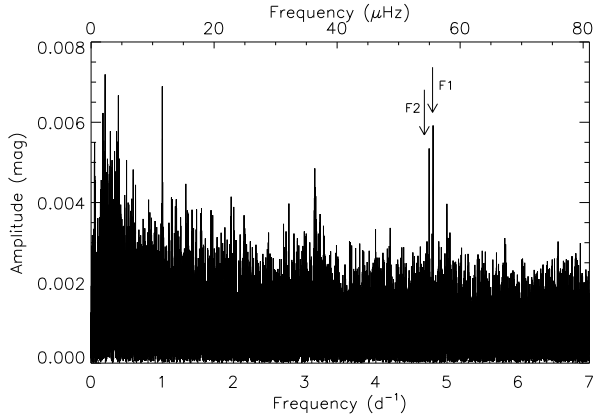

	Freq (d^{-1})	Amp (mag)	S/N
f_1	4.80378(4)	0.0059(9)	6.418
f_2	4.74834(5)	0.0053(9)	5.416

Figure 3.23: Amplitude spectrum of HIP 60710

Table 3.25: Significant frequencies identified in HIP 60710

HIP 60710 is a 4.8 magnitude star in a double system. Two frequencies (see Table 3.25) have been detected in the *SMEI* data which have not previously been reported. Estimates of the upper and lower stellar rotation limits do not provide evidence that either of these frequencies may be attributed to stellar rotation. The oscillations associated to these frequencies are small in amplitude and can be seen in the amplitude spectrum in Figure 3.23.

The frequencies presented here are unlikely to be from the second star (IDS 12211-5054 b) in the double system, as it is very faint (13.8 magnitudes).

HD 178329; HIP 93808

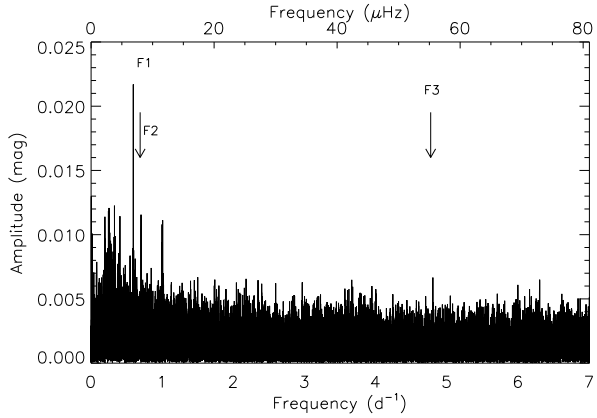

	Freq (d^{-1})	Amp (mag)	S/N
f_1	0.59276(2)	0.021(2)	8.422
f_2	0.70140(4)	0.011(2)	4.654
f_3	4.80108(6)	0.007(2)	4.133

Figure 3.24: Amplitude spectrum of HIP 93808

Table 3.26: Significant frequencies identified in HIP 93808

HIP 93808 is a spectroscopic binary with a magnitude of 6.49. The binary system has an orbital period of 1.0309 d (0.9700 d^{-1}) [Pourbaix et al., 2004], but unfortunately little information is known about its companion star such as spectral type and effective temperature. Stellar variability was reported in the Hipparcos and Tycho Catalogues [Perryman, 1997] at 1.687 d (0.593 d^{-1}). This frequency was the most dominant frequency observed in the *SMEI* data, with a S/N of 8.422 (see f_1, Table 3.26) and is clearly shown in Figure 3.24.

The other significant frequencies found in the light curve were not found in the literature and do not appear to be correlated with the binary period or the known stellar variability. They both have a very low S/N and are only just classed as significant. One frequency lies above 3 d^{-1} at 4.80 d^{-1} (f_3) while the other two frequencies (f_1 and f_2) are below 1 d^{-1}. The presence of frequencies in these ranges may suggest that the star has pulsations that are both SPB and β Cephei like in nature.

Although the frequencies in Table 3.26 meet the S/N criteria of 4.1, they are borderline, particularly f_3. As mentioned in Section 3.3.1, the S/N for the 5 year data set was calculated to be 4.1 with a 1% significance. With 126 frequencies detected in this survey, it would be expected that at least one of them would be a false positive

detection. Therefore it would be preferable to obtain further observations of this star to confirm the frequencies presented here, and hence confirm if this star pulsates with both SPB and β Cephei frequencies.

HD 214168; HIP 111544

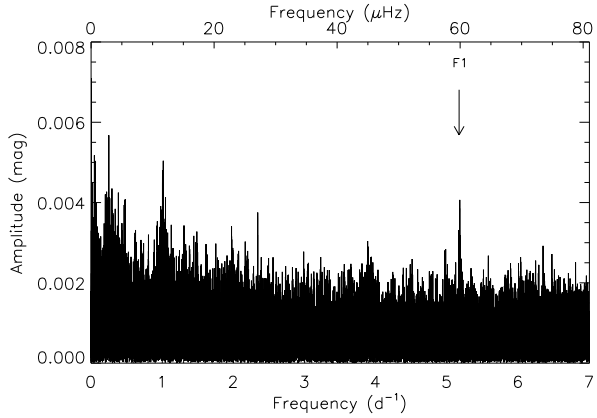

	Freq (d^{-1})	Amp (mag)	S/N
f_1	5.17887(4)	0.0041(7)	4.493

Figure 3.25: Amplitude spectrum of HIP 111544

Table 3.27: Significant frequencies identified in HIP 111544

HIP 111544 is a B2V star with an apparent magnitude of 6.48. It is a star which is in a double system, the second star being a confirmed Be star (HIP 111546, HD 214167) also of spectral type B2V with an apparent magnitude of 5.73. Both stars are of comparable brightness and of same spectral type which make it difficult to distinguish between them in the photometric data. Although it is the HIP 111544 light curve that is being analysed light from HIP 111546 may be contaminating the light curve and so it is possible that the frequency detected may be from either of the stars.

A low amplitude frequency of 5.179 d^{-1} was detected in the light curve as shown in Figure 3.25 and stated in Table 3.27. Estimates of the stellar rotation did not provide evidence to attribute this frequency to stellar rotation. It is the only star out of the six stars being analysed that has an effective temperature in the β Cephei range (between 20 000 K and 30 000 K).

3.3.4 Discussion

Many of the frequencies found in the six stars presented here have very low S/N and some are only just above the significance value of 4.1. The S/N level was recalculated so that the detection of an oscillation remained at a 1% significance (see Section 3.3.1). However, with 126 frequencies detected in the survey, it would be expected that at least one of the frequencies be a false positive detection. Therefore, the results presented here on these low amplitude oscillations would benefit from follow up observations to confirm their presence.

From the list of candidate β Cephei stars provided by Stankov and Handler [2005], 22 were included in the survey. None of these stars was found to have a frequency above 3 d^{-1} so we cannot provide evidence which would confirm these stars as β Cephei stars. However, two of the candidate β Cephei stars were found to have a frequency between 1 and 3 d^{-1}: HIP 25142 and HIP 78168. Many frequencies found in HIP 78168, were found to have an interval of approximately 0.22 d^{-1}. This is usually a characteristic of a star in a binary system, where the frequencies are that of the orbital period. However according to *The 9th catalogue of spectroscopic binary orbits* [Pourbaix et al., 2004] this star has a binary period of 10.0535 d, corresponding to a frequency of 0.0995 d^{-1}. The *SMEI* data give evidence to suggest that the binary period of this system is slightly different to the previously published value. This is something we suggest should be analysed more closely, not only with the *SMEI* instrument but other instruments as well.

The results presented in the survey on potential β Cephei stars does not mean to suggest that all possible β Cephei stars have been detected. It has already been established that not all of the confirmed β Cephei stars have been detected using the *SMEI* instrument, and there are three main reasons for this which are described below.

1. The oscillations frequencies for β Cephei stars range between 3 to 15 d^{-1}. However the Nyquist frequency for the *SMEI* instrument is only 7.08 d^{-1} and so frequencies above this are much harder to detect. It is therefore possible that

some of the stars in the survey are β Cephei, with frequencies higher than 7.08 d^{-1} and therefore cannot be detected with the *SMEI* instrument.

2. The analysis technique has also put restrictions on which frequencies could be detected. This was due to the alias frequencies at 1 d^{-1} and multiples thereof due to the Sun-synchronous orbit of the satellite round the Earth. So that these frequencies would not be included in the analysis, frequencies within 0.04 d^{-1} of the alias frequencies were ignored. This is the reason why the confirmed β Cephei star HIP 87812 was not detected in the survey.

3. It is possible that frequencies are present in the light curves which lie below 7.08 d^{-1} but the amplitudes are too low to be classed as a significant frequency. It was found that the light curves of stars where a frequency was detected had a mean RMS (root mean square) of 0.073 mag, whereas the mean RMS of the light curves of all the stars in the survey was 0.097 mag.

3.3.5 Conclusions

The aim of the survey was to detect potentially new β Cephei stars using data collected from the *SMEI* instrument. 213 stars, ranging from B0 to B3, were analysed to search for frequencies in the β Cephei range.

The overall results of the Kolomgorov-Smirnov tests found that stars where a frequency was found in the β Cephei range tended to have higher effective temperatures and luminosities than other stars included in the survey.

Of these stars, six were detected with an observed frequency in the β Cephei range, the frequencies of which were not attributed to binarity or stellar rotation and had not already been confirmed as β Cephei or Be stars. These six stars are: HIP 18724, HIP 30122, HIP 33558, HIP 60710, HIP 93808 and HIP 111544. The frequencies detected in these stars could be the results of β Cephei-like pulsations. Although the frequencies detected fulfil the S/N criterion of 4.1, many are still low in amplitude and have not

previously been published in the literature. The observations presented here would benefit from further observations to could confirm their presence.

The analysis of HIP 30122 detected frequencies that lay in both the β Cephei and SPB range. These frequencies were compared with current models and they were found to be compatible with a star of $8M_{\odot}$ and Z=0.02, where the frequencies detected relate to pure buoyancy and mixed mode oscillations.

The results presented in this survey do not mean to suggest that all possible β Cephei stars have been detected. This is not only due to instrumental effects but also that not all β Cephei oscillations are observed photometrically.

3.4 Conclusion

The results presented regarding the analysis of the confirmed β Cephei stars and the search for new β Cephei stars demonstrates the suitability of *SMEI* as an instrument for use in asteroseismology.

The lowest amplitude in a significant frequency that has been detected in the survey is 1.1 mmag. In order to compare this accuracy with ground based spectroscopic observations the following equation can be used from Kjeldsen and Bedding [1995]

$$(\delta L/L)_{\lambda} = \frac{v_{osc}/\mathrm{ms}^{-1}}{(\lambda/550\mathrm{nm})(T_{\mathrm{eff}}/5777\mathrm{K})^2} 20.1\mathrm{ppm} \tag{3.9}$$

where $\delta L/L$ is the observed luminosity amplitude, v_{osc} is the velocity of the oscillation, λ is the wavelength observed in and T_{eff} is the effective temperature of the star. Note that 1 ppm equals 1.086 μmag, for 1.1 mmag, this corresponds to 1012.9 ppm.

For *SMEI* the optical system is unfiltered, and so ranges between 460 nm and 990 nm, peaking at 700 nm. For the purpose of the following estimates λ=700 nm will be used. The effective temperature of the star also has significant influence over the velocity of the oscillation observed, so three effective temperatures will be used that cover the range of effective temperatures in the β Cephei survey. These are given in

Table 3.28: Equivalent minimum spectroscopic velocities that can be observed with the *SMEI* instrument, using effective temperatures that range across the β Cephei survey.

$T_{\rm eff}$ / K	v_{osc} / km s^{-1}
15 000	0.432
21 000	0.847
28 000	1.506

Table 3.28 along with the calculated scaled minimum velocities using Equation 3.9.

Ground based spectroscopic observations obtained on ν Eri show amplitudes of oscillation that range from 20.20 to 0.30 km s^{-1} [Aerts et al., 2004]. Comparing these amplitudes to the scaled ones with *SMEI*, it can be shown that *SMEI* gives a similar accuracy to current stellar spectroscopic observations, and so it is worth continuing to use this data for further asteroseismic studies.

SMEI also has many advantages when compared to space based instruments, such as *Kepler*. One such advantage regards the differences in their fields of view. The *Kepler* instrument, for example, is restricted to observing stars near the Cygnus constellation for which there are not many B-type stars in the field. As described in Chapter 2.1.2, *SMEI* produces an all sky image every 101 mins. Even though restrictions have been placed on which stars are targeted for analysis with the *SMEI* instrument (brighter than 6.5 magnitudes and observe stars only 10° from the Galactic Plane), there are a large number of stars which can be analysed for oscillations which cannot be seen with *Kepler*. A more detailed comparison is made between these instruments in the concluding chapter of this thesis (Chapter 5).

Chapter 4

Be stars

This chapter is dedicated to Be stars. Be stars are large, main sequence stars which show, or have shown, evidence for the presence of a circumstellar disc. The disc is formed from outburst material from the star, however the mechanism of the outburst is not fully understood, although it is believed that the fast rotation of these stars plays a large part in the cause. This is explained in further detail in Section 4.1.

Due to the long duration of the SMEI data, the oscillations present in Be stars can be analysed for evidence of amplitude and phase change. If these changes can be linked with an outburst event, this information can be used to help identify the extra mechanism required for large outbursts of material. The two stars analysed with the SMEI data are Achernar and ζ Oph, the results of which are presented in Sections 4.2 and 4.3 respectively.

4.1 Introduction to Be stars

Be stars are generally fast rotating main sequence B-type stars which show, or have shown, one or more Balmer lines in emission due to the presence of a circumstellar disc (this will be discussed in more detail in Section 4.1.2). The Italian astronomer Padre Angelo Secchi reported the first observations of a Be star in 1866 [Secchi, 1867]. His observations reported *emission* in the Hα line (one of the Balmer line series) in the

star γ Cassiopeia (HD 5394). The brightest stars observed at the time, for example Vega (HD 172167, HIP 91262) and Sirius (HD 48915, HIP 32349), were reported to have shown *absorption* in their Balmer lines.

Be stars are main sequence stars with spectral types ranging from late O- to early A-type stars, however the majority are B-type stars. Therefore their location on the asteroseismic HR diagram is the same as that of β Cephei and SPB stars (see Figure 1.9). However their location on the asteroseismic HR diagram is not marked as Be stars can show both β Cephei and SPB like pulsations. Of all the B-type stars in the Milky Way approximately 20 per cent are Be stars.

Previous observations of Be stars have shown variations on timescales ranging from days to years. Short variations of the order of days have been attributed to the rotation on the star, pulsations, magnetic fields and wind. Variations that occur on a much longer timescale, scaling from months to years, have been explained by the changes in the structure of the circumstellar disc, for example an outburst filling the circumstellar disc with new material. The pulsation behavior is similar to both β Cephei and Slowly Pulsating B-type (SPB) stars, where the pulsations are driven by the κ mechanism (see Section 1.5). These pulsations range between 0.5 d^{-1} (2 days) and 4 d^{-1} (0.25 days).

Be stars are generally extremely fast rotators, with the average rotational velocity found to be approximately 88 per cent of their critical limit [Frémat et al., 2005]. The critical limit is defined as where the outward centrifugal forces are balanced by the inward force of gravity. It is believed that this fast rotation, along with another mechanism, ejects material from the star to form a circumstellar disc. The adjoining mechanism for this is not fully understood and is discussed in the following section (Section 4.1.3).

The question of why Be stars rotate so fast has challenged our understanding of stellar evolution. Langer and Heger [1998] addressed the question, whether it is possible for an evolving massive star to increase its surface velocity until it reaches its critical limit. Langer and Heger find that the rotation rate of the surface may increase as a

result of the evolution of the star's angular momentum. However, the results of Langer and Heger would mean that Be stars should not lie on the main sequence, which we know is not true through observations. Due to observational evidence it is now thought that Be stars are already fast rotators when they arrive on the main sequence.

Martayan et al. [2006] and Martayan et al. [2007] conducted surveys of the SMC (Small Magellanic gas Cloud), LMC (Large Magellanic gas Cloud) and Milky Way and found that the metallicity of the environment affects the rotational velocity of Be stars. Their results show that B and Be stars in lower metallicity environments such as the SMC and LMC (with Z=0.002 and Z=0.004 respectively) have higher rotational velocities than those of the Milky Way (Z=0.020). This is expected since the stellar winds and stellar mass losses are lower at low metallicity than at higher metallicity [Bouret et al., 2003]. Therefore the loss in angular momentum in low metallicity environments is lower and hence the stellar rotation velocities are expected to be higher [Meynet and Maeder, 2000].

The effects of fast stellar rotation are explained in more detail in Section 4.1.1.

4.1.1 Fast rotation of Be stars

As mentioned previously, Be stars are active hot stars that form as very rapid rotators when they arrive on the main sequence.

Due to the high rotation rates of Be stars, the shape of the star is centrifugally distorted into an oblate spheroid. The most well known example is the Be star Achernar, for which a model of its oblateness is shown in Figure 4.1. The equatorial radius of Achernar was originally calculated to be 1.56 times bigger than its polar radius. However this value may have included the presence of a small circumstellar disc about the equator, so the ratio may not be as large as first suggested [Rozelot and Neiner, 2009].

As a result of the flattened spheroid, the surface of the star exhibits a change in radiative flux due to the change in local effective gravity, otherwise known as the Von Zeipel theorem [von Zeipel, 1924]. The Von Zeipel theorem establishes the relation

between the radiative flux at a considered latitude (ϑ) of a uniformly rotating star to the local effective gravity as a function of the angular velocity, Ω, and latitude, ϑ. This relation is given by Equation 4.1,

$$F(\Omega, \vartheta) = \frac{L}{4\pi G M_\star} g_{\text{eff}}(\Omega, \vartheta), \tag{4.1}$$

where F is the radiative flux, L is the luminosity, g_{eff} is the local effective gravity and $M_\star$ is given by

$$M_\star = M\left(1 - \frac{\Omega^2}{2\pi G \bar{\rho}_M}\right) \tag{4.2}$$

where M is the stellar mass and $\bar{\rho}_M$ is the average stellar density.

Equation 4.1 shows that the flux is proportional to the local effective gravity. By considering how the local effective gravity changes over the surface of the star, one sees that the local effective gravity at the equator is smaller than that at the poles. This means that the star is dimmer at the equator than it is at the poles as shown by Figure 4.1, an effect known as gravitational darkening.

The Von Zeipel theorem also suggests that with a change in the local radiative flux the local effective temperature would change as well. This is given by Equation 4.3:

$$T_{\text{eff}}(\Omega, \vartheta) = \left(\frac{L}{4\pi\sigma G M_\star}\right)^{1/4} [g_{\text{eff}}(\Omega, \vartheta)]^{1/4} \tag{4.3}$$

where σ is the Stefan-Boltzmann constant. From Equation 4.3 it is shown that the local effective temperature is proportional to the local effective gravity, so not only are Be stars dimmer at their equators but they must also be cooler.

It has been established that at low metallicity, stellar winds are less efficient and thus cannot evacuate enough angular momentum from fast rotators. This implies that the first generation of massive stars, which would have had very low metallicity, may have had a high percentage of critical rotators [Stee and Meilland, 2009].

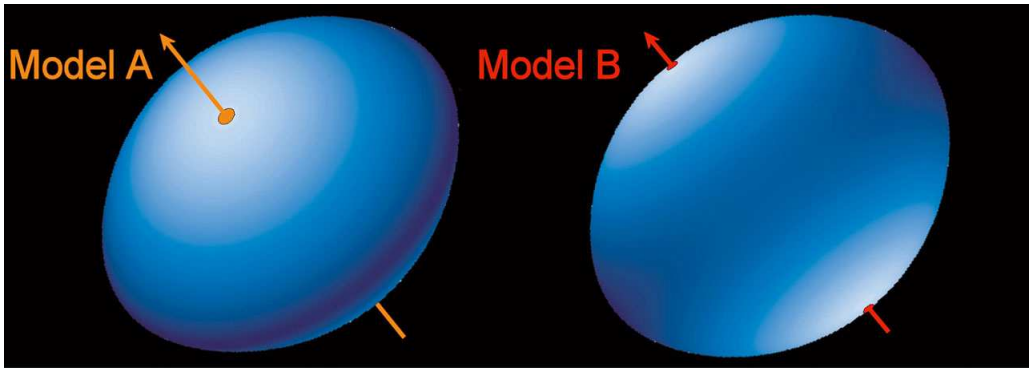

Figure 4.1: Model of a Be star showing an equatorial bulge at the equator due to its fast rotation. These models were based on observational data on the Be star Achernar. Copyright ESO.

4.1.2 Circumstellar Disc

Be stars are stars which show or have shown one or more Balmer lines in emission. These emission lines are brighter than the rest of the spectrum. This feature is explained by the presence of a circumstellar disc surrounding the star. Although the circumstellar disc is hot it is not as hot as the star. The electrons in the atoms of the circumstellar disc absorb high energy photons radiating away from the star, causing the electrons to move from a lower energy level to a higher one. The electron then de-excites emitting lower energy photons and producing emission lines in the spectrum. The emission in the Balmer line series relates to electrons de-exciting to the first excited state in hydrogen.

A complete knowledge of the physical structure of the circumstellar disc is still unknown, however analysis by Meilland et al. [2007] of the Be star α Arae produced evidence that the circumstellar disc has a Keplerian rotation.

4.1.3 The Be phenomenon

The cause of an outburst of material from the star filling the circumstellar disc has remained a mystery and is known as the *Be phenomenon*. Although Be stars rotate rapidly, the rotation alone in not enough to eject the material from the star and another mechanism needs to be included to provide the extra angular momentum required. A

number of explanations have been suggested. The most popular three are summarized below.

The first explanation is that Be stars could be part of a binary system, whereby the mass ejections are triggered by tidal effects. Although a high rotation rate may be the main physical process responsible for the disc formation, observations of two well known Be stars in binary systems, α Arae and Achernar, suggest that the companion star may trigger Be episodes. Observations of α Arae show that the circumstellar disc is a more permanent feature whereas the disc around Achernar forms and dissipates over a period of several years. The difference between disc formation of these two stars may be due to the orbit of the companion star forming the binary system they are in. In the case of α Arae, Chesneau et al. [2005] suggest the presence of a companion star with an orbital period of 70 days, however a direct detection of this companion star has not been confirmed. If the hypothetical companion has a circular orbit then the constant interaction between itself and α Arae may be producing the constant force forming the disc, and keeping the disc as a permanent feature about the star. A direct detection of a companion star about Achernar was found by Kervella et al. [2008] with a predicted orbital period of approximately 15 years. If the orbit of the companion star is more eccentric then strong tidal interactions contributing to disc formation would only happen around periastron. This topic is discussed in more detail in Section 4.2.5, with respect to Achernar. Although this may be the cause of mass ejection for some of the Be stars, many Be stars studied have not shown any evidence of being part of a binary system and so this explanation cannot explain the effect in all Be star cases.

Second, magnetic fields surrounding the star could force material from the star to travel along the magnetic field lines from the poles to the equator (assuming a dipole field). The material travelling from both the north and south pole would meet at the equator, and if the magnetic field were strong enough, would stay confined. However the evidence for strong magnetic fields in Be stars is sparse and although observations have been made of magnetic fields around Be stars (ω Orionis Neiner et al. [2003b]

and ζ Ophiuchi Hubrig et al. [2011]), it is thought that magnetic fields are rare, and if they are present they are weak. Like with the binary explanation presented above, although the existence of a magnetic field can explain the presence of a circumstellar disc for some Be stars, it does not explain the presence for all.

Finally, the beating of pulsation modes within the Be star could provide some angular momentum. Rivinius et al. [1998b] provide evidence of the beating of modes in the star μ Cen. Rivinius et al. [1998b] report that when oscillations that are closely spaced come into positive strong interference in μ Cen evidence of a circumstellar disc occurs. The combination of the angular momentum caused by the rotation of the star and the beating of pulsation modes could allow the star to reach the critical limit and hence a mass ejection from the star would occur. It has been shown by Rivinius et al. [1998a] with spectroscopic observations that the beating of pulsation modes in the Be star μ Cen coincides with the ejection of matter from the star.

Stee and Meilland [2009] have suggested that not all Be stars may be triggered by the same one physical process. The stars α Arae and Achernar (a photometric study of Achernar is presented in Section 4.2) both have rotation rates that are very close to their critical velocities. There are examples where this is not always true, although most Be stars do rotate rapidly. An example is the star κ CMa which was calculated to have a stellar rotation only 52 per cent of its critical rotation, much lower than the average rotation rate of 88 per cent for Be stars. Therefore other physical processes must dominate the triggering of the disc formation in this star. Radiative pressure on the gas may be responsible for the disc formation, as it is one of the more luminous Be stars in the sky. It is therefore possible that all Be stars do not need the same mechanism to trigger disc formation.

4.2 Achernar

The following results were published in Goss et al. [2011], which can be found in Appendix *A*.

Achernar, also known as α Eridani (HD 10144, HIP 7588), is one of the brightest stars in the southern hemisphere. With an apparent magnitude of 0.46 it is the eighth brightest star in the sky and one of the nearest Be stars to Earth [Rivinius et al., 2003]. Observations of Achernar measure the equatorial radius to be $12R_{\odot}$ and it has a rotational velocity of 225 km s^{-1} [Domiciano de Souza et al., 2003].

Achernar has been the target of many ground and space based observation using both photometry and spectroscopy. Previous observations of Achernar have been made by Balona et al. [1987], Porri and Stalio [1988], Smith [2001], Domiciano de Souza et al. [2003], Carciofi et al. [2007] and Kervella et al. [2008] to name a few.

4.2.1 Analysis of light curve

A 5-year light curve of Achernar was obtained by the *SMEI* instrument (see Section 2.1), which ran from 2003 June 13 to 2009 November 26. The complete light curve can be seen in Figure 4.2.

The light curve as a whole was analysed using Period04 [Lenz and Breger, 2005], (see Section 3.2.1 for an explanation as to how Period04 is used to analyse data). The amplitude spectrum for the entire light curve is shown in Figure 4.3. The figure clearly shows many frequencies with prominent power which are present in the data. As explained in Section 2.1.3 some of the frequencies present do not originate from the star and are instead effects from the Sun-synchronous orbit of the satellite. A cutoff of ± 0.04 d^{-1} around the 1 d^{-1} frequencies was made to distinguish between those frequencies that were analysed and those that were disregarded.

The significant frequencies seen in Figure 4.3 are listed in Table 4.1. A frequency is classed as significant if the S/N (signal to noise ratio) is four or higher (see Section 3.2.1 for justification of this level).

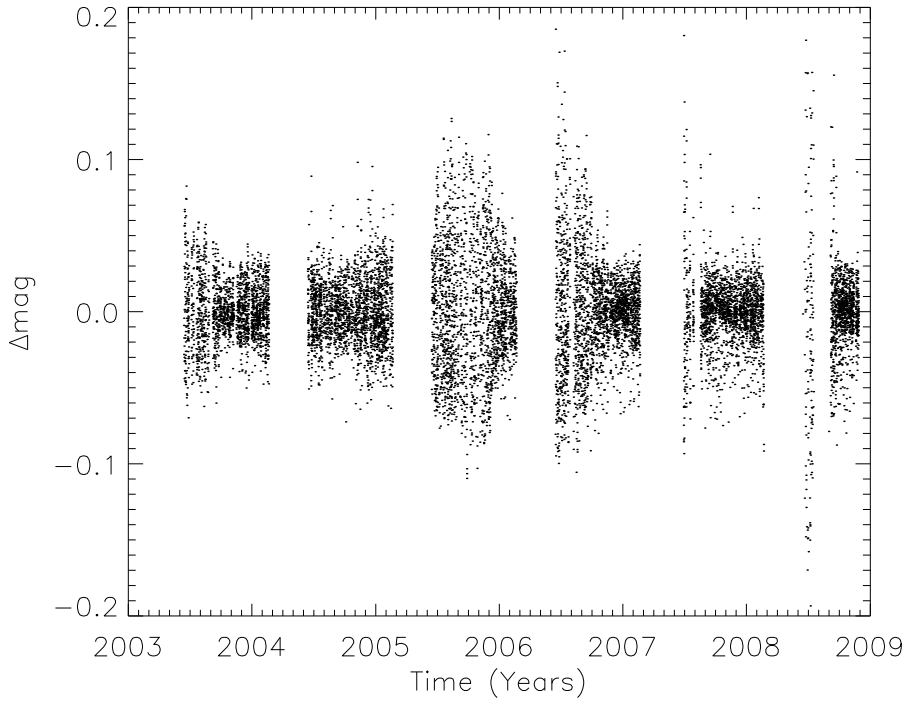

Figure 4.2: 5-year light curve of Achernar data before a running mean is subtracted.

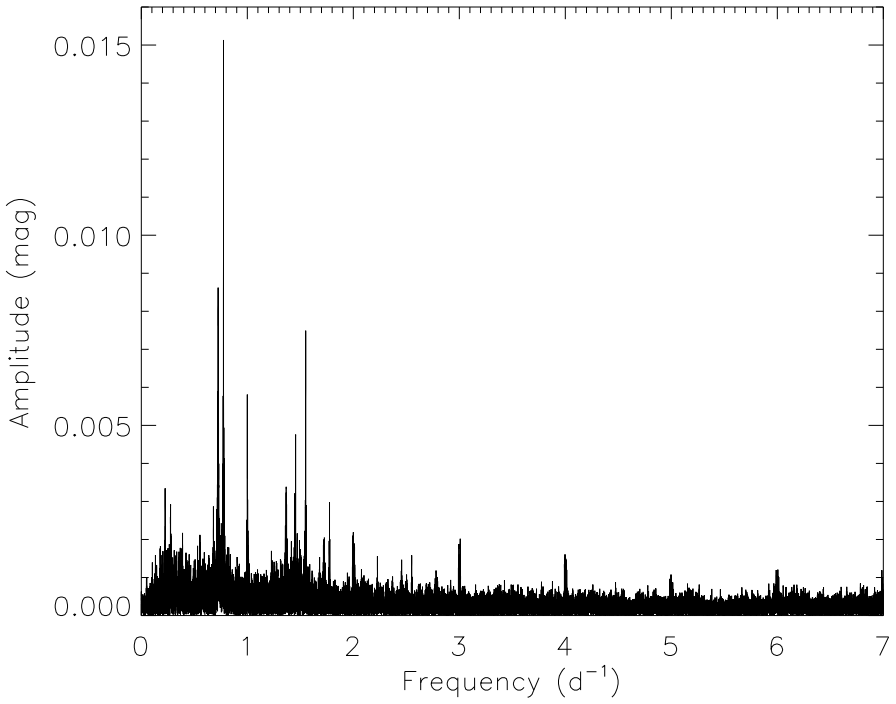

Figure 4.3: Amplitude spectrum of Achernar over 5 year light curve.

Table 4.1: A table to show the frequencies identified in Achernar for the complete 5 year light curve. The starred (*) frequencies represent frequencies where no published results have been found in the literature.

Frequency (d^{-1})	Amplitude (mag)	S/N
0.775177(5)	0.0165(3)	27.09
0.724854(6)*	0.0129(3)	19.05
0.68037(3)*	0.0027(3)	4.11

Of the frequencies listed in Table 4.1 only the 0.775 d^{-1} frequency was found to be published in the literature. Balona et al. [1987] published a frequency of 0.792 d^{-1}, obtained from simultaneous spectroscopy and photometry. When compared to the frequencies detected in the *SMEI* light curve, this does not quite match the value for the main oscillation. Later on a slightly different frequency of 0.7745 d^{-1} was then determined by Rivinius et al. [2003] which was based on spectroscopic observations between 1996 and 2000. The value Rivinius et al. [2003] published is the more widely accepted value for the frequency of the main oscillation in Achernar and it is this frequency which is observed in the *SMEI* data at 0.775 d^{-1}.

Vinicius et al. [2006] later reported further frequencies in Achernar using spectroscopic observations that were taken between 1991 November and 2000 October. The frequencies they found were: 0.49, 0.76, 1.27 and 1.72 d^{-1}. Only evidence of the 0.76 d^{-1} frequency, which is likely to be the same frequency that is reported in Rivinius et al. [2003], is evident in the *SMEI* light curve. In the amplitude spectrum of Achernar (Figure 4.3) there appears to be a grouping of frequencies around 1.72 d^{-1}. However, upon further analysis these frequencies were found to be combinations of the frequencies already given in Table 4.1 and the 1 d^{-1} harmonics from the orbit of the satellite.

The two starred (*) frequencies in Table 4.1 are frequencies where no published results were found in the literature. It is possible that the 1.72 d^{-1} frequency reported by Vinicius et al. [2006] could be the 0.72 d^{-1} frequency observed with *SMEI* but with an additional 1-day cycle effect. However this has not been confirmed.

While analysing the 5-year data with Period04 many frequencies around the

0.72 d^{-1} frequency were removed from the light curve, but evidence of this oscillation still remained. This also happened with the 0.77 d^{-1} frequency but to a much lesser extent. This is evidence of linewidth and suggests that the amplitudes and/or frequencies of the oscillations were changing during the observation. Gutierrez-Soto et al. [2008] also reported a similar result when analysing the first results on Be stars observed with the *CoRoT* satellite. In one Be star they reported that non-sinusoidal signals were present in the data after already removing approximately 50 frequencies and suggested that this was due to amplitude or frequency change during the observation period.

We therefore proceeded to look at how the amplitude and frequency of the 0.72 d^{-1} and 0.77 d^{-1} frequencies changed over the 5-year time period.

4.2.2 Splitting of the light curve

Since the *SMEI* light curve covers a period of 5 years it is long enough to be able to investigate whether the 0.77 d^{-1} and 0.72 d^{-1} frequencies are varying in either frequency or amplitude.

To do this the light curve was split into independent segments, each 50 days long. Each individual segment was analysed using Period04 to determine the frequency and amplitude of the 0.77 d^{-1} and 0.72 d^{-1} frequencies. The uncertainties on the amplitude and frequency were determined using the Monte Carlo simulations in Period04 [Lenz and Breger, 2005].

By experimenting with the window length of the segments, it was determined that the segments would be analysed in 50-day lengths. Shorter segments would reduce the number of points analysed and hence reduce the accuracy of the frequency and amplitude. A 50-day length was determined as the shortest time where accurate frequencies and amplitudes could be determined. If the window length were too long then detail would be lost in the variations of the frequency and amplitude over the 5-year time period.

In a 50-day period the maximum number of data that can be collected from the satellite is 712 points. In order to calculate an accurate frequency and amplitude, only segments where the total number of data exceeded 150 (fill factor of 20 per cent or more) were analysed. Segments where the number of data fell below this value did not create an amplitude spectrum of sufficiently high quality and had larger errors, hence their amplitude and frequency values could not be accepted with much confidence. The removal of segments where the data criteria was not made usually occurred at the start and at the end of the 6-month observing *SMEI* seasons. These 6-month observing seasons are clearly seen in Figure 4.2.

The 0.68 d^{-1} frequency was not analysed for change in amplitude and frequency, as this frequency had a very small amplitude when analysed with the whole 5-year light curve, with a S/N of 4.11. Once the light curve was split up into 50-day segments the amplitude of this frequency fell below a S/N of four and hence the amplitude and frequency could not be determined with confidence.

4.2.3 Results: Change in amplitude

Figure 4.4 shows how the amplitudes of the 0.77 d^{-1} and 0.72 d^{-1} frequencies changed over the observational period. As shown the amplitudes of the frequencies varied with a significant increase in amplitude of both frequencies over the same time period, roughly between 2004 October and 2007 January.

The 0.72 d^{-1} frequency started with a lower amplitude than the 0.77 d^{-1} frequency, but during the period when the amplitudes increased the amplitude of the 0.72 d^{-1} frequency increased above the amplitude of the 0.77 d^{-1} frequency. The amplitudes of both frequencies decreased around January 2007 with the 0.72 d^{-1} frequency decreasing to an undetectable level, while the 0.77 d^{-1} remained present in the light curve. It should be noted that the absence of the 0.72 d^{-1} frequency is not correlated to the lack of data. The 0.72 d^{-1} frequency could not be detected in the following 50 day segments starting at: 2006 January 18, 2007 September 10, 2007 October 30, 2008 August 25

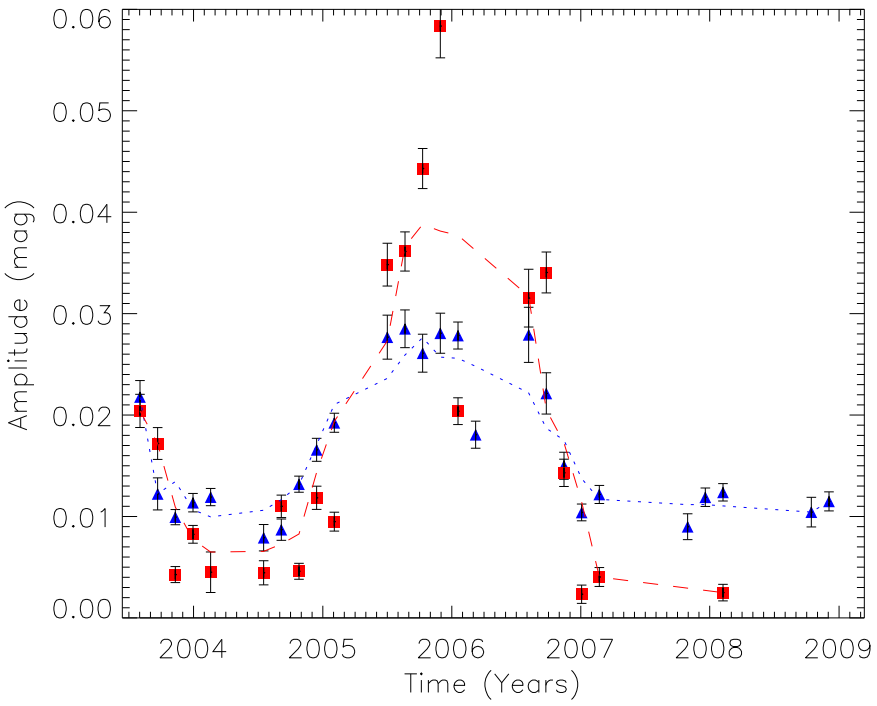

Figure 4.4: A graph to compare the change in amplitude of the 0.77 d^{-1} and 0.72 d^{-1} frequencies over the 5 year observation period. The blue triangles represent the change in amplitude of the 0.77 d^{-1} frequency and the red squares represent the change in amplitude of the 0.72 d^{-1} frequency. The blue dotted line shows a smooth fit through the 0.77 d^{-1} data and the red dashed line shows a smooth fit through the 0.72 d^{-1} data.

and 2008 October 14.

Figure 4.5 shows the amplitude spectra of Achernar at six different epochs which are separated by the large gaps in the light curve as seen in Figure 4.2. As shown in Figure 4.5, it is evident that the amplitude of both the 0.77 d^{-1} and 0.72 d^{-1} frequencies, marked as F1 and F2 respectively, varied significantly over the observational period. Here it is obvious that both of the frequencies increased in amplitude. The 0.72 d^{-1} frequency increased significantly more than the 0.77 d^{-1} frequency, and then proceeds to decrease to an undetectable level at the end of the observations. In the bottom two panels of Figure 4.5 the 0.72 d^{-1} frequency cannot be seen.

By comparing the top two panels of Figure 4.5 with the two middle panels (third and fourth panels down) it can be shown that the noise around the frequencies increases when the amplitudes of the frequencies increase. The fact that the noise increases around the frequencies when the amplitude increases suggests that the signal causing the frequencies may not be strictly coherent over time-scales of hundreds of days. A non-coherent signal would also be associated with random phase changes. Therefore analysis of the frequency and phase variations in these frequencies needed to be addressed, the results of which are presented in Section 4.2.4.

In order to rule out the increase in amplitude of the two frequencies being due to a satellite effect from the *SMEI* instrument, variations in the oscillations and light curves of other stars were analysed for comparison. Nine stars that were observed with *SMEI* were analysed with the selections made as described below. Their light curves were analysed for similar changes in amplitude of oscillation (if an oscillation was observed in the star) and for stability in the light curve over the same time period.

If the change in amplitude was dependent on the right ascension and declination of Achernar, other stars in the vicinity would also show this trend. Three stars in the vicinity of Achernar that were observed with *SMEI* were chosen to be analysed: HD 32249, HD 12311 and HD 3980. None of these stars showed variations in oscillations or the raw light curve that matched the trend present in Achernar.

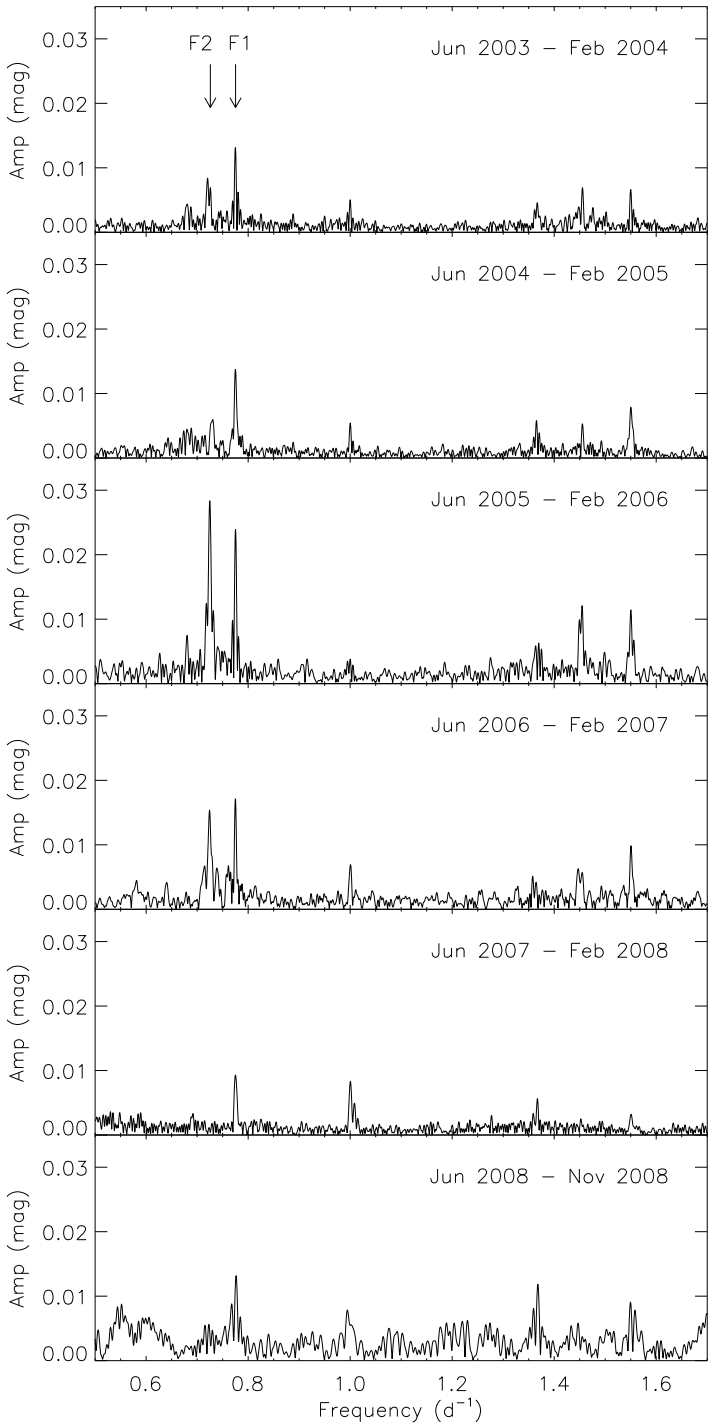

Figure 4.5: Six amplitude spectra of Achernar at different epochs during the 5 years of observation, showing the frequencies between 0.5 and 1.7 d^{-1}. The spectra are in chronological order with the observational period of each labelled respectively. Note that the 0.72 d^{-1} frequency, marked as F2 in the figure, is not present in the bottom two panels.

Since Achernar is the ninth brightest star in the sky another possibility is that the amplitude increase in the oscillations may only be obvious in the brightest of stars. Arcturus (HD 124897), Vega (HD 172167) and Capella (HD 34029), all stars which are brighter than Achernar at magnitudes -0.04, 0.03 and 0.08 respectively, were analysed. Again no patterns were found in the light curve that were similar to that of Achernar.

Finally three stars of photometric reference were analysed to look specifically for changes in the levels of noise. These stars are not known or expected to show any stellar variability and have had their light output very carefully measured [Tarrant, 2010]. Photometric standard stars are generally used to compare to other stellar observations to determine the exact brightness of the observed star. These were HD 168151, HD 155410 and HD 136064 which again showed null results.

4.2.4 Results: Change in frequency and phase

As mentioned in Section 4.2.3 it was observed that noise increases around the 0.77 d^{-1} and 0.72 d^{-1} frequencies as the amplitudes of these oscillations increase. This suggests that the frequencies may not be coherent. This would mean that an expected change in phase would occur when observing at a fixed frequency.

Figure 4.6 shows how the observed change in amplitude of the two frequencies correlate to their change in frequency and phase. The phases of both the 0.77 d^{-1} and 0.72 d^{-1} frequencies were analysed over the 5-year light curve. This was accomplished by fixing the frequency in Period04 at the frequencies given in Table 4.1, and calculating the phase in each 50-day segment. The change in frequency was determined by analysing the oscillations in each 50-day segment and determining the frequencies independently.

As shown in Figure 4.6 the 0.77 d^{-1} frequency is a coherent oscillation, with a constant frequency and phase over the 5-year time period. The 0.72 d^{-1} oscillation shows a decrease in frequency during 2004, just before the increase in amplitude, and what appears to be a random phase across the entire light curve. This suggests that

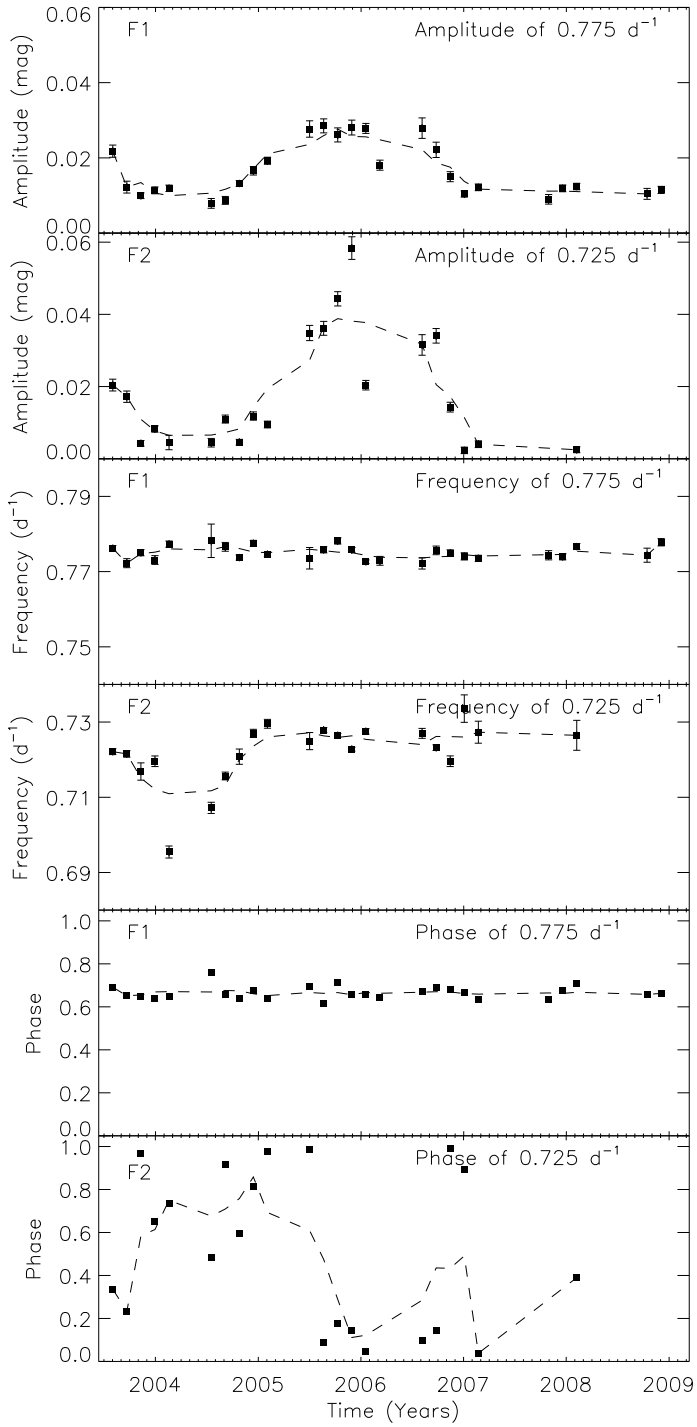

Figure 4.6: Panel 1: Amplitude variations in the 0.77 d^{-1} frequency. Panel 2: Amplitude variations in the 0.72 d^{-1} frequency. Panel 3: Frequency variations in the 0.77 d^{-1} frequency. Panel 4: Frequency variations in the 0.72 d^{-1} frequency. Panel 5: Phase variations in the 0.77 d^{-1} frequency. Panel 6: Phase variations of the 0.72 d^{-1} frequency. The dashed lines in the plots show a smooth fit through the data. Note that the errors on some of the panels are smaller than the symbols.

the 0.72 d^{-1} frequency is not coherent. However, the decrease in frequency appears when the amplitude of the frequency is low and thus a low S/N (below four), so it is unclear whether the change in frequency is correlated with the change in amplitude.

The results suggest that the 0.72 d^{-1} frequency may not be fully coherent and so it is possible that it is due to rotational modulation. However the oscillation scenario cannot be completely ruled out. Firstly, the similar changes in amplitudes of the 0.77 d^{-1} and 0.72 d^{-1} frequencies suggest a common origin. Also, as already stated, it is not clear whether the change in frequency of the 0.72 d^{-1} oscillation is significant as this occurs when the amplitude of the frequency is low.

4.2.5 Discussion

The amplitudes of the 0.77 d^{-1} and 0.72 d^{-1} frequencies were found to significantly increase and then decrease over a 5-year time period, with amplitude of the 0.72 d^{-1} frequencies changing by up to a factor of eight. While the frequency and phase of the 0.77 d^{-1} oscillation remained constant suggesting a coherent oscillation, the 0.72 d^{-1} oscillation shows evidence for a decrease in frequency and what appears to be a random phase change, suggesting that it is not a fully coherent oscillation. The nature of this event may be explained by a transient frequency during a stellar outburst. This is discussed by Rivinius et al. [2003] who report on non-radially pulsating Be stars. Be stars are known for their stellar outbursts where a large transfer of mass from the star to the circumstellar disc occurs. In a survey of 27 known Be stars, Rivinius et al. [2003] report that four of the stars show a secondary transient period within 10 per cent of their main oscillation period which appeared during outbursts only. In the oscillations of Achernar, the 0.72 d^{-1} oscillation is within 10 per cent of the 0.77 d^{-1} frequency. Rivinius et al. [2003] conclude that the secondary periods are attributed to the circumstellar disc surrounding the star, whether it be the period of the ejected gas from the star or other processes that interact with the disc. However the lack of data in this area, for the time being, does not allow conclusive remarks to be made on the

nature of transient frequencies in Be stars.

Huat et al. [2009] report on the photometric analysis on the Be star HD 49330, which was observed using the *CoRoT* satellite. The star was observed undergoing an outburst event. They report on a direct correlation between the changes in amplitude of oscillation with the outburst event. The amplitudes of the main frequencies (p-modes oscillations) decrease just before and during the outburst and increase after the outburst. Other groups of frequencies (g-mode oscillations) appear just before the outburst with their amplitudes reaching a maximum during the outburst, and then decrease and disappear after the outburst has finished. However, it has not yet been determined whether the variations in the pulsation modes triggered the outburst event, or whether the occurrence of such an outburst led to the excitation of the modes.

The changes in stellar oscillations from stellar outbursts, reported in Huat et al. [2009], last up to tens of days. The changes in Achernar however last much longer, up to approximately 1000 days. Long-term variations in Be stars that last from months to years have been attributed to structural change in the circumstellar disc, for example a one-armed oscillation of the disc (one section of the disc having a higher density of material than other sections) or an outburst filling the circumstellar disc with new material [Neiner and Hubert, 2009].

Following the publication of this analysis in Goss et al. [2011], T. Rivinius made direct contact with the author confirming that Achernar was indeed in strong emission during 2006 using spectroscopic data from the ESO archive. These data therefore confirmed the presence of a circumstellar disc about Achernar.

Carciofi et al. [2007] indicate that after a near-quiescent period from 1998 to 2002, observations carried out on Achernar in 2006 showed that the star was in an active phase and that it had built up a circumstellar disc. Their results confirm that the variations reported here may be directly connected to the presence of a circumstellar disc around the star.

Assuming that the amplitude variations observed are due to an outburst event

relating to the circumstellar disc, one of the triggers for the creation of the circumstellar disc (as mentioned in Section 4.1.3) is the presence of another star orbiting the Be star in a binary system. Kervella et al. [2008] reported that Achernar does have a companion star with an orbital period of approximately 15 years. It was suggested in Kervella et al. [2008] that the interaction between the companion star and Be star at their closest point could be the trigger of the Be episodes. If this is correct, it was predicted that the next such passage would occur around 2010. However the amplitude variations presented here suggest that the Be episode occurred around 2006 and so the companion star was unlikely to be the cause.

4.2.6 Conclusion

Analysis of the 5-year photometric data from *SMEI* has uncovered three significant frequencies in the Be star Achernar: 0.775 d^{-1}, 0.725 d^{-1} and 0.680 d^{-1}. Only the 0.775 d^{-1} has been previously published in the literature [Rivinius et al., 2003].

The long duration of the photometric data collected using the *SMEI* instrument has allowed us to study the variations in oscillations of the two main oscillations (0.775 d^{-1} and 0.725 d^{-1}). The analysis of independent 50-day time segments showed that the amplitude of these frequencies increased significantly and then decreased over the same time period.

The 0.72 d^{-1} frequency is believed to be of a transient nature. The low-amplitude of the 0.680 d^{-1} frequency does not allow us to distinguish whether this oscillation is a pulsation or transient frequency, as it cannot be analysed accurately in the independent 50-day segments.

The variations in the amplitudes of oscillation of Achernar could be explained by the presence of a stellar outburst creating a circumstellar disc about the star.

4.3 ζ Oph

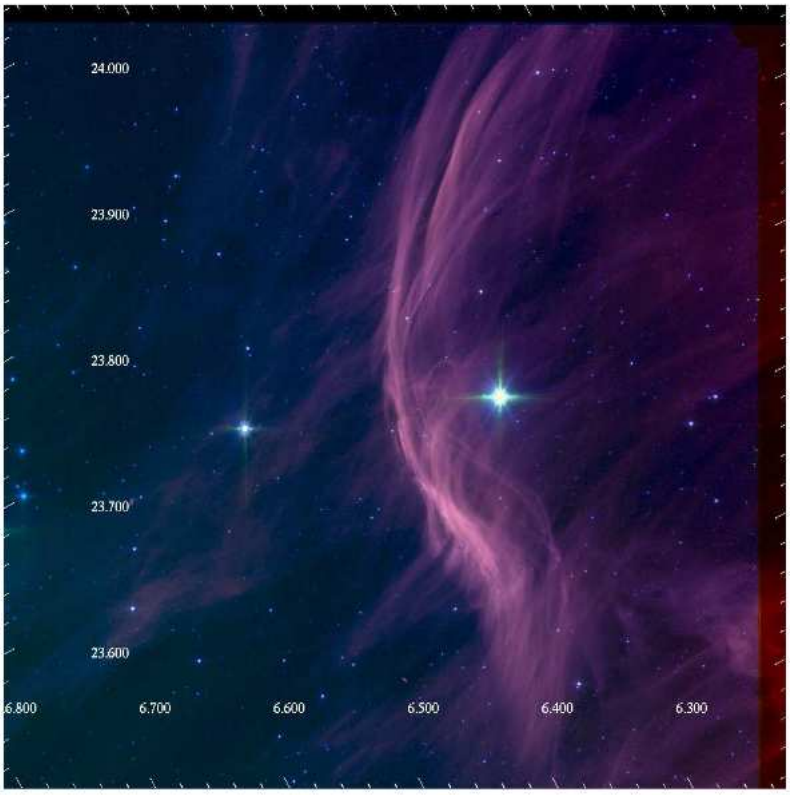

Figure 4.7: IR Spitzer image of bow shock around ζ Oph [Hubrig et al., 2011].

ζ Oph (also known as HD 149757, HIP 81377) is a late O-type star. It is therefore referred to as an Oe star rather than a Be star, but the signature Be characteristics remain the same (remember that Be stars range from late O to early A type stars). It is a bright star with an apparent magnitude of 2.57 and rapidly rotates with a $v\sin i$ of 400 km s^{-1}.

ζ Oph is also a well-known runaway star, as first identified by Blaauw [1961]. A runaway star is one that was once part of a binary system with an even more massive primary component. When the primary component reached the end of its life it exploded as a supernova and propelled ζ Oph away at an approximate velocity of 30 km s^{-1}. The former primary component of the binary system has been identified by Hoogerwerf et al. [2001] as the pulsar PSR J1932+1059.

The bright blue star on the right-hand side of Figure 4.7 is ζ Oph. To the left of

Table 4.2: Observation times of ζ Oph using the *MOST* and *WIRE* data.

Satellite	Observational Period	Nos. data	RMS (mmag)
WIRE	18/02/04 - 27/02/04	6663	6.1
MOST	18/05/04 - 11/06/04	9084	6.1
WIRE	28/08/05 - 30/09/05	40730	4.8
WIRE	08/08/06 - 09/09/06	28113	7.8

ζ Oph is a bright pink curve, known as a bow shock. In Figure 4.7 ζ Oph is travelling from right to left. As it moves its stellar winds pushes gas and dust out of its way. Therefore the gas that lies directly in the path of the star gets compressed together creating the bow shock.

4.3.1 Analysis of light curve

The photometric data analysed for ζ Oph were collected by *SMEI*, *MOST* and *WIRE* (see Sections 2.1, 2.2 and 2.3 respectively for details on these satellites). As shown in Figure 4.8, the data span a period of 5 years running from 2003 February 10 to 2008 September 27. The top panel of Figure 4.8 shows the photometric data collected by the *WIRE* and *MOST* satellites. The first, third and fourth segments of data were collected by *WIRE* and the second segment of data were collected by *MOST*. The bottom panel of Figure 4.8 shows the photometric data collected by the *SMEI* instrument. The crosses indicate the dates the spectroscopic data were obtained were obtained to observe the Hα line.

Tables 4.2 and 4.3 show how the photometric data collected by the different instruments compare to each other. As shown from the RMS (root mean square) values in Tables 4.2 and 4.3 the *WIRE* and *MOST* instruments have a greater precision in their light curves than the *SMEI* instrument. This is also obvious by eye when directly comparing their light curves in Figure 4.8 (it is evident here that *SMEI* has a far more scattered light curve than the *WIRE* and *MOST* instruments). However, *SMEI* has the advantage of obtaining a light curve which covers a period of 5 years (see Table 4.3). Both *WIRE* and *MOST* only observed ζ Oph for a month at a time.

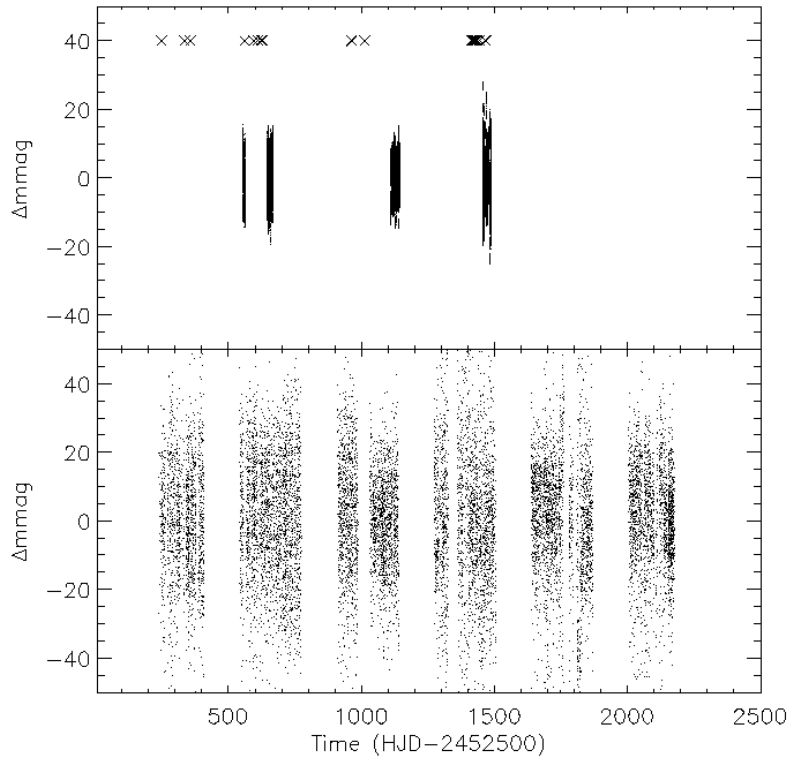

Figure 4.8: Light curves for ζ Oph spanning a period of 5 years. The top panel shows the data collected by the *WIRE* and *MOST* satellites. The first, third and fourth sections of data in the top panel were collected by the *WIRE* satellite, while the second section of data in the top panel was collected by the *MOST* instrument. The bottom panel shows the data collected by the *SMEI* instrument. The crosses indicate the dates the spectroscopic data were obtained were obtained to observe the Hα line.

Table 4.3: Observation times of ζ Oph using the *SMEI* data.

Satellite	Observational Period	Nos. data	RMS (mmag)
SMEI	10/02/03 - 25/09/03	1467	17.0
SMEI	07/02/04 - 25/09/04	2473	20.0
SMEI	06/02/05 - 25/06/05	2255	18.0
SMEI	06/02/06 - 26/09/06	2194	24.0
SMEI	07/02/07 - 25/09/07	2340	24.0
SMEI	07/02/08 - 27/09/08	2123	22.0

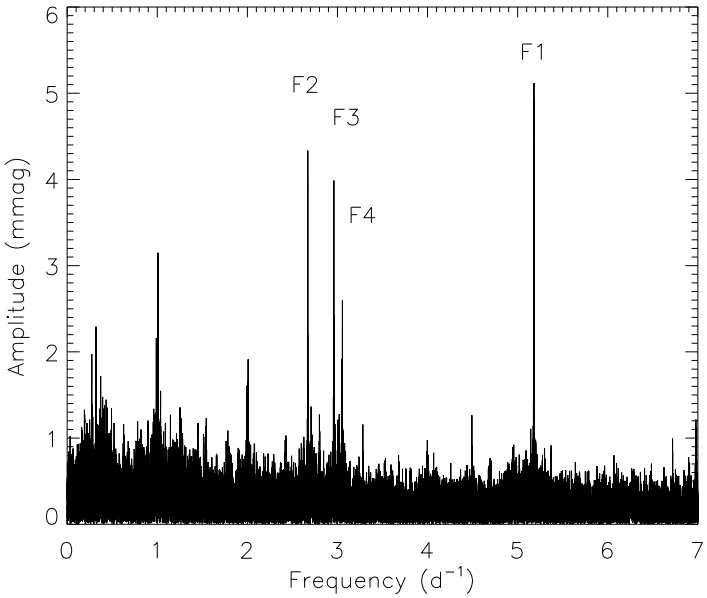

Figure 4.9: Amplitude spectrum of ζ Oph using 5 year time series collected by *SMEI*.

The initial analysis of the *SMEI*, *WIRE* and *MOST* data was conducted using Period04 [Lenz and Breger, 2005], the light curves analysed for frequencies between 0.00 and 7.08 d^{-1}. The amplitude spectrum for the whole 5-year *SMEI* light curve can be seen in Figure 4.9 and the individual amplitude spectra for the *WIRE* and *MOST* instruments are shown in chronological order in the right-hand column of Figure 4.10. Remember that frequencies at 1 d^{-1} and multiples thereof are present in the *SMEI* data due to the Sun synchronous orbit of the satellite (see Section 2.1.3 for further details) and are disregarded in the analysis.

As shown in Figures 4.9 and 4.10 there are a number of significant frequencies present within the ζ Oph light curves. The complete 5-year light curve for *SMEI* and the individual observing segments for *WIRE* and *MOST* were analysed for significant frequencies i.e, where the S/N ratio was greater than four. The uncertainties on the frequency and amplitude were calculated using Monte Carlo simulations in Period04 [Lenz and Breger, 2005]. The significant frequencies found in the 5-year *SMEI* light curve are shown in ascending order in Table 4.4. The significant frequencies found in the *MOST* and *WIRE* light curves are shown in ascending order in Table 4.5.

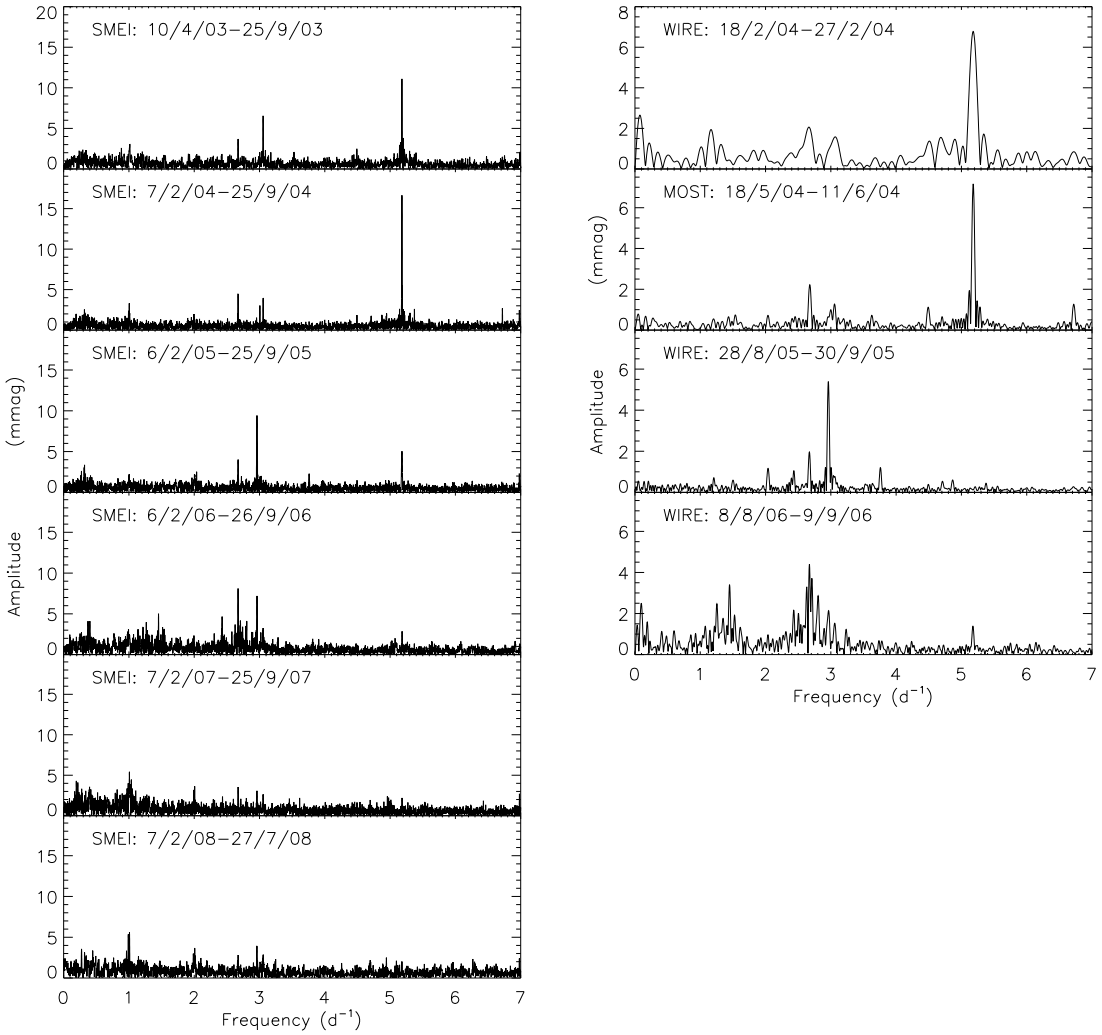

Figure 4.10: Amplitude spectra of ζ Oph over different epochs using different satellites, the epoch and satellite are stated in their respective panels. The left-hand column presents six amplitude spectra of ζ Oph collected using the *SMEI* instrument showing frequencies between 0 and 7 d^{-1}, with the panels ordered chronologically. The right-hand column presents the amplitude spectra of the *MOST* and *WIRE* instruments, also showing frequencies between 0 and 7 d^{-1} and are ordered chronologically.

Table 4.4: Frequencies identified in ζ Oph using the *SMEI* instrument, ordered by ascending frequency. Note: these frequencies were found when analysing the entire light curve. The starred (*) frequencies represent frequencies where no published results have been found in the literature.

Frequency (d^{-1})	Amplitude (mmag)	S/N
2.67137(2)	4.3(3)	10.93
2.96041(2)*	4.0(3)	9.84
3.05498(3)*	2.6(3)	6.92
5.18082(1)	5.1(3)	10.25

Table 4.5: Frequencies identified in ζ Oph with the *WIRE* and *MOST* instruments. The frequencies are listed in ascending order.

WIRE 2004		*MOST* 2004		*WIRE* 2005		*WIRE* 2006	
Frequency (d^{-1})	Amplitude (mmag)	Frequency (d^{-1})	Amplitude (mmag)	Frequency (d^{-1})	Amplitude (mmag)	Frequency (d^{-1})	Amplitude (mmag)
1.165(2)	1.77(5)	-	-	-	-	-	-
-	-	-	-	-	-	1.2537(2)	2.82(3)
-	-	-	-	-	-	1.3549(3)	2.02(3)
-	-	-	-	-	-	1.4480(2)	3.40(3)
-	-	-	-	2.0385(2)	1.13(1)	-	-
-	-	-	-	-	-	2.3816(4)	1.54(3)
-	-	-	-	2.4334(3)	0.90(1)	2.4297(2)	2.55(3)
-	-	-	-	-	-	2.6269(2)	2.43(3)
2.648(1)	2.16(5)	2.6762(4)	2.24(4)	2.6706(1)	1.86(1)	2.6800(1)	4.63(3)
-	-	-	-	-	-	2.7014(1)	4.31(3)
-	-	-	-	-	-	2.8060(2)	3.51(3)
-	-	2.953(1)	0.76(4)	2.96120(5)	5.32(1)	2.9581(3)	2.31(3)
-	-	3.0153(8)	1.11(4)	-	-	-	-
3.085(2)	1.49(5)	3.0481(6)	1.50(4)	3.0557(3)	0.90(1)	3.0578(4)	1.51(3)
-	-	-	-	3.7588(2)	1.16(1)	-	-
-	-	4.4906 (8)	1.07(4)	-	-	-	-
-	-	-	-	4.7092(5)	0.53(1)	-	-
-	-	-	-	4.8650(5)	0.53(1)	-	-
5.1792(5)	6.68(5)	5.1805(1)	7.22(4)	-	-	5.1763(4)	1.32(3)
-	-	5.371(1)	0.70(4)	-	-	-	-
-	-	6.7209(7)	1.28(4)	-	-	-	-

The data from the *MOST* satellite collected in 2004 on ζ Oph were previously analysed and published in Walker et al. [2005]. The frequencies identified in the *MOST* data in Table 4.5 are the same as those found by Walker et al.

Comparison of the frequencies presented in Table 4.5 and the spectrum in the right-hand column of Figure 4.10 shows similar frequencies in the *WIRE* and *MOST* data. The amplitudes of the most dominant frequencies in the light curves vary significantly over time and it should be noted that some frequencies are only present at certain epochs.

The frequencies identified in the 5-year *SMEI* light curve are presented in Table 4.4 and are shown in the amplitude spectra in Figure 4.9. Comparison of the *SMEI* data with the *WIRE* and *MOST* data show that the same frequencies are present in both. By looking at the *MOST* and *WIRE* amplitude spectra in chronological order it is obvious that there is a change in amplitude in the most dominant frequencies. We use the data collected by *SMEI* to analyse how these frequencies change in amplitude and phase over time. The frequencies that were analysed in detail are: 2.67 d^{-1}, 2.96 d^{-1} and 5.18 d^{-1}, the results of which are discussed in the following sections.

4.3.2 Splitting of the light curve

The most dominant frequencies were analysed in the *SMEI* light curve in order to determine how their amplitude and phase change over time.

The light curve was analysed in 50-day sections moving the window along every 10 days so that there is an overlap between adjacent windows. The frequencies originally measured in the *SMEI* light curve using Period04 (see Table 4.4) were used as a fixed frequency in each of the segments. An amplitude and phase for the fixed frequencies were then calculated in each of the 50-day sections. Sections were only analysed when the number of data were greater than 150 (duty cycle for that section greater than 20 per cent). Sections where the number of data were below 150 were ignored. This analysis was accomplished by using a pipeline which incorporated a Least-Squares

spectrum [Frandsen et al., 1995], the result of which was a calculated amplitude at a fixed frequency.

Due to a fixed stepping rate in the Least-Squares spectrum of the pipeline, the amplitudes calculated needed to be refined. This was accomplished by using a program to best fit a sine wave to the light curve, determining the amplitude and phase at the fixed frequencies being analysed. The program could not have been used directly, as it requires an estimate of the value it is trying to accurately determine, therefore the above procedure needed to be accomplished first. The uncertainties on the amplitude and phase change were calculated using the equations given by Montgomery and Odonoghue [1999].

4.3.3 Results: Change in amplitude

As already stated in Section 4.3.1, Figure 4.10 shows that the main oscillation frequencies observed in ζ Oph have significantly changed in amplitude over 5 years.

Figure 4.11 shows a graph of how the amplitudes of the three most significant frequencies change with respect to each to other using observations from the *SMEI* instrument. The black triangles show the change in amplitude of the 5.18 d^{-1} frequency. The red crosses show the change in amplitude of the 2.96 d^{-1} frequency. The blue squares show the change in amplitude of the 2.67 d^{-1} frequency.

Comparison of the left and right-hand columns of Figure 4.10 shows a dominant frequency at 5.18 d^{-1} during 2003 and 2004, which then decreases in amplitude and disappears. Figure 4.11 clearly shows that the amplitude of the 5.18 d^{-1} frequency increases during the first 500 days of the *SMEI* observations, peaking in amplitude at 23 mmag. This is an increase by over a factor of four since the start of the *SMEI* observations. After 500 days the amplitude drops rapidly over a period of approximately 300 days. After 800 days since the start of the *SMEI* observations the S/N of the 5.18 d^{-1} frequency drops below four and remains below this level until the end of the observations.

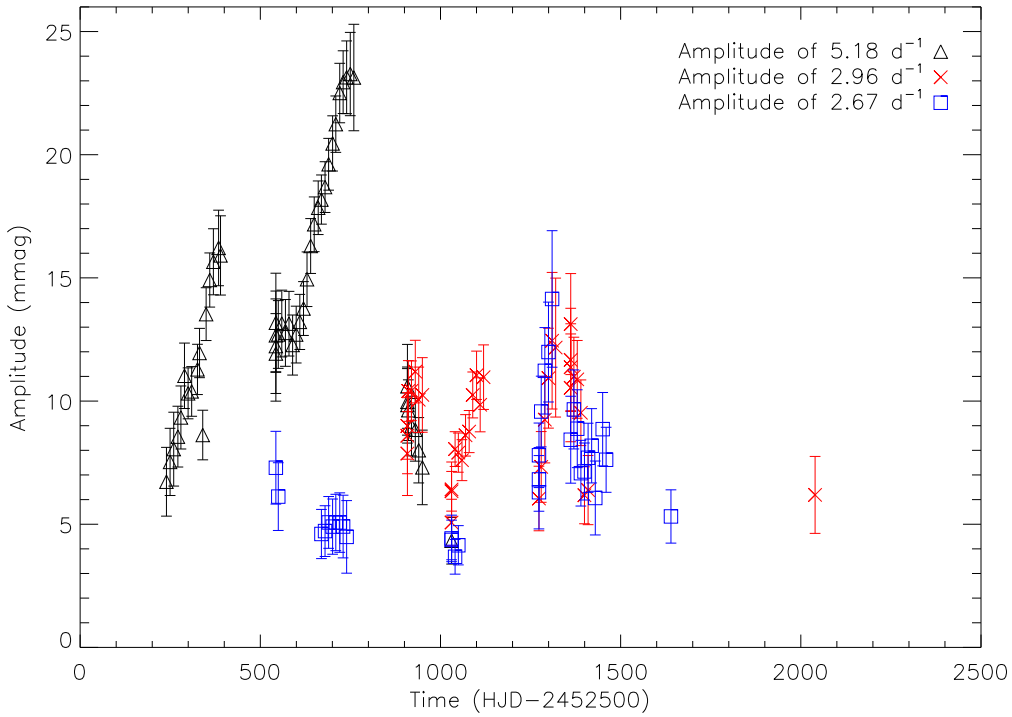

Figure 4.11: A graph to compare the change in amplitude of the three main frequencies observed in ζ Oph using the *SMEI* instrument. The black triangles represent the change in amplitude of the 5.18 d^{-1} frequency. The red crosses represent the change in amplitude of the 2.96 d^{-1} frequency. The blue squares represent the change in amplitude of the 2.67 d^{-1} frequency.

It should be noted that the noise level does not change over this time period, it is the amplitude of the three main frequencies which are changing. Also the variations in amplitude are not correlated with the variations in the fill of the time series.

The 2.96 d^{-1} frequency present in the data also shows significant change in the amplitude of the oscillation. Figure 4.11 shows that it is after 600 days when this frequency becomes significant, and it remains significant for 600 days thereafter. The amplitude of the 2.96 d^{-1} frequency varies between 5 and 13 mmag, increasing by up to a factor of 2.6.

The change in amplitude of the 2.67 d^{-1} frequency is also shown in Figures 4.10 and 4.11. This frequency is present at the start of the observations but at a very low amplitude. Once the amplitude of the 5.18 d^{-1} frequency falls below a S/N of four the amplitude of the 2.67 d^{-1} frequency increases from 3 mmag to 14 mmag, increasing by a factor of 4.67. This rise in amplitude appears at the same time the 2.96 d^{-1} frequency rises in amplitude and also disappears at the same time.

After 1300 days the amplitude of all three frequencies have fallen below the S/N of four and do not rise again thereafter.

It should be noted that although these are the main frequencies found in the light curve of ζ Oph, when the light curve is split into its 50 day sections other frequencies were detected where the S/N was greater than four. This occurs in particular around the time period when the 2.67 and 2.96 d^{-1} frequencies are the most significant in the spectrum but persists for no longer than 100 days. This is shown more clearly in Figure 4.12 which shows a time frequency analysis for the *SMEI* light curve, performed by Buzasi (private communication). Not only does Figure 4.12 show the amplitude change of the three main frequencies explained above, but also shows the presence of other frequencies that occur within the time series. In particular there is an increase in amplitude of low frequencies (roughly between 0 d^{-1} and 2.5 d^{-1}) at around 1200 days and 1500 days. The appearance of these significant frequencies does not correlate with a low duty cycle at these times.

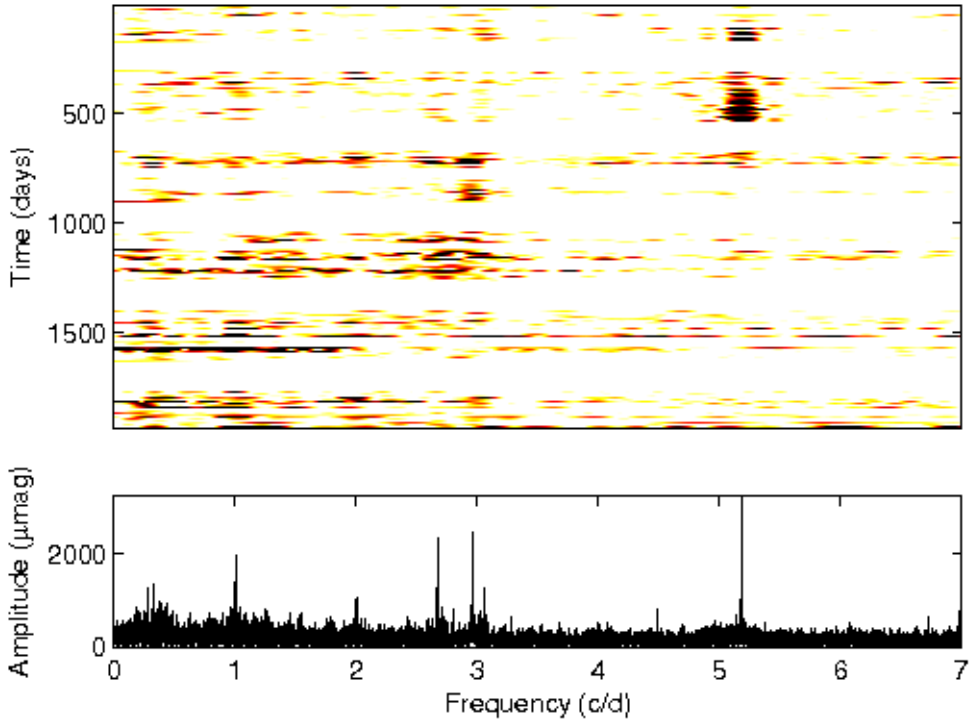

Figure 4.12: Time frequency analysis of *SMEI* light curve. The top panel shows how the amplitudes of the frequencies within the ζ Oph light curve change with respect to time. The bottom panel indicates the position of the frequencies in the top panel by use of the ζ Oph amplitude spectrum (Buzasi, private communication).

4.3.4 Results: Change in frequency and phase

The expected change in phase of the frequencies due to amplitude modulation is approximately 0.002 radians. This was inferred by simulating a light curve and modulating the amplitude by the same amount as was observed in the real observations to infer by how much the phase should change. The 0.002 radian change in phase due to amplitude modulation cannot be detected with the *SMEI* data and falls well within the uncertainty in the phase.

Figure 4.13 shows the change in amplitude and phase of the three frequencies being analysed. The black symbols show the significant data where the S/N for the frequency was calculated to be greater than four. The grey points show data where the S/N fell below four. The black lines in the phase plots show the mean phase of the significant points while the dashed and dotted lines represent one and two sigma errors on this respectively.

The results show that the oscillations of the 2.67 d^{-1} and 5.18 d^{-1} frequencies do not show evidence for significant change in phase. However the oscillation of the 2.96 d^{-1} frequency does show evidence of more variation.

Spectroscopic observations

As mentioned in Section 4.1.2, the presence of a circumstellar disc gives rise to emission in the Balmer line series. A series of spectroscopic data were obtained through a researcher, Dr Harmanec. These spectroscopic data were collected by a number of Czech stellar astronomers [1]. These data were analysed for signs of emission in the Hα line, which lies at approximately 656 nm. The results of some spectroscopic observations were also obtained from Rivinius (private communication).

Spectroscopic data where an emission was observed in the Hα line are indicated by red crosses in Figure 4.14, while black crosses indicate the absence of Hα emission. As shown from this figure, an emission in the Hα line was observed in ζ Oph for one

[1] Dr Pavel Koubsky, Dr Miroslav Slechta, Dr Petr Harmanec, Dr Petr Skoda, Dr Daniela Korcakova, Dr Viktor Votruba, Ms Sejnova, Mr M. Ceniga

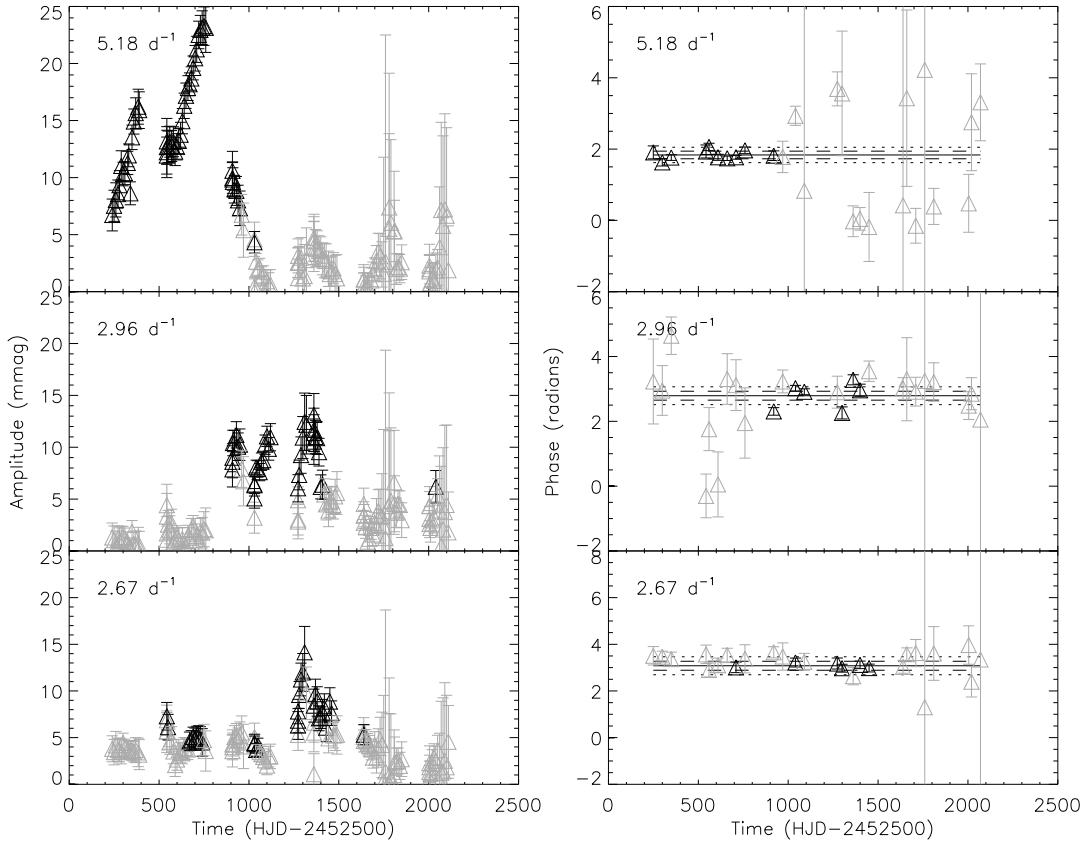

Figure 4.13: Amplitude and phase changes of the three main frequencies observed in ζ Oph using data from the *SMEI* instrument. The left-hand column shows the change in amplitude of the frequencies 5.18, 2.96 and 2.67 d^{-1} respectively. The right-hand column shows their respective change in phase. The black symbols represent significant data, where the S/N for that frequency at that time was greater than or equal to 4. The grey points represent those data where the S/N was below 4. The black lines in the phase plots represent the mean phase of the significant data. The dashed lines represent a one sigma error on the significant phase points and the dotted lines represent a two sigma error.

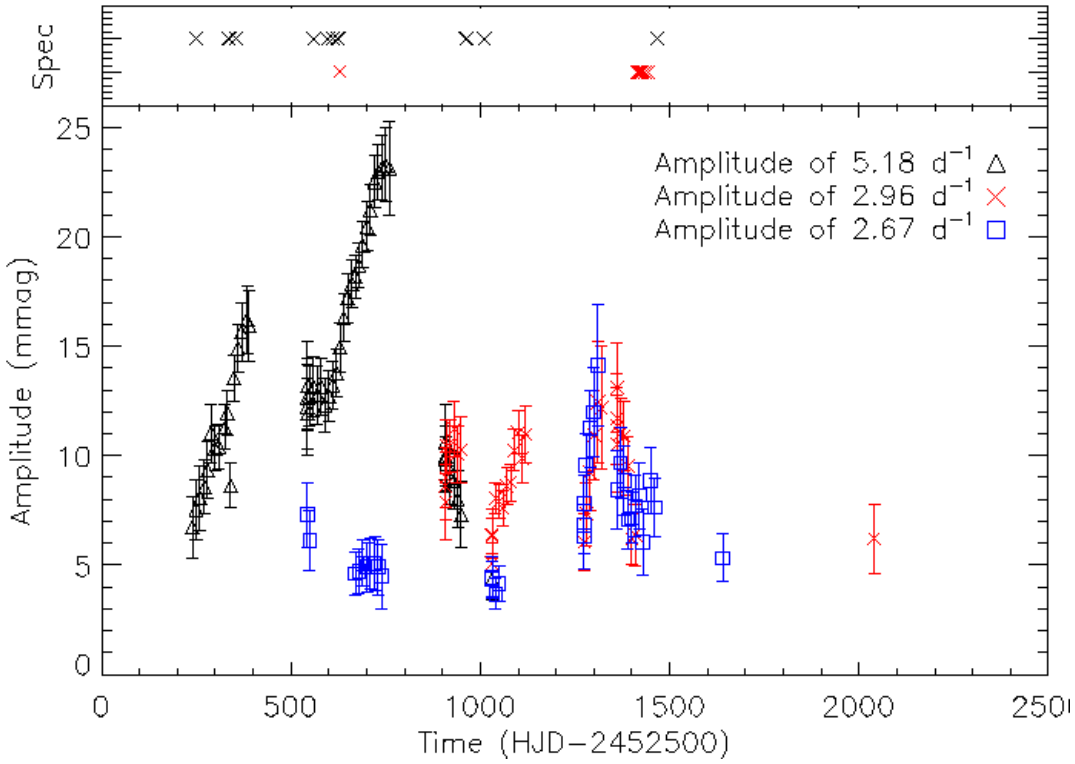

Figure 4.14: A graph to compare the results of the spectroscopic data to the amplitude changes in the photometric frequencies. The red crosses in the top panel indicate spectra where an emission was observed in the Hα line, while the black crosses indicate the absence of Hα emission.

month, between June 26 to July 26 in 2006. Unfortunately the spectroscopic data have a large gap before this time period and so it is unknown whether the emission started at an earlier time.

A weak emission in the Hα line was also detected in ζ Oph on 2004 May 5 (Rivinius, private communication). From the spectroscopic data available to us, the closest spectroscopic observation to this date is 2004 April 29, which unfortunately does not show evidence of emission in the Hα line. It is therefore concluded that either the emission began between the two dates, or that the emission was not strong enough to be detected in the data presented here. Rivinius also reports detecting no emission in the Hα on 21^{st} May 2004, which further suggests that the emission was of short duration.

As shown in Figure 4.14, the presence of the main Hα emission does not coincide with the main amplitude variation in the 5.18 d^{-1} oscillations. Instead, the emission occurs at the end of the amplitude variations in the 2.67 and 2.96 d^{-1} oscillations, when the amplitudes of these oscillations are decreasing. However, due to the lack of spectroscopic data it is not possible to determine whether the emission was of longer duration. It may be therefore possible that the 2.67 and 2.96 d^{-1} oscillations are linked with the presence of a circumstellar disc.

Figure 4.15 shows a sample of spectroscopic data taken before (top panel), during (middle panels) and after (bottom panel) the emission in the Hα line was observed. The middle three spectra show two emission peaks around the Hα absorption dip. This feature shows us that we are observing the circumstellar disc from the side, rather than looking down on the disc from the stellar rotational axis. By making the approximation that i=90° an estimate of the velocity of the circumstellar disc surrounding the star was found to be approximately 310 km s^{-1}.

An emission is also seen at approximately 668 nm, corresponding to an emission in ionised Helium. The emission occurs over the same time period as the Hα emission and also shows two emission peaks around the absorption dip. It can also be concluded

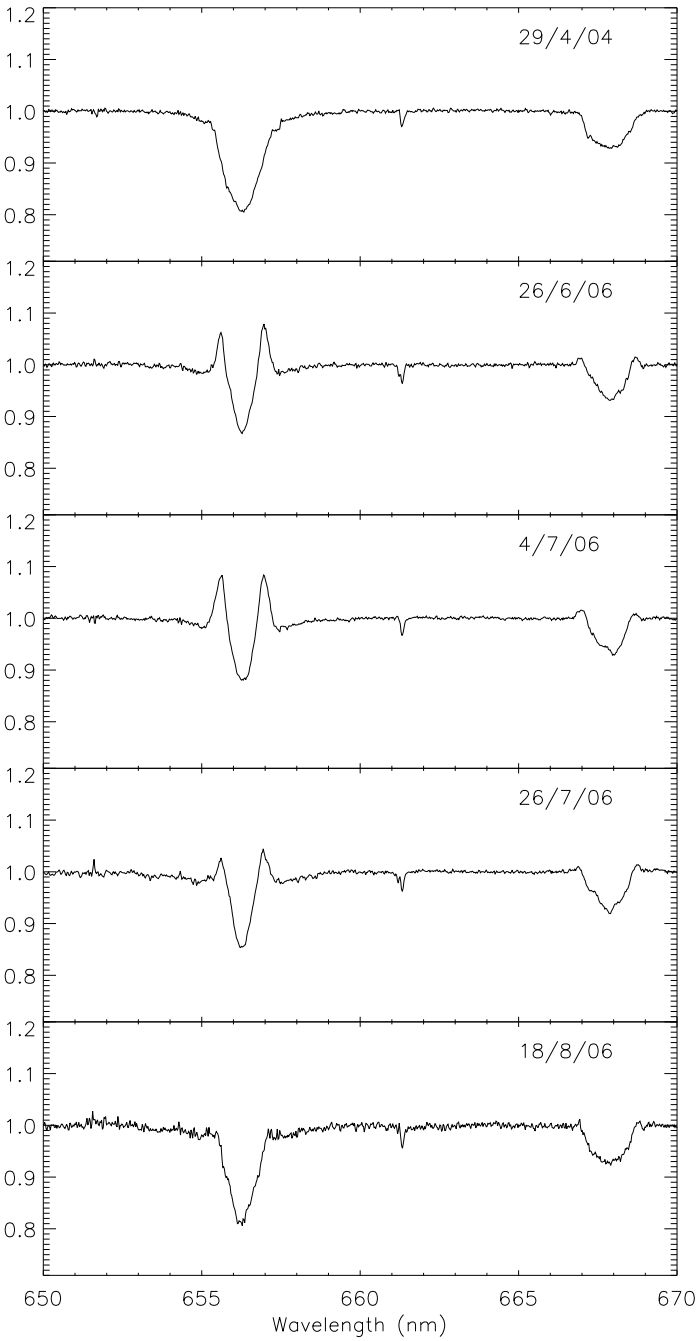

Figure 4.15: Spectroscopic observations of ζ Oph showing variations in the Hα line taken before (top panel), during (middle panels) and after (bottom panel) the emission in the Hα line.

that this emission is also associated with the presence of a circumstellar disc.

4.3.5 Discussion

As already mentioned in Section 4.3.1, the *MOST* data for ζ Oph have already been analysed and published in Walker et al. [2005]. The same oscillations were found as are presented here. Walker et al. [2005] conclude that the oscillations observed in ζ Oph can be explained by β Cephei-like pulsations driven by the κ-mechanism associated with the iron opacity bump.

The 5.18 d^{-1} frequency presented here has also been seen before in photometric observations made in 1985 by Balona [1992]. However, this frequency was not present in subsequent observations made in the following year. The only other confirmation of this frequency is in Walker et al. [2005].

However, in the subsequent observations that Balona [1992] made in 1989, it was observed that there was another dominant oscillation with a period of 0.376 d (2.66 d^{-1}). It is possible that the frequency Balona [1992] observed is the 2.67 d^{-1} frequency observed in the *SMEI*, *WIRE* and *MOST* data. Observations made by Balona [1992] in 1990 suggested that frequencies of 2.30 and 2.66 d^{-1} were present in the time series, but that neither of them were very convincing.

Balona [1992] observed a very similar pattern in the oscillations of ζ Oph between 1985 and 1990 as the pattern is presented here between 2003 and 2008. In both cases a convincing dominant frequency at 5.18 d^{-1} is present in the star at the start of the observations which then disappears. A frequency of 2.67 d^{-1} (2.66 d^{-1} for Balona [1992]) then appears after the 5.18 d^{-1} frequency has disappeared. Balona [1992] commented that (later on in the observations) this frequency becomes unconvincing, and as shown in the data presented here the amplitude of the 2.67 d^{-1} frequency decreases, with the S/N of this frequency falling below four. Balona [1992] fails to mention any of the other frequencies that are reported here with the *SMEI*, *WIRE* and *MOST* data.

There are however differences between the observations presented here and those by Balona [1992]. Balona [1992] conclude that ζ Oph was in a stage of constant light during observations made in June and July of 1987 and also in early 1988. These observations are between when the 5.18 d^{-1} and 2.66 d^{-1} frequencies were observed. The results from the *SMEI* instrument show that a frequency of 2.96 d^{-1} (a frequency which Balona [1992] does not mention in the analysis) is present in the light curve at the end of the 5.18 d^{-1} amplitude variation, and that the 2.67 d^{-1} frequency is also present. Figure 4.11 shows that the 2.67 d^{-1} frequency observed by *SMEI* has a low amplitude at this point and does not begin to rise until approximately 300 days after the amplitude of the 5.18 d^{-1} frequency has fallen. It is possible that the observations made by Balona [1992] were not able to detect the 2.67 d^{-1} frequency at this point if the amplitude was too low.

Both Walker et al. [2005] and Balona [1992] conclude from their observations that the oscillations observed in ζ Oph are not stable over a long period of time.

Both ζ Oph and Achernar (presented in Section 4.2) undergo significant amplitude change in their oscillations. The oscillations of Achernar were found to simultaneously increase and then decrease over a 5-year period, whereas the oscillations observed in ζ Oph find that the amplitude changes occur over different time periods. This may suggest that the origin of the oscillation changes is different.

Long-term variations in Be stars that last from months to years have been attributed to structural change in the circumstellar disc. For example an outburst from the star filling the circumstellar disc with new material [Neiner and Hubert, 2009]. As stated in Section 4.1.2 the presence of a circumstellar disc will result in emission in the Hα line.

However, a firm confirmation of the Hα emission only occurs at the end of the amplitude variation in the 2.67 and 2.96 d^{-1} oscillations. It may be possible that the increase in the amplitude of the 5.18 d^{-1} frequency gave the extra force required, along with the fast stellar rotation, for the star to eject material to form a circumstellar disc.

It is also possible that the pulsations are not in anyway linked to the formation or presence of the circumstellar disc. If not, then this probes the question of why would the amplitudes of the oscillations be varying.

4.3.6 Conclusion

By combining photometric data from the *MOST*, *WIRE* and *SMEI* instruments, significant frequencies have been identified in the Oe star ζ Oph. The long duration of the *SMEI* data has allowed us to analyse how the amplitude and phase of the most significant frequencies have changed over a 5-year period, with data from the *MOST* and *WIRE* satellites backing up these results.

Analysis of the photometric data has identified three main oscillation frequencies, 5.18, 2.96 and 2.67 d^{-1}, whose amplitudes have changed significantly. Balona [1992] reported similar observations between 1985 and 1990. Long-term variations in Oe/Be stars have been attributed to the presence of a circumstellar disc, however the mechanism for the creation of a circumstellar disc is still not clear.

The presence of a circumstellar disc gives rise to an emission in the Hα line. Spectroscopic data ranging over the photometric observational period were analysed for evidence of a circumstellar disc. Evidence of a disc was only found for a period of 1 month near the end of the amplitude variations (with a possible weak emission earlier on in the observations).

The spectroscopic data have been analysed further to show phase variations, the results of which are shown in Figure 4.16. This work was completed by Ian Howarth and will accompany the results presented here to create a paper. This extra analysis not only shows the presence of the 5.18, 2.96 and 2.67 d^{-1} frequencies presented here, but also frequencies at 7.19, 9.86 and 11.89 d^{-1} which have previously been confirmed in Kambe et al. [1997]. This analysis may also help shed light on the origin of the oscillations. Howarth suggests that the 5.18 d^{-1} oscillation has characteristics of a non-radial pulsation. However the origin of the 2.96 and 2.67 d^{-1} oscillations is unclear.

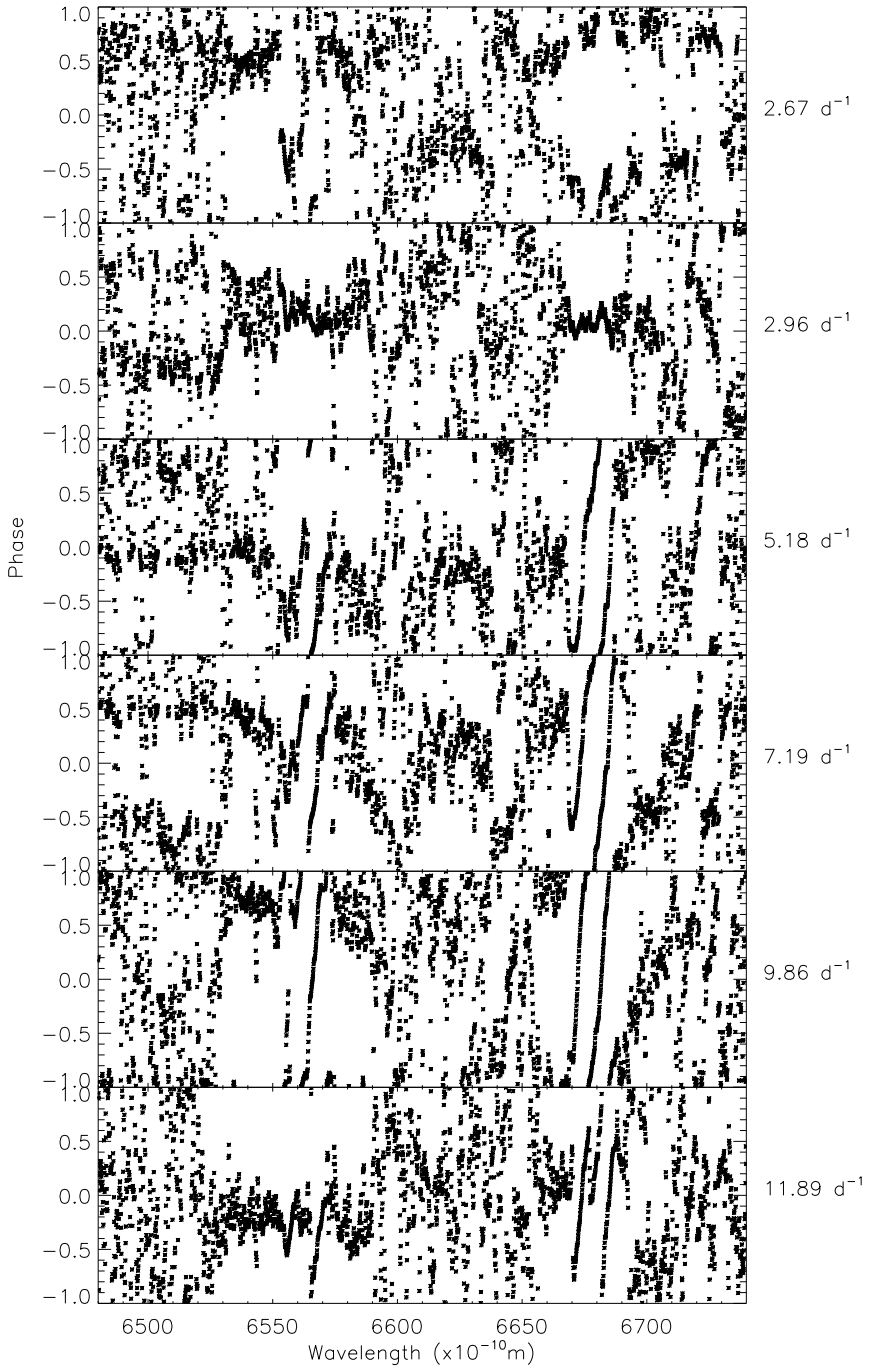

Figure 4.16: Phase variations of 2.67, 2.96, 5.18, 7.19, 9.86 and 11.89 d^{-1} frequencies in the spectroscopic observations, courtesy of Ian Howarth.

A possible explanation is that the oscillation in the 5.18 d^{-1} frequency may have been the extra force required for the star to eject material to form a circumstellar disc, while the origins of the 2.96 and 2.67 d^{-1} frequencies remain unclear. It is also possible that the results presented here have no link to the presence of the circumstellar disc.

Chapter 5

Conclusion

The main focus of this thesis was to study the stellar oscillations of some of the largest stars in the sky using photometric data provided by the *SMEI* instrument. This study was particularly focused on identifying oscillations in β Cephei and Be type stars and observing change in the amplitudes of the oscillations, so that this information may be used in further work to help model stellar interiors and the study of stellar characteristics.

As mentioned in Section 1.6 other space-based instruments also observe stellar oscillations. The following discusses the advantages and disadvantages of *SMEI* as an instrument to observe stellar oscillations, in comparison to the most recent space-based instrument, *Kepler*.

Kepler collects high quality photometric data and, as mentioned in Section 1.6, many significant papers have been published using this data with regards to extrasolar planet detection and asteroseismology. As shown in Figure 5.1 the *Kepler* field of view is restricted to a small region close to the Cygnus constellation. Since the primary focus of *Kepler* is to study transiting extrasolar planets a dedicated field of view is required. This is because the instrument needs to have the ability to continuously observe its target stars so that measurements of the light intensity may be collected every 30 minutes. A dedicated field of view is also required as an extrasolar planet can only be confirmed if three transits of the planet have been observed. This also

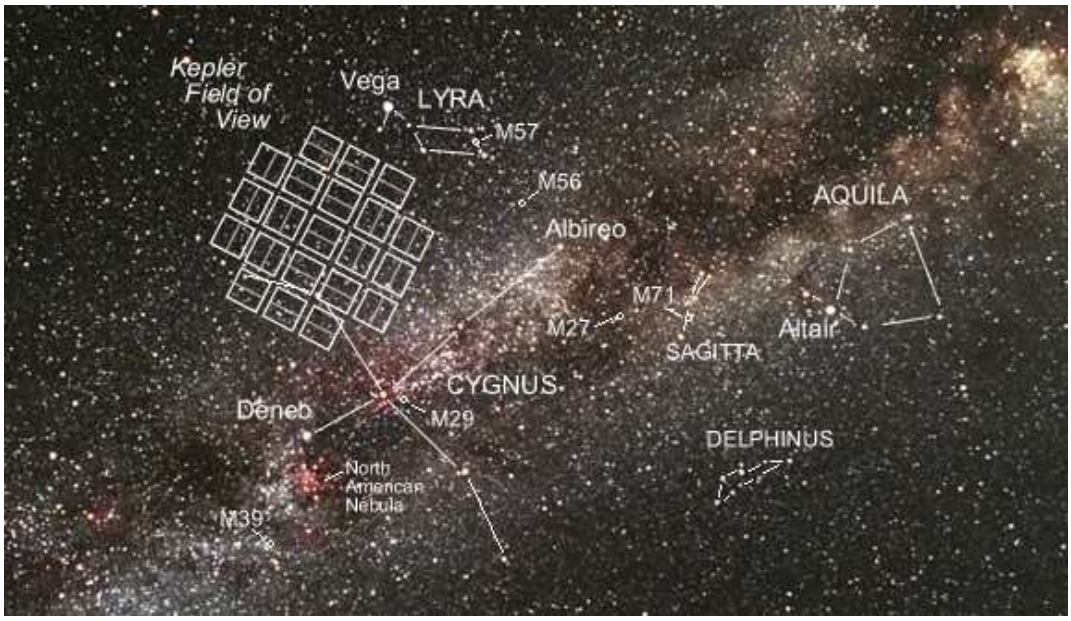

Figure 5.1: The *Kepler* field of view superimposed on the night sky [Roberts, 2012].

means that the field of view cannot be obstructed at any point during the Earth's orbit round the Sun, so the field of view needs to not only lie outside of the ecliptic plane but far enough away so that no light from the Sun shines onto the telescope's cameras. By residing off the ecliptic plane this also means that confusion resulting from occultations by asteroids and Kuiper Belt objects are avoided. Another requirement is that the *Kepler* field of view must have a large number of stars, but not lie on the Galactic Plane to reduce confusion with other stars in the field.

The selected *Kepler* field of view also favours observations of older stars. The majority of stars tend to form in dense regions on the Galactic Plane, an area known as the young thin disk, which has a vertical scale height of approximately 50 pc [Carroll and Ostlie, 2006]. As the stars get older they progress away from the Galactic Plane and begin to oscillate about it. Therefore the older the star, the more likely that it will lie away from the Galactic Plane. As B-type stars are much larger stars, they evolve much more quickly than solar like stars and do not live long in comparison. They therefore do not have much opportunity to move away from the Galactic Plane. As mentioned above, *Kepler* observes stars just off the Galactic Plane, and so it is expected that older stars will be present in its field of view, with few B-type stars

observed. The aim of the *Kepler* mission is to detect Earth-like extrasolar planets in the habitable zone, which means that it is the cooler stars that are targeted for further analysis. This again reduces the number of B-type stars that *Kepler* collects data on.

Kepler observes up to 223,000 stars in its field of view, detecting photometric variations in stars from a magnitude of 8 up to 14. Of these stars approximately 61% are estimated to be main sequence stars [NASA, 2012].

In comparison, *SMEI* is only capable of detecting the brightest stars in the sky, down to a magnitude of 6.5. However the field of view of the *SMEI* instrument covers almost the entire sky, which means that data on approximately 12,000 stars are available for analysis (see Chapter 2.1.2). Observations of the brightest stars in the sky also mean that the instrument is biased towards the largest stars in the sky, and is therefore more likely to observe stars further along the main sequence than the Sun and older stars that have evolved into giants. This is why there is a larger selection of B-type stars available for asteroseismic analysis with the *SMEI* instrument than there is with *Kepler*.

Even though the *Kepler* instrument far exceeds the *SMEI* instrument in terms of its accuracy, the *SMEI* data could still hold a lot of valuable information that is not available with *Kepler*, particularly for large main sequence stars.

5.1 β Cephei stars

The data on 27 known β Cephei stars were obtained from the *SMEI* instrument. These data were not only used to identify new pulsation frequencies in some of the stars, but also provided tighter constraints on frequencies which had previously been determined from other sources.

With the successful detection of new and known pulsation frequencies, the *SMEI* data were then analysed to search for potentially new β Cephei stars. Of the 213 stars observed with *SMEI*, ranging from B0 to B3, six stars were found with frequencies in the β Cephei range which were not attributed to stellar rotation or binarity and were

not previously confirmed as β Cephei stars.

The results of one star in particular, ζ CMa (HIP 30122), detected frequencies in both the β Cephei and SPB range. When these frequencies were compared to current stellar models, it was found that they were compatible with a star of $8M_{\odot}$ and Z=0.02. Furthermore, this demonstrates the capabilities of *SMEI* in detecting enough frequencies in a single star for modelling to occur.

5.2 Be stars

Photometric variations in Be stars have been observed for several decades. However these observations have been intermittent for example, the observations of ζ Oph between 1985 and 1990 as stated in Balona [1992], where observations detected frequencies in one time epoch but not others. Gutierrez-Soto et al. [2008] also report evidence for amplitude and/or phase change of oscillations in Be stars observed by *CoRoT*.

However, the research presented in this thesis specifically shows *how* the amplitude of the oscillations change over the light curves, and are shown in plots of amplitude vs. time. This analysis is the first of its kind performed on Be stars and has only been possible due to the long continuous light curves provided by the *SMEI* instrument. It is hoped that the results presented on Achernar and ζ Oph will help further our understanding of Be stars and if the variations found are linked with the Be phenomenon.

5.3 Future prospects

As shown from the results of the Be stars, the *SMEI* data can be used to observe amplitude changes in stellar oscillations. It is also possible that the data collected by *SMEI* may also be used to detect significant changes in the phase. The light curves of approximately 12 000 stars collected by the *SMEI* instrument are available covering a time period of 3 years. This archive could not only confirm the presence of previously undetected oscillations but also hold a wealth of interesting changes in amplitudes and

phases of these oscillations. However, 12 000 stars is too great a number to analyse individually and so an automated method was devised, which is described below.

The best chances of observing changes in amplitude and phase occur in stars where the S/N ratio of the oscillation is quite high. Therefore before any analysis regarding amplitude and phase changes began, stars which did not show oscillations with a high S/N ratio were immediately removed from the analysis. This was completed using a code similar to that used in *The search for new β Cephei stars* (Chapter 3.3.1). The only difference between that code and the one used here is the boundary condition used in the cutoff for the S/N. In the β Cephei survey all significant oscillations were searched for (where the S/N was greater than or equal to 4.1). To detected significant changes in amplitude and/or phase using the *SMEI* data the S/N of the oscillation was estimated to be approximately 20, the determination of which is described below.

When calculating the amplitude changes in the oscillations of Achernar and ζ Oph, the light curves needed to be split into 50-day time periods. In order to detect a change in amplitude and/or phase, the S/N of the oscillation in the 50-day time period must be greater than 4 for the results to be significant.

A light curve was simulated in order to determine what the S/N of an oscillation must be over a 3-year period for the S/N to be significant over a 50-day period. The simulation created a light curve to cover a 50-day time period with an oscillation of S/N of 4 running through it. The same simulation was then extended to cover a 3-year period so that the amplitude of the oscillation could be determined. The S/N in the 3-year light curve was found to be approximately 20, assuming that the amplitude of the oscillation remains constant during that time.

As shown in the results of Achernar and ζ Oph, the amplitudes of oscillations can change significantly, going from high S/N ratios to those below 4. With this in mind, the S/N cutoff was reduced to 15, so that interesting changes in amplitude that vary from very low amplitudes to higher amplitudes were not excluded.

Of the 12 000 stars in the survey, 245 stars were found to have one or more oscil-

lations where the S/N was greater than or equal to 15. The oscillations detected were then analysed further to search for amplitude and phase variations. This was accomplished using a similar code to that used for the ζ Oph results (Chapter 4.3.2) whereby the amplitude and phase were determined for each oscillation at the fixed frequency it was originally calculated at.

The final results were then plotted, an example of which is shown in Figure 5.2 which shows the variations in the 0.82 d^{-1} oscillation in γ Cas. There are six panels for each individual oscillation showing (i) amplitude variation (top), (ii) phase variation (middle) and (iii) duty cycle (bottom). The left-hand column shows the results of all of the amplitude and phase variation points in the light curve while the right-hand column only shows these results if the S/N of the oscillation was greater than 4. The points are also colour coded to show how the S/N of the oscillation changes over time. The colour coding is shown in the colour bar on the right-hand side of Figure 5.2. Dark blue points signify an oscillation with a high S/N, with the colour lightening to cyan for lower values of S/N. Once below a S/N of 4 the colour of the points turns to green, until it reaches dark green at 0.

The analysis of the 245 stars resulted in approximately 1 500 oscillations where the S/N was greater than 15. In some of these cases it is the harmonics which have also been detected. In other stars multiple fittings were removed from the same frequency which still had a S/N above 15. This suggests that a single sinusoidal model does not fit well with the data, possibly due to oscillation not being sinusoidal or possibly due to amplitude and/or phase variations of the oscillation. Taking this into consideration it is estimated that approximately 700 oscillation were detected.

Further analysis of these results is yet to begin. One possible aspect to investigate is how the phase of a stellar oscillation might vary due to the presence of a secondary star or planetary system. This has already been investigated by Silvotti et al. [2007] where a planet was found in orbit about a hot subdwarf B star with a period of 3.2 years. This was accomplished by observing how the phase of an oscillation changed

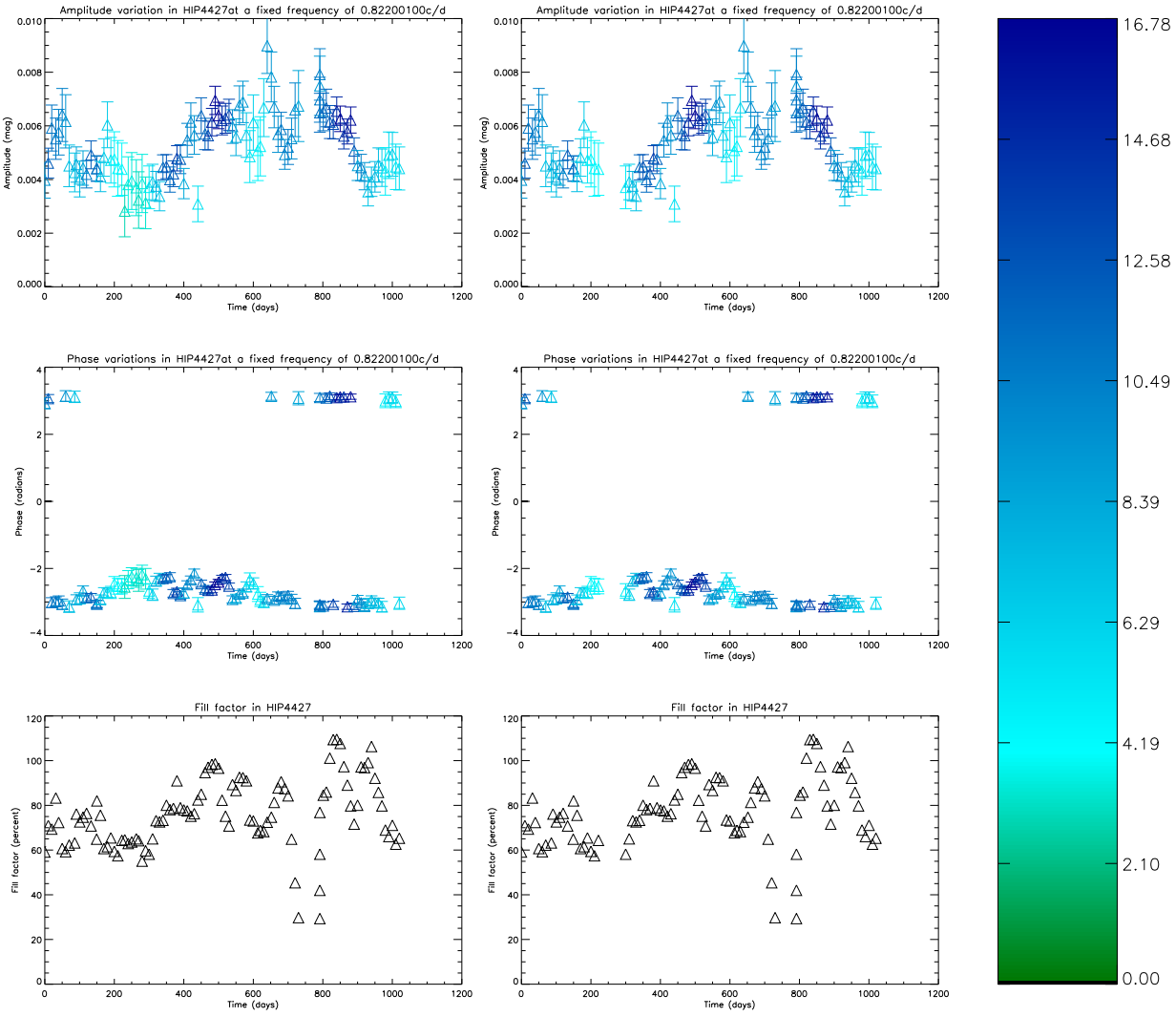

Figure 5.2: Example of amplitude and phase change results in the star γ Cas, HIP 4427, on the oscillation 0.82 d^{-1}. In ascending order the panels show amplitude variation, phase variation and duty cycle. The left-hand column shows all amplitude and phase results over the light curve. The right-hand side only shows amplitude and phase results where the oscillation had a S/N greater than or equal to 4. The points are coloured to indicate S/N, where dark blue represents high S/N turning to green for a S/N below 4.

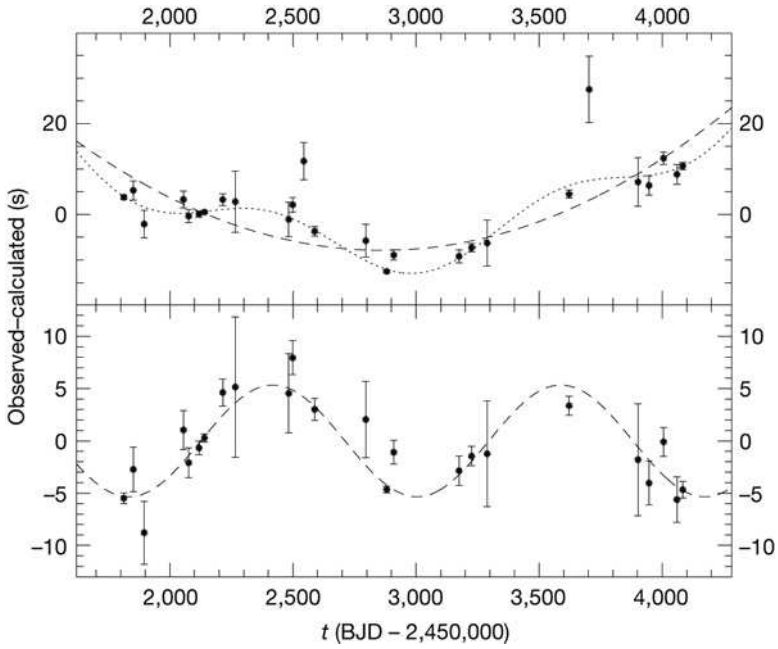

Figure 5.3: O-C diagram showing the variation in phase of the main pulsation frequency in the star V 391 Peg [Silvotti et al., 2007]. The top panel shows the original data with a second order polynomial and sinusoidal fit. The bottom panel shows only the sinusoidal component of the fit, once the long term trend had been removed.

as the star orbited about the centre of mass of the system. Figure 5.3 shows an O-C diagram, which shows how the phase varies in the main pulsation frequency of the star analysed by Silvotti et al. [2007]. The top panel of Figure 5.3 shows the O-C results with a second order polynomial and sinusoidal fit. The polynomial trend is due to the pulsation period changing with time, this trend has been confirmed in previous observations. The bottom panel shows only the sinusoidal fit with the trend removed. From these observations it was estimated that a planet was is orbit about the star with a period of 3.2 years, orbital distance of 1.7 AU and $M\sin i = 3.2\mathrm{M}_{Jup}$.

With the long duration of the *SMEI* light curves and results already obtained on high S/N oscillations, it is possible that the results from *SMEI* are able to detect extrasolar planets. For a significant oscillation in the phase to be detected, the change in phase must be larger than the error on the phase. A small error on the phase requires the S/N in the 50-day sections to be quite large. Typical results from the survey show that a S/N of four gives an error in phase of approximately 0.2 radians. While a S/N of 20 typically gives an error in phase of 0.06 radians, going down to 0.04 radians for

a S/N of 80.

Taking a star with a S/N of 40 in each 50-day section, the error on the phase was approximately 0.05 radians. Depending on the frequency of the oscillation, this gives an error in the timing of the oscillation between 100 and 200 seconds (assuming that the frequency lies between 3 and 7 d^{-1}). If a star were orbiting around a centre of mass due to a planetary or binary system, then the distance between the centre of mass of the system and the star is required to be between 0.2 and 0.4 AU or higher.

This is a rather large orbit for a star, particularly if it is due to a planetary system. For such an effect to be observed would depend on the mass of the star and the mass of the planet. However, the results in general indicate that the mass and semi major axis of the planet would be required to be large e.g. $20M_{jup}$ with a semi major axis of 10 AU, with a stellar mass not to much higher than the Sun. Due to the large semi-major axis of the planet, a complete cycle of the orbital period would not be detected in the 3 year *SMEI* data.

This is an example estimate and values will of course alter depending on the masses of the bodies in the system and also its inclination with respect to the observer. To detect a change in phase of the star due to its motion about the centre of mass of the system it is required that the motion of the star is parallel (or near parallel) to the observer. This orientation requirement is similar to that used in the detection of extrasolar planets using the Doppler Wobble. This requirement is so the maximum change in phase in the oscillation will occur. If the star's orbital orientation was such that it was perpendicular to the observer, orientation conditions required for astrometry, then no change in the phase of the oscillation would be observed.

It is more likely the phase results may be used in the detection of binary systems, rather than planetary systems, where the change in phase would be much larger. However this work would require further analysis than what has already been accomplished and so it is suggested that it be made available to others for future work. Even if no significant results are found regarding the phase change due to a planetary or bi-

nary system, interesting results regarding the phase change of oscillations may still be found. Indeed it has already been demonstrated with the observations on Be stars that interesting results can be found in the amplitude variations of the oscillations.

The results of this analysis have already proven useful. Researchers that already know of the amplitude and phase variation results from *SMEI* have queried the results for individual stars. In some cases this has provided confirmation of oscillations that have been detected. In others, the amplitude and phase variations look initially interesting and further analysis is now required. The code used in this analysis can also be used to look at other frequencies, where the S/N did not meet the criterion specified above, but where an amplitude variation may still be detected even if the phase variation cannot. The complete archive of 12 000 stars is still in demand by other researchers.

It is hoped that the results on the amplitude and phase variations will remain accessible to those who wish to use the information in further research, along with the rest of the data in the *SMEI* archive. It is important not to forget the significance of the results already obtained with the *SMEI* instrument and how much is still yet to be discovered.

The results presented in this thesis show the advantages of having photometric data with good coverage and over a long duration. Not only can these data be used to identify stellar oscillations, but with a long time duration the amplitude and phase changes of these oscillations may also be established.

Appendix A

Published results

The research that was undertaken on Achernar (see Chapter 4.2) was successfully published in a scientific paper, a copy of which can be found on the following pages.

The results presented on ζ Oph (see Chapter 4.3) are currently in preparation to be published in a scientific paper. The results on the confirmed β Cephei stars (see Chapter 3.2) and the β Cephei survey (see Chapter 3.3) are also planned to be published as two separate scientific papers.

[Full text not available in the digital version of this thesis.
See:
K. J. F. Goss, C. Karoff, W. J. Chaplin, Y. Elsworth, and I. R. Stevens. Variations of the amplitudes of oscillation of the Be star Achernar. MNRAS, 411:162–166, February 2011. doi: 10.1111/j.1365-2966.2010.17665.x.]

Bibliography

H. A. Abt, H. Levato, and M. Grosso. Rotational Velocities of B Stars. ApJ, 573: 359–365, July 2002. doi: 10.1086/340590.

C. Aerts and P. De Cat. β Cep stars from a spectroscopic point of view. Space Sci. Rev., 105:453–492, January 2003. doi: 10.1023/A:1023983704925.

C. Aerts, P. Mathias, D. Gillet, and C. Waelkens. Multiperiodicity and pulsation characteristics of β Cephei. A&A, 286:109–120, June 1994.

C. Aerts, P. De Cat, G. Handler, U. Heiter, L. A. Balona, J. Krzesinski, P. Mathias, H. Lehmann, I. Ilyin, J. De Ridder, S. Dreizler, A. Bruch, I. Traulsen, A. Hoffmann, D. James, E. Romero-Colmenero, T. Maas, M. A. T. Groenewegen, J. H. Telting, K. Uytterhoeven, C. Koen, P. L. Cottrell, J. Bentley, D. J. Wright, and J. Cuypers. Asteroseismology of the β Cephei star ν Eridani - II. Spectroscopic observations and pulsational frequency analysis. MNRAS, 347:463–470, January 2004. doi: 10.1111/j.1365-2966.2004.07215.x.

C. Aerts, J. Christensen-Dalsgaard, and D. W. Kurtz. *Asteroseismology*. 2010. doi: 10.1007/978-1-4020-5803-5.

T. Appourchaux, T. Toutain, U. Telljohann, A. Jimenez, M. C. Rabello-Soares, B. N. Andersen, and A. R. Jones. Frequencies and splittings of low-degree solar P modes: results of the Luminosity Oscillations Imager. A&A, 294:L13–L16, February 1995.

M. Asplund, N. Grevesse, A. J. Sauval, C. Allende Prieto, and R. Blomme. Line

formation in solar granulation. VI. [C I], C I, CH and C_2 lines and the photospheric C abundance. A&A, 431:693–705, February 2005. doi: 10.1051/0004-6361:20041951.

Nancy Atkinson. Kepler mission extended to 2016, 2012. URL http://www.universetoday.com/94423/kepler-mission-extended-to-2016/.

M. Ausseloos, C. Aerts, K. Uytterhoeven, C. Schrijvers, C. Waelkens, and J. Cuypers. beta Centauri: An eccentric binary with two beta Cep-type components. A&A, 384: 209–214, March 2002. doi: 10.1051/0004-6361:20020004.

M. Ausseloos, C. Aerts, K. Lefever, J. Davis, and P. Harmanec. High-precision elements of double-lined spectroscopic binaries from combined interferometry and spectroscopy. Application to the β Cephei star β Centauri. A&A, 455:259–269, August 2006. doi: 10.1051/0004-6361:20064829.

N. R. Badnell, M. A. Bautista, K. Butler, F. Delahaye, C. Mendoza, P. Palmeri, C. J. Zeippen, and M. J. Seaton. Updated opacities from the Opacity Project. MNRAS, 360:458–464, June 2005. doi: 10.1111/j.1365-2966.2005.08991.x.

Emily Baldwin. What is asteroseismology, March 2012. URL http://www.astronomynow.com/nam09/2009/04/what-is-asteroseismology.html.

L. A. Balona. Calibration of effective temperature, bolometric correction and mass for early-type stars using Stroemgren photometric indices. MNRAS, 211:973–979, December 1984.

L. A. Balona. Photometric monitoring of O-type stars. MNRAS, 254:404–+, February 1992.

L. A. Balona and J. Cuypers. The extraordinary early-type eclipsing binary HR 2680. MNRAS, 261:1–10, March 1993.

L. A. Balona, C. A. Engelbrecht, and F. Marang. Achernar. MNRAS, 227:123–133, July 1987.

L. A. Balona, J. Cuypers, and F. Marang. Intensive photometry of southern Be variables. II - Summer objects. A&AS, 92:533–563, February 1992.

T. R. Bedding, B. Mosser, D. Huber, J. Montalbán, P. Beck, J. Christensen-Dalsgaard, Y. P. Elsworth, R. A. García, A. Miglio, D. Stello, T. R. White, J. De Ridder, S. Hekker, C. Aerts, C. Barban, K. Belkacem, A.-M. Broomhall, T. M. Brown, D. L. Buzasi, F. Carrier, W. J. Chaplin, M. P. di Mauro, M.-A. Dupret, S. Frandsen, R. L. Gilliland, M.-J. Goupil, J. M. Jenkins, T. Kallinger, S. Kawaler, H. Kjeldsen, S. Mathur, A. Noels, V. S. Aguirre, and P. Ventura. Gravity modes as a way to distinguish between hydrogen- and helium-burning red giant stars. Nature, 471: 608–611, March 2011. doi: 10.1038/nature09935.

L. N. Berdnikov and I. R. Stevens. Search for Random Fluctuations in Periods of Short-period Cepheids. In C. Sterken, N. Samus, & L. Szabados, editor, *Variable Stars, the Galactic halo and Galaxy Formation*, pages 207–+, February 2010.

A. Blaauw. On the origin of the O- and B-type stars with high velocities (the "runaway" stars), and some related problems. Bull. Astron. Inst. Netherlands, 15:265–+, May 1961.

J.-C. Bouret, T. Lanz, D. J. Hillier, S. R. Heap, I. Hubeny, D. J. Lennon, L. J. Smith, and C. J. Evans. Quantitative Spectroscopy of O Stars at Low Metallicity: O Dwarfs in NGC 346. ApJ, 595:1182–1205, October 2003. doi: 10.1086/377368.

M. Breger, J. Stich, R. Garrido, B. Martin, S. Y. Jiang, Z. P. Li, D. P. Hube, W. Ostermann, M. Paparo, and M. Scheck. Nonradial Pulsation of the Delta-Scuti Star Bu-Cancri in the Praesepe Cluster. A&A, 271:482–+, April 1993.

H. Bruntt, H. Kjeldsen, D. L. Buzasi, and T. R. Bedding. Evidence for Granulation and Oscillations in Procyon from Photometry with the WIRE Satellite. ApJ, 633: 440–446, November 2005. doi: 10.1086/462401.

H. Bruntt, D. W. Kurtz, M. S. Cunha, I. M. Brandão, G. Handler, T. R. Bedding, T. Medupe, D. L. Buzasi, D. Mashigo, I. Zhang, and F. van Wyk. Asteroseismic analysis of the roAp star α Circini: 84d of high-precision photometry from the WIRE satellite. MNRAS, 396:1189–1201, June 2009. doi: 10.1111/j.1365-2966.2009.14804.x.

D. Buzasi, J. Catanzarite, R. Laher, T. Conrow, D. Shupe, T. N. Gautier, III, T. Kreidl, and D. Everett. The Detection of Multimodal Oscillations on α Ursae Majoris. ApJ, 532:L133–L136, April 2000. doi: 10.1086/312573.

A. C. Carciofi, A. M. Magalhães, N. V. Leister, J. E. Bjorkman, and R. S. Levenhagen. Achernar: Rapid Polarization Variability as Evidence of Photospheric and Circumstellar Activity. ApJ, 671:L49–L52, December 2007. doi: 10.1086/524772.

B. W. Carroll and D. A. Ostlie. *An introduction to modern astrophysics and cosmology*. July 2006.

E. Chapellier and J. C. Valtier. Pulsation and binarity in Beta Cephei Stars. I - Sigma Scorpii. A&A, 257:587–593, April 1992.

W. J. Chaplin, T. Appourchaux, Y. Elsworth, R. A. García, G. Houdek, C. Karoff, T. S. Metcalfe, J. Molenda-Żakowicz, M. J. P. F. G. Monteiro, M. J. Thompson, T. M. Brown, J. Christensen-Dalsgaard, R. L. Gilliland, H. Kjeldsen, W. J. Borucki, D. Koch, J. M. Jenkins, J. Ballot, S. Basu, M. Bazot, T. R. Bedding, O. Benomar, A. Bonanno, I. M. Brandão, H. Bruntt, T. L. Campante, O. L. Creevey, M. P. Di Mauro, G. Doğan, S. Dreizler, P. Eggenberger, L. Esch, S. T. Fletcher, S. Frandsen, N. Gai, P. Gaulme, R. Handberg, S. Hekker, R. Howe, D. Huber, S. G. Korzennik, J. C. Lebrun, S. Leccia, M. Martic, S. Mathur, B. Mosser, R. New, P.-O. Quirion, C. Régulo, I. W. Roxburgh, D. Salabert, J. Schou, S. G. Sousa, D. Stello, G. A. Verner, T. Arentoft, C. Barban, K. Belkacem, S. Benatti, K. Biazzo, P. Boumier, P. A. Bradley, A.-M. Broomhall, D. L. Buzasi, R. U. Claudi, M. S. Cunha, F. D'Antona, S. Deheuvels, A. Derekas, A. García Hernández, M. S.

Giampapa, M. J. Goupil, M. Gruberbauer, J. A. Guzik, S. J. Hale, M. J. Ireland, L. L. Kiss, I. N. Kitiashvili, K. Kolenberg, H. Korhonen, A. G. Kosovichev, F. Kupka, Y. Lebreton, B. Leroy, H.-G. Ludwig, S. Mathis, E. Michel, A. Miglio, J. Montalbán, A. Moya, A. Noels, R. W. Noyes, P. L. Pallé, L. Piau, H. L. Preston, T. Roca Cortés, M. Roth, K. H. Sato, J. Schmitt, A. M. Serenelli, V. Silva Aguirre, I. R. Stevens, J. C. Suárez, M. D. Suran, R. Trampedach, S. Turck-Chièze, K. Uytterhoeven, R. Ventura, and P. A. Wilson. The Asteroseismic Potential of Kepler: First Results for Solar-Type Stars. ApJ, 713:L169–L175, April 2010. doi: 10.1088/2041-8205/713/2/L169.

W. J. Chaplin, H. Kjeldsen, J. Christensen-Dalsgaard, S. Basu, A. Miglio, T. Appourchaux, T. R. Bedding, Y. Elsworth, R. A. García, R. L. Gilliland, L. Girardi, G. Houdek, C. Karoff, S. D. Kawaler, T. S. Metcalfe, J. Molenda-Żakowicz, M. J. P. F. G. Monteiro, M. J. Thompson, G. A. Verner, J. Ballot, A. Bonanno, I. M. Brandão, A.-M. Broomhall, H. Bruntt, T. L. Campante, E. Corsaro, O. L. Creevey, G. Doğan, L. Esch, N. Gai, P. Gaulme, S. J. Hale, R. Handberg, S. Hekker, D. Huber, A. Jiménez, S. Mathur, A. Mazumdar, B. Mosser, R. New, M. H. Pinsonneault, D. Pricopi, P.-O. Quirion, C. Régulo, D. Salabert, A. M. Serenelli, V. Silva Aguirre, S. G. Sousa, D. Stello, I. R. Stevens, M. D. Suran, K. Uytterhoeven, T. R. White, W. J. Borucki, T. M. Brown, J. M. Jenkins, K. Kinemuchi, J. Van Cleve, and T. C. Klaus. Ensemble Asteroseismology of Solar-Type Stars with the NASA Kepler Mission. *Science*, 332:213–, April 2011. doi: 10.1126/science.1201827.

O. Chesneau, A. Meilland, T. Rivinius, P. Stee, S. Jankov, A. Domiciano de Souza, U. Graser, T. Herbst, E. Janot-Pacheco, R. Koehler, C. Leinert, S. Morel, F. Paresce, A. Richichi, and S. Robbe-Dubois. First VLTI/MIDI observations of a Be star: Alpha Arae. A&A, 435:275–287, May 2005. doi: 10.1051/0004-6361:20041954.

J. Christensen-Dalsgaard. *Lecture Notes on Stellar Structure and Evolution.* Aarhus Universitet, 1991. URL `http://books.google.co.uk/books?id=B2VOQwAACAAJ`.

J. Christensen-Dalsgaard. On the Asteroseismic HR Diagram. In T. M. Brown, editor,

GONG 1992. Seismic Investigation of the Sun and Stars, volume 42 of *Astronomical Society of the Pacific Conference Series*, page 347, January 1993.

J. Christensen-Dalsgaard. *Lecture notes on stellar oscillations*. Institut for Fysik og Astronomi, Aarhus Universitet, 1998. URL `http://books.google.co.uk/books?id=FD55cgAACAAJ`.

J. Christensen-Dalsgaard. *Lecture notes on stellar oscillations*. Institut for Fysik og Astronomi, Aarhus Universitet, 2003. URL `http://books.google.co.uk/books?id=FD55cgAACAAJ`.

J. Christensen-Dalsgaard. An Overview of Helio- and Asteroseismology. In D. Danesy, editor, *SOHO 14 Helio- and Asteroseismology: Towards a Golden Future*, volume 559 of *ESA Special Publication*, pages 1–+, October 2004.

J. Cuypers. New observations and frequency analysis of the Beta Cephei star Tau1 LUPI. A&AS, 69:445–449, June 1987.

J. De Ridder, C. Barban, F. Baudin, F. Carrier, A. P. Hatzes, S. Hekker, T. Kallinger, W. W. Weiss, A. Baglin, M. Auvergne, R. Samadi, P. Barge, and M. Deleuil. Non-radial oscillation modes with long lifetimes in giant stars. Nature, 459:398–400, May 2009. doi: 10.1038/nature08022.

P. Degroote, C. Aerts, M. Ollivier, A. Miglio, J. Debosscher, J. Cuypers, M. Briquet, J. Montalbán, A. Thoul, A. Noels, P. De Cat, L. Balaguer-Núñez, C. Maceroni, I. Ribas, M. Auvergne, A. Baglin, M. Deleuil, W. W. Weiss, L. Jorda, F. Baudin, and R. Samadi. CoRoT's view of newly discovered B-star pulsators: results for 358 candidate B pulsators from the initial run's exoplanet field data. A&A, 506:471–489, October 2009. doi: 10.1051/0004-6361/200911884.

P. Degroote, C. Aerts, A. Baglin, A. Miglio, M. Briquet, A. Noels, E. Niemczura, J. Montalban, S. Bloemen, R. Oreiro, M. Vučković, K. Smolders, M. Auvergne, F. Baudin, C. Catala, and E. Michel. Deviations from a uniform period spacing of

gravity modes in a massive star. Nature, 464:259–261, March 2010. doi: 10.1038/nature08864.

M. Desmet, M. Briquet, A. Thoul, W. Zima, P. De Cat, G. Handler, I. Ilyin, E. Kambe, J. Krzesinski, H. Lehmann, S. Masuda, P. Mathias, D. E. Mkrtichian, J. Telting, K. Uytterhoeven, S. L. S. Yang, and C. Aerts. An asteroseismic study of the β Cephei star 12 Lacertae: multisite spectroscopic observations, mode identification and seismic modelling. MNRAS, 396:1460–1472, July 2009. doi: 10.1111/j.1365-2966.2009.14790.x.

P. D. Diago, J. Gutiérrez-Soto, J. Fabregat, C. Martayan, and J. Suso. Pulsating B and Be Stars in the Magellanic Clouds. In *Highlights of Spanish Astrophysics V*, page 401, 2010.

A. Domiciano de Souza, P. Kervella, S. Jankov, L. Abe, F. Vakili, E. di Folco, and F. Paresce. The spinning-top Be star Achernar from VLTI-VINCI. A&A, 407:L47–L50, August 2003. doi: 10.1051/0004-6361:20030786.

M.-A. Dupret, J. De Ridder, P. De Cat, C. Aerts, R. Scuflaire, A. Noels, and A. Thoul. A photometric mode identification method, including an improved non-adiabatic treatment of the atmosphere. A&A, 398:677–685, February 2003. doi: 10.1051/0004-6361:20021679.

W. A. Dziembowski and A. A. Pamiatnykh. The opacity mechanism in B-type stars. I - Unstable modes in Beta Cephei star models. MNRAS, 262:204–212, May 1993.

W. A. Dziembowski, P. Moskalik, and A. A. Pamyatnykh. The Opacity Mechanism in B-Type Stars - Part Two - Excitation of High-Order G-Modes in Main Sequence Stars. MNRAS, 265:588–+, December 1993.

A. S. Eddington. *The Internal Constitution of the Stars*. 1926.

C. J. Eyles, G. M. Simnett, M. P. Cooke, B. V. Jackson, A. Buffington, P. P. Hick,

N. R. Waltham, J. M. King, P. A. Anderson, and P. E. Holladay. The Solar Mass Ejection Imager (Smei). Sol. Phys., 217:319–347, November 2003.

F. C. Fekel, Jr. and J. Tomkin. Secondaries of eclipsing binaries. IV - The triple system Lambda Tauri. ApJ, 263:289–301, December 1982. doi: 10.1086/160503.

B. H. Foing, C. Catala, J. M. Oliveira, A. M. Hubert, M. Floquet, J. X. Hao, T. Kennelly, L. Balona, H. Henrichs, and J. de Jong. Asteroseismology from MUSICOS multi-site campaigns. *Advances in Space Research*, 24:251–257, 1999. doi: 10.1016/S0273-1177(99)00510-4.

S. Frandsen, A. Jones, H. Kjeldsen, M. Viskum, J. Hjorth, N. H. Andersen, and B. Thomsen. CCD photometry of the δ-Scuti star $\kappa\hat{}2\hat{}$ Bootis. A&A, 301:123, September 1995.

Y. Frémat, J. Zorec, A.-M. Hubert, and M. Floquet. Effects of gravitational darkening on the determination of fundamental parameters in fast-rotating B-type stars. A&A, 440:305–320, September 2005. doi: 10.1051/0004-6361:20042229.

E. B. Frost. The sprectroscopic binary beta Cephei. ApJ, 15:340–341, June 1902. doi: 10.1086/140929.

E. B. Frost. The period of beta Cephei. ApJ, 24:259–262, November 1906. doi: 10.1086/141389.

S. J. George, I. R. Stevens, and S. A. Spreckley. Is Shedir Variable? *ArXiv e-prints*, May 2009.

R. L. Gilliland, T. M. Brown, J. Christensen-Dalsgaard, H. Kjeldsen, C. Aerts, T. Appourchaux, S. Basu, T. R. Bedding, W. J. Chaplin, M. S. Cunha, P. De Cat, J. De Ridder, J. A. Guzik, G. Handler, S. Kawaler, L. Kiss, K. Kolenberg, D. W. Kurtz, T. S. Metcalfe, M. J. P. F. G. Monteiro, R. Szabó, T. Arentoft, L. Balona, J. Debosscher, Y. P. Elsworth, P.-O. Quirion, D. Stello, J. C. Suárez, W. J. Borucki, J. M.

Jenkins, D. Koch, Y. Kondo, D. W. Latham, J. F. Rowe, and J. H. Steffen. Kepler Asteroseismology Program: Introduction and First Results. PASP, 122:131–143, February 2010. doi: 10.1086/650399.

S. Giridhar. Spectral Classification: Old and Contemporary. In A. Goswami & B. E. Reddy, editor, *Principles and Perspectives in Cosmochemistry*, pages 165–+, 2010. doi: 10.1007/978-3-642-10352-0_3.

R. Glebocki and P. Gnacinski. Catalog of Stellar Rotational Velocities (Glebocki+ 2005). *VizieR Online Data Catalog*, 3244:0–+, 2005.

K. J. F. Goss, C. Karoff, W. J. Chaplin, Y. Elsworth, and I. R. Stevens. Variations of the amplitudes of oscillation of the Be star Achernar. MNRAS, 411:162–166, February 2011. doi: 10.1111/j.1365-2966.2010.17665.x.

M. Gruberbauer, H. Saio, D. Huber, T. Kallinger, W. W. Weiss, D. B. Guenther, R. Kuschnig, J. M. Matthews, A. F. J. Moffat, S. Rucinski, D. Sasselov, and G. A. H. Walker. MOST photometry and modeling of the rapidly oscillating (roAp) star γ Equulei. A&A, 480:223–232, March 2008. doi: 10.1051/0004-6361:20078830.

F. Grundahl, T. Arentoft, J. Christensen-Dalsgaard, S. Frandsen, H. Kjeldsen, and P. K. Rasmussen. Stellar Oscillations Network Group SONG. *Journal of Physics Conference Series*, 118(1):012041, October 2008. doi: 10.1088/1742-6596/118/1/012041.

J. Gutierrez-Soto, C. Neiner, A.-M. Hubert, M. Floquet, A.-L. Huat, P. D. Diago, J. Fabregat, B. Leroy, B. De Batz, L. Andrade, M. Emilio, W. Facanha, Y. Fremat, E. Janot-Pacheco, C. Martayan, and J. Suso. First results on the Be stars observed with the CoRoT satellite. *Communications in Asteroseismology*, 157:70–74, December 2008.

G. M. H. J. Habets and J. R. W. Heintze. Empirical bolometric corrections for the main-sequence. A&AS, 46:193–237, November 1981.

P. Hadrava and P. Harmanec. New aspects of the variability of β Cep. A&A, 315: L401–L404, November 1996.

Steven Hale. Bison background: An overview, March 2012. URL `http://bison.ph.bham.ac.uk/index.php?page=bison`.

G. Handler. β Cephei and Slowly Pulsating B stars as targets for BRITE- Constellation. *Communications in Asteroseismology*, 152:160–165, January 2008. doi: 10.1553/cia152s160.

G. Handler, M. Jerzykiewicz, E. Rodríguez, K. Uytterhoeven, P. J. Amado, T. N. Dorokhova, N. I. Dorokhov, E. Poretti, J.-P. Sareyan, L. Parrao, D. Lorenz, D. Zsuffa, R. Drummond, J. Daszyńska-Daszkiewicz, T. Verhoelst, J. De Ridder, B. Acke, P.-O. Bourge, A. I. Movchan, R. Garrido, M. Paparó, T. Sahin, V. Antoci, S. N. Udovichenko, K. Csorba, R. Crowe, B. Berkey, S. Stewart, D. Terry, D. E. Mkrtichian, and C. Aerts. Asteroseismology of the β Cephei star 12 (DD) Lacertae: photometric observations, pulsational frequency analysis and mode identification. MNRAS, 365:327–338, January 2006. doi: 10.1111/j.1365-2966.2005.09728.x.

G. Handler, J. M. Matthews, J. A. Eaton, J. Daszyńska-Daszkiewicz, R. Kuschnig, H. Lehmann, E. Rodríguez, A. A. Pamyatnykh, T. Zdravkov, P. Lenz, V. Costa, D. Díaz-Fraile, A. Sota, T. Kwiatkowski, A. Schwarzenberg-Czerny, W. Borczyk, W. Dimitrov, M. Fagas, K. Kamiński, A. Rożek, F. van Wyk, K. R. Pollard, P. M. Kilmartin, W. W. Weiss, D. B. Guenther, A. F. J. Moffat, S. M. Rucinski, D. D. Sasselov, and G. A. H. Walker. Asteroseismology of Hybrid Pulsators Made Possible: Simultaneous MOST Space Photometry and Ground-Based Spectroscopy of γ Peg. ApJ, 698:L56–L59, June 2009. doi: 10.1088/0004-637X/698/1/L56.

B. Hauck and M. Mermilliod. uvby-beta Catalogue (Hauck+ 1997). *VizieR Online Data Catalog*, 2215:0–+, October 1997.

D. Heynderickx. A photometric study of Beta Cephei stars. I - Frequency analyses. A&AS, 96:207–254, December 1992.

D. Hoffleit. History of the Discovery of Mira Stars. *Journal of the American Association of Variable Star Observers (JAAVSO)*, 25:115–136, 1997.

D. Hoffleit and C. —. Jaschek. *The Bright star catalogue*. 1991.

M. M. Hohle, R. Neuhäuser, and B. F. Schutz. Masses and luminosities of O- and B-type stars and red supergiants. *Astronomische Nachrichten*, 331:349, April 2010. doi: 10.1002/asna.200911355.

R. Hoogerwerf, J. H. J. de Bruijne, and P. T. de Zeeuw. On the origin of the O and B-type stars with high velocities. II. Runaway stars and pulsars ejected from the nearby young stellar groups. A&A, 365:49–77, January 2001. doi: 10.1051/0004-6361:20000014.

R. Hounsell, M. F. Bode, P. P. Hick, A. Buffington, B. V. Jackson, J. M. Clover, A. W. Shafter, M. J. Darnley, N. R. Mawson, I. A. Steele, A. Evans, S. P. S. Eyres, and T. J. O'Brien. Exquisite Nova Light Curves from the Solar Mass Ejection Imager (SMEI). ApJ, 724:480–486, November 2010. doi: 10.1088/0004-637X/724/1/480.

A.-L. Huat, A.-M. Hubert, F. Baudin, M. Floquet, C. Neiner, Y. Frémat, J. Gutiérrez-Soto, L. Andrade, B. de Batz, P. D. Diago, M. Emilio, F. Espinosa Lara, J. Fabregat, E. Janot-Pacheco, B. Leroy, C. Martayan, T. Semaan, J. Suso, M. Auvergne, C. Catala, E. Michel, and R. Samadi. The B0.5IVe CoRoT target HD 49330. I. Photometric analysis from CoRoT data. A&A, 506:95–101, October 2009. doi: 10.1051/0004-6361/200911928.

S. Hubrig, L. M. Oskinova, and M. Schöller. First detection of a magnetic field in the fast rotating runaway Oe star ζ Ophiuchi. *Astronomische Nachrichten*, 332:147–+, 2011. doi: 10.1002/asna.201111516.

C. Jaschek, M. Jaschek, and B. Kucewicz. A Survey of Southern Be Stars. ZAp, 59: 108–+, 1964.

M. Jerzykiewicz. HR 6684: A New Beta Cephei Type Variable Star. PASP, 84:718–+, October 1972. doi: 10.1086/129368.

M. Jerzykiewicz, G. Handler, R. R. Shobbrook, A. Pigulski, R. Medupe, T. Mokgwetsi, P. Tlhagwane, and E. Rodríguez. Asteroseismology of the β Cephei star ν Eridani - IV. The 2003-2004 multisite photometric campaign and the combined 2002-2004 data. MNRAS, 360:619–630, June 2005. doi: 10.1111/j.1365-2966.2005.09088.x.

E. Kambe, R. Hirata, H. Ando, J. Cuypers, M. Katoh, E. J. Kennelly, G. A. H. Walker, S. Stefl, and A. E. Tarasov. Multiperiodicity of zeta Ophiuchi from Multisite Observations. ApJ, 481:406, May 1997. doi: 10.1086/304025.

P. Kervella, A. Domiciano de Souza, and P. Bendjoya. The close-in companion of the fast rotating Be star Achernar. A&A, 484:L13–L16, June 2008. doi: 10.1051/0004-6361:200809765.

R. Kippenhahn and A. Weigert. *Stellar Structure and Evolution*. 1990.

H. Kjeldsen and T. R. Bedding. Amplitudes of stellar oscillations: the implications for asteroseismology. A&A, 293:87–106, January 1995.

Z. Kołaczkowski, A. Pigulski, I. Soszyński, A. Udalski, M. Kubiak, M. Szymański, K. Żebruń, G. Pietrzyński, P. R. Woźniak, O. Szewczyk, and Ł. Wyrzykowski. Hot pulsators in the Magellanic Clouds . Mem. Soc. Astron. Italiana, 77:336, 2006.

D. W. Kurtz, C. Cameron, M. S. Cunha, N. Dolez, G. Vauclair, E. Pallier, A. Ulla, S. O. Kepler, A. da Costa, A. Kanaan, L. Fraga, O. Giovannini, M. A. Wood, N. Silvestri, S. D. Kawaler, R. L. Riddle, M. D. Reed, T. K. Watson, T. S. Metcalfe, A. Mukadam, R. E. Nather, D. E. Winget, A. Nitta, S. J. Kleinman, J. A. Guzik, P. A. Bradley, J. M. Matthews, K. Sekiguchi, D. J. Sullivan, T. Sullivan,

R. Shobbrook, X. Jiang, P. V. Birch, B. N. Ashoka, S. Seetha, V. Girish, S. Joshi, P. Moskalik, S. Zola, D. O'Donoghue, G. Handler, M. Mueller, J. M. Gonzalez Perez, J.-E. Solheim, F. Johannessen, and L. Bigot. Pushing the ground-based limit: 14-μmag photometric precision with the definitive Whole Earth Telescope asteroseismic data set for the rapidly oscillating Ap star HR1217. MNRAS, 358:651–664, April 2005. doi: 10.1111/j.1365-2966.2005.08807.x.

R. Kuschnig, W. W. Weiss, R. Gruber, P. Y. Bely, and H. Jenkner. Microvariability survey with the Hubble Space Telescope Fine Guidance Sensors. Exploring the instrumental properties. A&A, 328:544–550, December 1997.

N. Langer and A. Heger. The Evolution of Surface Parameters of Rotating Massive Stars. In I. Howarth, editor, *Properties of Hot Luminous Stars*, volume 131 of *Astronomical Society of the Pacific Conference Series*, pages 76–+, 1998.

T. Lebzelter. The shapes of light curves of Mira-type variables. *Astronomische Nachrichten*, 332:140, February 2011. doi: 10.1002/asna.201011469.

R. B. Leighton, R. W. Noyes, and G. W. Simon. Velocity Fields in the Solar Atmosphere. I. Preliminary Report. ApJ, 135:474, March 1962. doi: 10.1086/147285.

P. Lenz and M. Breger. Period04 User Guide. *Communications in Asteroseismology*, 146:53–136, June 2005. doi: 10.1553/cia146s53.

J. R. Lesh and M. L. Aizenman. The observational status of the Beta Cephei stars. ARA&A, 16:215–240, 1978. doi: 10.1146/annurev.aa.16.090178.001243.

C. Lloyd and C. D. Pike. The radial velocity variations and evolutionary status of Delta LUPI. A&AS, 76:121–125, November 1988.

N. R. Lomb. The decline of the Beta Canis Majoris pulsation in Alpha Virginis. MNRAS, 185:325–333, November 1978.

N. R. Lomb and R. R. Shobbrook. New radial velocities and further photometric observations of lambda Sco and kappa Sco. MNRAS, 173:709–728, December 1975.

A. Maeder. *Physics, Formation and Evolution of Rotating Stars*. 2009.

C. Martayan, Y. Frémat, A.-M. Hubert, M. Floquet, J. Zorec, and C. Neiner. Effects of metallicity, star-formation conditions, and evolution in B and Be stars. I. Large Magellanic Cloud, field of NGC 2004. A&A, 452:273–284, June 2006. doi: 10.1051/0004-6361:20053859.

C. Martayan, Y. Frémat, A.-M. Hubert, M. Floquet, J. Zorec, and C. Neiner. Effects of metallicity, star-formation conditions, and evolution in B and Be stars. II. Small Magellanic Cloud, field of NGC330. A&A, 462:683–694, February 2007. doi: 10.1051/0004-6361:20065076.

P. Mathias, C. Aerts, M. de Pauw, D. Gillet, and C. Waelkens. A Spectroscopic Analysis of the Beta-Cephei Star Alpha-Lupi. A&A, 283:813–+, March 1994a.

P. Mathias, C. Aerts, D. Gillet, and C. Waelkens. A spectroscopic analysis of the beta Cephei star 12 Lacertae. A&A, 289:875–884, September 1994b.

J. M. Matthews, R. Kuschnig, G. A. H. Walker, J. Pazder, R. Johnson, K. Skaret, E. Shkolnik, T. Lanting, J. P. Morgan, and S. Sidhu. Ultraprecise Photometry from Space: The MOST Microsat Mission. In L. Szabados & D. Kurtz, editor, *IAU Colloq. 176: The Impact of Large-Scale Surveys on Pulsating Star Research*, volume 203 of *Astronomical Society of the Pacific Conference Series*, pages 74–75, 2000.

A. Meilland, P. Stee, M. Vannier, F. Millour, A. Domiciano de Souza, F. Malbet, C. Martayan, F. Paresce, R. G. Petrov, A. Richichi, and A. Spang. First direct detection of a Keplerian rotating disk around the Be star α Arae using AMBER/VLTI. A&A, 464:59–71, March 2007. doi: 10.1051/0004-6361:20064848.

G. Meynet and A. Maeder. Stellar evolution with rotation. V. Changes in all the outputs of massive star models. A&A, 361:101–120, September 2000.

E. Michel, J. A. Belmonte, M. Alvarez, S. Y. Jiang, M. Chevreton, M. Auvergne, M. J. Goupil, A. Baglin, A. Mangeney, T. Roca Cortes, Y. Y. Liu, J. N. Fu, and N. Dolez. Multi-periodicity of the Delta Scuti star GX Pegasi - Second photometry campaign of the STEPHI network. A&A, 255:139–148, February 1992.

A. Miglio, J. Montalbán, and M.-A. Dupret. Instability strips of slowly pulsating B stars and β Cephei stars: the effect of the updated OP opacities and of the metal mixture. MNRAS, 375:L21–L25, February 2007a. doi: 10.1111/j.1745-3933.2006.00267.x.

A. Miglio, J. Montalbán, and M.-A. Dupret. Revised instability domains of SPB and β Cephei stars. *Communications in Asteroseismology*, 151:48–56, August 2007b. doi: 10.1553/cia151s48.

Chris Mihos. Late stage nuclear burning in high mass stars, March 2012. URL `http://burro.astr.cwru.edu/Academics/Astr221/LifeCycle/highmassburn.html`.

E. Miller-Ricci, J. F. Rowe, D. Sasselov, J. M. Matthews, D. B. Guenther, R. Kuschnig, A. F. J. Moffat, S. M. Rucinski, G. A. H. Walker, and W. W. Weiss. MOST Space-based Photometry of the Transiting Exoplanet System HD 209458: Transit Timing to Search for Additional Planets. ApJ, 682:586–592, July 2008a. doi: 10.1086/587446.

E. Miller-Ricci, J. F. Rowe, D. Sasselov, J. M. Matthews, R. Kuschnig, B. Croll, D. B. Guenther, A. F. J. Moffat, S. M. Rucinski, G. A. H. Walker, and W. W. Weiss. MOST Space-based Photometry of the Transiting Exoplanet System HD 189733: Precise Timing Measurements for Transits across an Active Star. ApJ, 682:593–601, July 2008b. doi: 10.1086/587634.

M. H. Montgomery and D. Odonoghue. A derivation of the errors for least squares fitting to time series data. *Delta Scuti Star Newsletter*, 13:28–+, July 1999.

NASA. Kepler: Target stars, 2012. URL `http://kepler.nasa.gov/Science/about/targetFieldOfView/`.

R. E. Nather, D. E. Winget, J. C. Clemens, C. J. Hansen, and B. P. Hine. The whole earth telescope - A new astronomical instrument. ApJ, 361:309–317, September 1990. doi: 10.1086/169196.

C. Neiner and A.-M. Hubert. The pulsations of Be stars. *Communications in Asteroseismology*, 158:194–+, July 2009.

C. Neiner, H. F. Henrichs, M. Floquet, Y. Frémat, O. Preuss, A.-M. Hubert, V. C. Geers, A. H. Tijani, J. S. Nichols, and S. Jankov. Rotation, pulsations and magnetic field in ¡ASTROBJ¿V 2052 Ophiuchi¡/ASTROBJ¿: A new He-strong star. A&A, 411:565–579, December 2003a. doi: 10.1051/0004-6361:20031342.

C. Neiner, A.-M. Hubert, Y. Frémat, M. Floquet, S. Jankov, O. Preuss, H. F. Henrichs, and J. Zorec. Rotation and magnetic field in the Be star ¡ASTROBJ¿omega Orionis¡/ASTROBJ¿. A&A, 409:275–286, October 2003b. doi: 10.1051/0004-6361:20031086.

A. A. Pamyatnykh. Pulsational Instability Domains in the Upper Main Sequence. , 49:119–148, June 1999.

M. A. C. Perryman. The HIPPARCOS Catalogue Contents. In R. M. Bonnet, E. Høg, P. L. Bernacca, L. Emiliani, A. Blaauw, C. Turon, J. Kovalevsky, L. Lindegren, H. Hassan, M. Bouffard, B. Strim, D. Heger, M. A. C. Perryman, & L. Woltjer, editor, *Hipparcos - Venice '97*, volume 402 of *ESA Special Publication*, pages 1–4, August 1997.

A. Pigulski and D. A. Boratyn. The orbit of Beta Cephei derived from the light-time effect. A&A, 253:178–184, January 1992.

K. R. Pollard, D. J. Wright, W. Zima, P. L. Cottrell, and P. De Cat. High-resolution spectroscopy and mode identification in non-radially pulsating stars. *Communications in Asteroseismology*, 157:118–123, December 2008.

A. Porri and R. Stalio. Short term profile variations in Alpha Eridani (B4Ve), P Carinae (B4Ve), and Epsilon Capricorni (B3IIIe). A&AS, 75:371–380, November 1988.

D. Pourbaix, A. A. Tokovinin, A. H. Batten, F. C. Fekel, W. I. Hartkopf, H. Levato, N. I. Morrell, G. Torres, and S. Udry. S$_{B⁹}$: The ninth catalogue of spectroscopic binary orbits. A&A, 424:727–732, September 2004. doi: 10.1051/0004-6361:20041213.

D. Pourbaix, A. A. Tokovinin, A. H. Batten, F. C. Fekel, W. I. Hartkopf, H. Levato, N. I. Morell, G. Torres, and S. Udry. SB9: 9th Catalogue of Spectroscopic Binary Orbits (Pourbaix+ 2004-2011). *VizieR Online Data Catalog*, 1:2020–+, August 2009.

Richard Powell. The hertzsprung russell diagram, February 2012. URL `http://www.atlasoftheuniverse.com/hr.html`.

H. Rauer and C. Catala. The PLATO mission. In A. Sozzetti, M. G. Lattanzi, & A. P. Boss, editor, *IAU Symposium*, volume 276 of *IAU Symposium*, pages 354–358, November 2011. doi: 10.1017/S1743921311020436.

A. Retter, T. R. Bedding, D. L. Buzasi, H. Kjeldsen, and L. L. Kiss. Oscillations in Arcturus from WIRE Photometry. ApJ, 591:L151–L154, July 2003. doi: 10.1086/377211.

T. Rivinius, D. Baade, S. Stefl, O. Stahl, B. Wolf, and A. Kaufer. Stellar and circumstellar activity of the Be star MU Centauri. II. Multiperiodic low-order line-profile variability. A&A, 336:177–190, August 1998a.

T. Rivinius, D. Baade, S. Stefl, O. Stahl, B. Wolf, and A. Kaufer. Multiperiodic Line-profile Variability and a Tentative Ephemeris for Line-Emission Outbursts of the Be Star MU CEN. In P. A. Bradley and J. A. Guzik, editors, *A Half Century of Stellar Pulsation Interpretation*, volume 135 of *Astronomical Society of the Pacific Conference Series*, page 343, 1998b.

T. Rivinius, D. Baade, and S. Štefl. Non-radially pulsating Be stars. A&A, 411: 229–247, November 2003. doi: 10.1051/0004-6361:20031285.

Carter Roberts. Kepler field of view, March 2012. URL http://kepler.nasa.gov/multimedia/photos/?ImageID=9.

F. J. Rogers and C. A. Iglesias. Radiative atomic Rosseland mean opacity tables. ApJS, 79:507–568, April 1992. doi: 10.1086/191659.

J. F. Rowe, J. M. Matthews, S. Seager, E. Miller-Ricci, D. Sasselov, R. Kuschnig, D. B. Guenther, A. F. J. Moffat, S. M. Rucinski, G. A. H. Walker, and W. W. Weiss. The Very Low Albedo of an Extrasolar Planet: MOST Space-based Photometry of HD 209458. ApJ, 689:1345–1353, December 2008. doi: 10.1086/591835.

J.-P. Rozelot and C. Neiner, editors. *The Rotation of Sun and Stars*, volume 765 of *Lecture Notes in Physics, Berlin Springer Verlag*, 2009.

S. Salmon, J. Montalbán, T. Morel, A. Miglio, M. Dupret, and A. Noels. Testing the effects of opacity and the chemical mixture on the excitation of pulsations in B stars of the Magellanic Clouds. *ArXiv e-prints*, March 2012.

M. Schönberg and S. Chandrasekhar. On the Evolution of the Main-Sequence Stars. ApJ, 96:161–+, September 1942. doi: 10.1086/144444.

C. Schrijvers, J. H. Telting, and C. Aerts. Line-profile variability in the β Cephei star ϵ Centauri. A&A, 416:1069–1079, March 2004. doi: 10.1051/0004-6361:20031731.

R. Scuflaire, J. Montalbán, S. Théado, P.-O. Bourge, A. Miglio, M. Godart, A. Thoul, and A. Noels. The Liège Oscillation code. Ap&SS, 316:149–154, August 2008a. doi: 10.1007/s10509-007-9577-6.

R. Scuflaire, S. Théado, J. Montalbán, A. Miglio, P.-O. Bourge, M. Godart, A. Thoul, and A. Noels. CLÉS, Code Liégeois d'Évolution Stellaire. Ap&SS, 316:83–91, August 2008b. doi: 10.1007/s10509-007-9650-1.

M. J. Seaton, C. J. Zeippen, J. A. Tully, A. K. Pradhan, C. Mendoza, A. Hibbert,

and K. A. Berrington. The Opacity Project - Computation of Atomic Data. , 23:19, March 1992.

A. Secchi. Schreiben des herrn prof. secchi, dir. der sternwarte des collegio romano, an den herausgeber. *Astronomische Nachrichten*, 68(4):63–64, 1867. ISSN 1521-3994. doi: 10.1002/asna.18670680405. URL http://dx.doi.org/10.1002/asna.18670680405.

R. R. Shobbrook. Two new Beta Canis Majoris variables: epsilon Cen and delta Lup. MNRAS, 157:5P–9P, 1972.

R. Silvotti, S. Schuh, R. Janulis, J.-E. Solheim, S. Bernabei, R. Østensen, T. D. Oswalt, I. Bruni, R. Gualandi, A. Bonanno, G. Vauclair, M. Reed, C.-W. Chen, E. Leibowitz, M. Paparo, A. Baran, S. Charpinet, N. Dolez, S. Kawaler, D. Kurtz, P. Moskalik, R. Riddle, and S. Zola. A giant planet orbiting the 'extreme horizontal branch' star V391 Pegasi. Nature, 449:189–191, September 2007. doi: 10.1038/nature06143.

M. A. Smith. The nonradial oscillations of Spica. I - Two commensurable modes. II - A 'quasi-toroidal' mode. ApJ, 297:206–232, October 1985a. doi: 10.1086/163517.

M. A. Smith. The Nonradial Oscillations of SPICA - Part Two - a Quasi-Toroidal Mode. ApJ, 297:224–+, October 1985b. doi: 10.1086/163518.

M. A. Smith. Ultraviolet Spectrophotometry of Variable Early-Type Be and B Stars Derived from High-Resolution IUE Data. ApJ, 562:998–1011, December 2001. doi: 10.1086/323846.

J. Southworth, H. Bruntt, and D. L. Buzasi. Eclipsing binaries observed with the WIRE satellite. II. β Aurigae and non-linear limb darkening in light curves. A&A, 467:1215–1226, June 2007. doi: 10.1051/0004-6361:20077184.

S. A. Spreckley and I. R. Stevens. The period and amplitude changes of Polaris (α UMi) from 2003 to 2007 measured with SMEI. MNRAS, 388:1239–1244, August 2008. doi: 10.1111/j.1365-2966.2008.13439.x.

Steven Spreckley. A study of variable stars and search for extrasolar planets with the space based photometers smei and stereo. PhD thesis, October 2008.

A. Stankov and G. Handler. Catalog of Galactic β Cephei Stars. ApJS, 158:193–216, June 2005. doi: 10.1086/429408.

P. Stee and A. Meilland. Is the Critical Rotation of Be Stars Really Critical for the Be Phenomenon? In *The Rotation of Sun and Stars*, volume 765 of *Lecture Notes in Physics, Berlin Springer Verlag*, pages 195–205, 2009. doi: 10.1007/978-3-540-87831-5_8.

D. Stello, H. Bruntt, H. Preston, and D. Buzasi. Oscillating K Giants with the WIRE Satellite: Determination of Their Asteroseismic Masses. ApJ, 674:L53–L56, February 2008. doi: 10.1086/528936.

N. J. Tarrant, W. J. Chaplin, Y. Elsworth, S. A. Spreckley, and I. R. Stevens. Asteroseismology of red giants: photometric observations of Arcturus by SMEI. MNRAS, 382:L48–L52, November 2007. doi: 10.1111/j.1745-3933.2007.00387.x.

N. J. Tarrant, W. J. Chaplin, Y. Elsworth, S. A. Spreckley, and I. R. Stevens. Oscillations in β Ursae Minoris. Observations with SMEI. A&A, 483:L43–L46, June 2008a. doi: 10.1051/0004-6361:200809738.

N. J. Tarrant, W. J. Chaplin, Y. P. Elsworth, S. A. Spreckley, and I. R. Stevens. SMEI observations of previously unseen pulsation frequencies in γ Doradus. A&A, 492: 167–169, December 2008b. doi: 10.1051/0004-6361:200810952.

Neil James Tarrant. Asteroseismology from the main sequence to giant stars. Two papers based on this thesis, and originally included in Appendix 2 are available at http://eprints.bham.ac.uk/380/ http://eprints.bham.ac.uk/381/, July 2010. URL `http://etheses.bham.ac.uk/736/`.

J. H. Telting and C. Schrijvers. A new bright beta Cephei star: line-profile variability in omegaˆ1 SCO. A&A, 339:150–158, November 1998.

J. H. Telting, C. Aerts, and P. Mathias. A period analysis of the optical line variability of β Cephei: evidence for multi-mode pulsation and rotational modulation. A&A, 322:493–506, June 1997.

J. H. Telting, C. Schrijvers, I. V. Ilyin, K. Uytterhoeven, J. De Ridder, C. Aerts, and H. F. Henrichs. A high-resolution spectroscopy survey of β Cephei pulsations in bright stars. A&A, 452:945–953, June 2006. doi: 10.1051/0004-6361:20054730.

N. Tetzlaff, R. Neuhäuser, and M. M. Hohle. A catalogue of young runaway Hipparcos stars within 3 kpc from the Sun. MNRAS, 410:190–200, January 2011. doi: 10.1111/j.1365-2966.2010.17434.x.

D. G. Turner. Monitoring the Evolution of Cepheid Variables. *Journal of the American Association of Variable Star Observers (JAAVSO)*, 26:101–111, 1998.

K. Uytterhoeven, J. H. Telting, C. Aerts, and B. Willems. Interpretation of the variability of the β Cephei star λ Scorpii. II. The line-profile diagnostics. A&A, 427: 593–605, November 2004a. doi: 10.1051/0004-6361:20041224.

K. Uytterhoeven, B. Willems, K. Lefever, C. Aerts, J. H. Telting, and U. Kolb. Interpretation of the variability of the β Cephei star λ Scorpii. I. The multiple character. A&A, 427:581–592, November 2004b. doi: 10.1051/0004-6361:20041223.

M. M. F. Vinicius, J. Zorec, N. V. Leister, and R. S. Levenhagen. α Eridani: rotational distortion, stellar and circumstellar activity. A&A, 446:643–660, February 2006. doi: 10.1051/0004-6361:20053029.

H. von Zeipel. The radiative equilibrium of a rotating system of gaseous masses. MNRAS, 84:665–683, June 1924.

G. Walker, J. Matthews, R. Kuschnig, R. Johnson, S. Rucinski, J. Pazder, G. Burley, A. Walker, K. Skaret, R. Zee, S. Grocott, K. Carroll, P. Sinclair, D. Sturgeon, and J. Harron. The MOST Asteroseismology Mission: Ultraprecise Photometry from Space. PASP, 115:1023–1035, September 2003. doi: 10.1086/377358.

G. A. H. Walker, R. Kuschnig, J. M. Matthews, P. Reegen, T. Kallinger, E. Kambe, H. Saio, P. Harmanec, D. B. Guenther, A. F. J. Moffat, S. M. Rucinski, D. Sasselov, W. W. Weiss, D. A. Bohlender, H. Božić, O. Hashimoto, P. Koubský, R. Mann, D. Ruždjak, P. Škoda, M. Šlechta, D. Sudar, M. Wolf, and S. Yang. Pulsations of the Oe Star ζ Ophiuchi from MOST Satellite Photometry and Ground-based Spectroscopy. ApJ, 623:L145–L148, April 2005. doi: 10.1086/430254.

G. A. H. Walker, B. Croll, R. Kuschnig, A. Walker, S. M. Rucinski, J. M. Matthews, D. B. Guenther, A. F. J. Moffat, D. Sasselov, and W. W. Weiss. The Differential Rotation of κ^1 Ceti as Observed by MOST. ApJ, 659:1611–1622, April 2007. doi: 10.1086/511851.

G. A. H. Walker, B. Croll, J. M. Matthews, R. Kuschnig, D. Huber, W. W. Weiss, E. Shkolnik, S. M. Rucinski, D. B. Guenther, A. F. J. Moffat, and D. Sasselov. MOST detects variability on τ Bootis A possibly induced by its planetary companion. A&A, 482:691–697, May 2008. doi: 10.1051/0004-6361:20078952.

D. F. Webb, D. R. Mizuno, A. Buffington, M. P. Cooke, C. J. Eyles, C. D. Fry, L. C. Gentile, P. P. Hick, P. E. Holladay, T. A. Howard, J. G. Hewitt, B. V. Jackson, J. C. Johnston, T. A. Kuchar, J. B. Mozer, S. Price, R. R. Radick, G. M. Simnett, and S. J. Tappin. Solar Mass Ejection Imager (SMEI) observations of coronal mass ejections (CMEs) in the heliosphere. *Journal of Geophysical Research (Space Physics)*, 111: A12101, December 2006. doi: 10.1029/2006JA011655.

M. Wenger, F. Ochsenbein, D. Egret, P. Dubois, F. Bonnarel, S. Borde, F. Genova, G. Jasniewicz, S. Laloë, S. Lesteven, and R. Monier. The SIMBAD astronomical database. The CDS reference database for astronomical objects. A&AS, 143:9–22, April 2000. doi: 10.1051/aas:2000332.

W. Zima. The Campaigns of the Delta Scuti Network. *Delta Scuti Star Newsletter*, 11:37, July 1997.